8-31-2022

Performance analysis of the dominant mode rejection beamformer

Enlong Hu
New Jersey Institute of Technology

Copyright Warning & Restrictions

The copyright law of the United States (Title 17, United States Code) governs the making of photocopies or other reproductions of copyrighted material.

Under certain conditions specified in the law, libraries and archives are authorized to furnish a photocopy or other reproduction. One of these specified conditions is that the photocopy or reproduction is not to be "used for any purpose other than private study, scholarship, or research." If a, user makes a request for, or later uses, a photocopy or reproduction for purposes in excess of "fair use" that user may be liable for copyright infringement,

This institution reserves the right to refuse to accept a copying order if, in its judgment, fulfillment of the order would involve violation of copyright law.

Please Note: The author retains the copyright while the New Jersey Institute of Technology reserves the right to distribute this thesis or dissertation

Printing note: If you do not wish to print this page, then select "Pages from: first page # to: last page #" on the print dialog screen

ABSTRACT

PERFORMANCE ANALYSIS OF THE DOMINANT MODE REJECTION BEAMFORMER

by
Enlong Hu

In array signal processing over challenging environments, due to the non-stationarity nature of data, it is difficult to obtain enough number of data snapshots to construct an adaptive beamformer (ABF) for detecting weak signal embedded in strong interferences. One type of adaptive method targeting for such applications is the dominant mode rejection (DMR) method, which uses a reshaped eigen-decomposition of sample covariance matrix (SCM) to define a subspace containing the dominant interferers to be rejected, thereby allowing it to detect weak signal in the presence of strong interferences. The DMR weight vector takes a form similar to the adaptive minimum variance distortion-less response (MVDR), except with the SCM being replaced by the DMR-SCM.

This dissertation studies the performance of DMR-ABF by deriving the probability density functions of three important metrics: notch depth (ND), white noise gain (WNG), and signal-to-interference-and-noise ratio (SINR). The analysis contains both single interference case and multiple interference case, using subspace transformation and the random matrix theory (RMT) method for deriving and verifying the analytical results. RMT results are used to approximate the random matrice. Finally, the analytical results are compared with RMT Monte-Carlo based empirical results.

PERFORMANCE ANALYSIS OF THE DOMINANT MODE REJECTION BEAMFORMER

by
Enlong Hu

A Dissertation
Submitted to the Faculty of
New Jersey Institute of Technology
in Partial Fulfillment of the Requirements for the Degree of
Doctor of Philosophy in Electrical Engineering

Helen and John C. Hartmann
Department of Electrical and Computer Engineering

August 2022

APPROVAL PAGE

PERFORMANCE ANALYSIS OF THE DOMINANT MODE REJECTION BEAMFORMER

Enlong Hu

Dr. Hongya Ge, Dissertation Advisor — Date
Associate Professor of Electrical and Computer Engineering, NJIT

Dr. Alexander M. Haimovich, Committee Member — Date
Distinguished Professor of Electrical and Computer Engineering, NJIT

Dr. Ali Abdi, Committee Member — Date
Professor of Electrical and Computer Engineering, NJIT

Dr. Yunqing Shi, Committee Member — Date
Professor of Electrical and Computer Engineering, NJIT

Dr. Zoi-Heleni Michalopoulou, Committee Member — Date
Professor of Mathematical Sciences, NJIT

BIOGRAPHICAL SKETCH

Author: Enlong Hu

Degree: Doctor of Philosophy

Date: August 2022

Undergraduate and Graduate Education:

- Doctor of Philosophy in Electrical Engineering,
  New Jersey Institute of Technology, Newark, NJ, 2022
- Master of Science in Electrical Engineering,
  New Jersey Institute of Technology, Newark, NJ, 2012
- Bachelor of Science in Electrical Engineering,
  Zhejiang University, Hangzhou, P.R.China, 2010

Major: Electrical Engineering

Presentations and Publications:

Enlong Hu and Hongya Ge, "The probability density function of SINR loss of the dominant mode rejection beamformer," *in Proc. 52nd Annual Conference on Information Sciences and Systems (CISS),Princeton, NJ, USA*, Mar 2018, pp. 1-6.

Enlong Hu and Hongya Ge, "Probability density function of notch depth for dominant mode rejection beamformer," *Electronics Letters*, Vol. 55, No.23, pp. 1255-1258, Nov 2019.

This dissertation is my family, friends, teachers and colleagues who have supported and inspired me.

ACKNOWLEDGMENT

First, I wish to express my sincere gratitude to my advisor, Prof. Hongya Ge, for introducing me into this research area. Without Dr. Ge's consistent guidance and support throughout my whole Ph.D program, I would not be able to reach this point.

Second, I want to thank Dr. Alexander M. Haimovich, Dr. Ali Abdi , Dr. Yunqing Shi from Electrical and Computer Engineering Department of NJIT and Dr. Zoi-Heleni Michalopoulou from Mathematical Sciences Department of NJIT to be the members of committee. I appreciate their insight and suggestions.

Thank you to the Center for Wireless Information Processing and all my labmates for their help in technicalities, feedback and valuable suggestions. Thank you to the ECE department for the teacher assistant job. Thank you to Dr. Ge for the research assistant offer.

Finally, Id like to thank all the people who helped, guided and encouraged me in my whole life.

TABLE OF CONTENTS

TABLE OF CONTENTS
(Continued)

Chapter **Page**

TABLE OF CONTENTS
(Continued)

Chapter **Page**

TABLE OF CONTENTS
(Continued)

Chapter **Page**

LIST OF FIGURES

LIST OF FIGURES
(Continued)

Figure **Page**

LIST OF FIGURES
(Continued)

Figure **Page**

LIST OF FIGURES
(Continued)

Figure **Page**

LIST OF FIGURES
(Continued)

Figure **Page**

LIST OF FIGURES
(Continued)

Figure **Page**

CHAPTER 1

INTRODUCTION

1.1 Overview of Adaptive Beamforming

An adaptive beamformer (ABF) is a widely used system with an array of transmitters or receivers that performs adaptive spatial signal processing to filter out weak signal of interest (SOI) in the presence of strong interferences. ABFs rely on the knowledge of the data covariance matrix to compute the beamformer weights. For example, the minimum variance distortionless response (MVDR) beamformer, also known as the Capon's beamformer, is derived by minimizing output power $\mathbf{w}_{MVDR} = \arg\min_{\mathbf{w}} E\left\{\left|\mathbf{w}^H\mathbf{p}\left(l\right)\right|^2\right\}$ subject to a unity gain constraint $\mathbf{w}^H\mathbf{v}_s = 1$ in the SOI's look direction: $\mathbf{w}_{MVDR} = \arg\min_{\mathbf{w}}\left\{\mathbf{w}^H\mathbf{\Sigma}_{I+N}\mathbf{w}\right\}, \quad s.t.\ \mathbf{w}^H\mathbf{v}_s = 1$, where $\mathbf{p}\left(l\right)$ is the data vector, Σ_{I+N} is the ensemble covariance matrix (ECM) and $\mathbf{v}_s$ is the steering vector..

Note under H_0 (signal absent case), the data vector $\mathbf{p}\left(l\right)$ contains only D planewave interferences and noise: $\mathbf{p}\left(l\right) = \sum_{i=1}^{D} b_i\left(l\right)\mathbf{v}_i + \mathbf{n}\left(l\right)$ where b_i is the amplitude of the ith planewave interference $\mathbf{v}_i$, $\mathbf{n}$ is a vector of complex noise samples $\mathbf{n} \sim CN\left(\mathbf{0}, \sigma_n^2\mathbf{I}\right)$. The ECM under H_0 is represented as $\mathbf{\Sigma}_{I+N} = \sum_{i=1}^{D}\sigma_i^2\mathbf{v}_i\mathbf{v}_i^{\mathbf{H}} + \sigma_n^2\mathbf{I}$. While on the other hand, under H_1 (signal present case), the data vector $\mathbf{p}\left(l\right)$ contains SOI, D planewave interferences and noise: $\mathbf{p}\left(l\right) = b_s\left(l\right)\mathbf{v}_s + \sum_{i=1}^{D} b_i\left(l\right)\mathbf{v}_i + \mathbf{n}\left(l\right)$ where b_s is the amplitude of the signal vector $\mathbf{v}_s$. The ECM under H_1 is represented as $\mathbf{\Sigma}_{S+I+N} = \sigma_s^2\mathbf{v}_s\mathbf{v}_s^{\mathbf{H}} + \sum_{i=1}^{D}\sigma_i^2\mathbf{v}_i\mathbf{v}_i^{\mathbf{H}} + \sigma_n^2\mathbf{I}$

Using the method of Lagrange multipliers, we can transform the constrained optimization above into an unconstrained one. The Lagrangian function is given by $\mathcal{L}(\mathbf{w}, \lambda) = \mathbf{w}^H\mathbf{\Sigma}_{I+N}\mathbf{w} + \lambda\left(\mathbf{w}^H\mathbf{v}_s - 1\right) + \left(\mathbf{v}_s^H\mathbf{w} - 1\right)\lambda^*$. By equating $\dfrac{\partial\mathcal{L}}{\partial\mathbf{w}}$ to zero and solving for $\mathbf{w}$, we can obtain: $\mathbf{w}_{MVDR} = \left(\mathbf{\Sigma}_{I+N}^{-1}\mathbf{v}_s\right) / \left(\mathbf{v}_s^{\mathbf{H}}\mathbf{\Sigma}_{I+N}^{-1}\mathbf{v}_s\right)$. The above results

are in the case of H_0 (signal absent). Note that under H1 (signal present) case, the $\mathbf{\Sigma}_{I+N}$ is replaced with $\mathbf{\Sigma}_{S+I+N}$ (signal partial cancellation issue may arise).

The MVDR weight vector is a function of the inverse of the ECM. In reality, the ECM for data is not available, so that in the data-driven adaptive MVDR, the ECM is replaced by the sample covariance matrix (SCM) $\mathbf{S} = \frac{1}{L}\sum_{l=1}^{L}\mathbf{p}(l)\,\mathbf{p}(l)^{\mathrm{H}}$. The SCM is computed from a collection of L data snapshots. For stationary data set, SCM approximates to ECM well. However, if there is only a limited amount of data snapshots, the sample covariance matrix could be singular (non-invertible) and/or resulting a bad estimate of ECM.

1.2 Overview of Dominant Mode Rejection (DMR) Beamformer

For large arrays or fast-changing environments, it is not always easy to obtain enough number of snapshots because the data are not stationary over long enough time intervals. Therefore, these cases require beamformers that achieve faster convergence by reducing the adaptive degrees of freedom. The classical adaptive methods rely on the eigendecomposition of the SCM. There are two main types of eigenvector beamforming algorithms: The first type is Eigenspace-ABF. It projects the data into a subspace formed from the eigenvectors associated with the largest eigenvalues. The second type is DMR-ABF. We will discuss these two methods in detail in later chapters.

The DMR is a type of adaptive beamformer proposed by Abraham and Owsley [1]. DMR weight vector is the MVDR weight vector with the ECM replaced by $\mathbf{\Sigma}_{DMR}$: $\mathbf{w}_{DMR} = \left(\mathbf{\Sigma}_{DMR}^{-1}\mathbf{v}_s\right) / \left(\mathbf{v}_s^{\mathbf{H}}\mathbf{\Sigma}_{DMR}^{-1}\mathbf{v}_s\right)$. In practice, the ECM is not available, so $\mathbf{\Sigma}_{DMR}$ cannot be constructed. Instead, the structured covariance matrix required for DMR is computed using the SCM $\mathbf{S}_{DMR}$ based on snapshots. Therefore, the adaptive DMR weight vector is: $\mathbf{w}_{DMR} = \left(\mathbf{S}_{DMR}^{-1}\mathbf{v}_s\right) / \left(\mathbf{v}_s^{\mathbf{H}}\mathbf{S}_{DMR}^{-1}\mathbf{v}_s\right)$. DMR covariance matrix $\mathbf{S}_{DMR}$ uses a reshaped eigen-decomposition of SCM to define a subspace containing the

dominant interference to be rejected, thereby allowing it to detect weak SOI in the presence of strong interference. DMR decomposes the $N \times N$ covariance matrix into a dominant interferer subpace and a noise subspace. The dominant subspace is denoted by the eigenvectors associated with the D largest eigenvalues of the sample covariance matrix while the all the eigenvalues for the $N-D$ dim noise subspace in the SCM are replaced by their mean value $\left(\frac{1}{N-D}\right)\sum_{n=D+1}^{N}\lambda_n$. The number of dominant eigenvalues determines the dominant subspace rank. When the background noise is spatially white, the rank of the noise subspace is known, ensemble statistics are accessible, $\mathbf{\Sigma}_{DMR} = \mathbf{\Sigma}_{I+N}$ or $\mathbf{\Sigma}_{DMR} = \mathbf{\Sigma}_{S+I+N}$ (e.g., ensemble covariance matrix under H_0 is represented as $\mathbf{\Sigma}_{I+N} = \sum_{i=1}^{D}\sigma_i^2\mathbf{v}_i\mathbf{v}_i^{\mathbf{H}} + \sigma_n^2\mathbf{I}$ and under H_1 is $\mathbf{\Sigma}_{S+I+N} = \sigma_s^2\mathbf{v}_s\mathbf{v}_s^{\mathbf{H}} + \sum_{i=1}^{D}\sigma_i^2\mathbf{v}_i\mathbf{v}_i^{\mathbf{H}} + \sigma_n^2\mathbf{I}$), then DMR ABF becomes equal to the MVDR beamformer.

1.3 Literature Review of DMR ABF

There exist a number of papers exploring how to make DMR ABF robust to mismatch [5, 8, 13, 21, 25], but few considering the performance analysis of the algorithm. For practical applications, there exist some papers [24,31] investigating DMR performance using deep-water and shallow-water sonar data results. The experimental analysis of in these papers supports the claim that the DMR ABF requires fewer snapshots than the MVDR ABF to achieve the same performance, but these papers [5,8,13,21,24,25, 31] do not extend the empirical results to predict the relationship between snapshots and performance for an arbitrary array.

In this work, we focus on two main types of eigenvector beamforming algorithms: Eigenspace-ABF and DMR-ABF, there have been many studies done on them. Eigenspace-ABF requires the desired signal to be loud enough that it is included in the reduced-rank subspace used for the projection, whereas the DMR-ABF depends on the desired signal being quiet enough that it is not included in its dominant interferer subspace. The difference in assumptions leads to a fundamental

performance difference between DMR and other eigenspace methods, particularly when the subspace must be estimated from the SCM. We would like to extend the research work of DMR-ABF from some of the above results and methods.

The recent DMR research works by Wage and Buck [37–41] focus on the snapshot performance of the DMR algorithm. Their analyses emphasize on the fundamental case of a single interference in white noise, and using theoretical calculations for the ensemble case reveal the relationships among white noise gain (WNG), notch depth (ND), and signal-to-interference-plus-noise ratio (SINR). But the theoretical derivation to support their snapshot-based results/conjectures yet to be developed.

The focus of this dissertation is on the performance analysis of DMR ABF, by deriving the theoretic results on the probability density distributions (PDFs) of WNG, ND and SINR. We study the performance through investigating adaptive dimensionality reduction and subspace formulation techniques. Closed-form derivations of the PDFs for WNG, ND and SINR are presented to confirm conjectures [37–41]. The performance analysis contains both single interference case and multiple interference case, along with the RMT method for deriving and verifying the analytical results. Finally, the analytical results are compared with RMT Monte-Carlo based empirical results.

1.4 Organization

This dissertation studies the performance of DMR-ABF through the probability density functions of three standard metrics: WNG, ND, and SINR. We expand our study through investigating adaptive dimensionality reduction and subspace formulation techniques. The analysis contains both single interference case and multiple interference case, along with the RMT method for deriving and verifying the analytical results.

This dissertation is organized as following:

(1) Chapter 1 introduces the background knowledge of DMR ABF, illustrates the focus of our research and outlines the organizations.

(2) In Chapter 2, three approaches for handling rank deficient sample covariance matrices are summarized. ND histograms generated through Monte-Carlo simulations are used to show the performance of approaches. Among the comparison, an adaptive dimensionality reduction and subspace formulation technique is develpoed to study the performance of DMR-ABF.

(3) The performance analysis of DMR ABF is presented in Chapter 3-5. First, Chapter 3 shows that the distribution of SINR loss ratio of the DMR beamformer for single interference case. The distribution can be simplified into a beta distribution function. Second, Chapter 4 presents a theoretical analysis for the ND of the DMR based ABF for single interference case. A closed-form expression has been derived for the PDF of ND. Finally, the performance analysis of DMR ABF for the multiple interference case is discussed in Chapter 5, along with the RMT method for deriving and verifying the analytical results.

CHAPTER 2

APPROACHES FOR HANDLING RANK DEFICIENT COVARIANCE MATRICES

2.1 Introduction

The estimation of covariance matrix is required in many data-driven signal processing applications. In array signal processing over challenging environments, it is difficult to obtain enough number of data snapshots to construct an ABF for detecting weak signal embedded in strong interference due to the non-stationarity nature of data. In most practical applications, ensemble statistics required in implementing the ABF are typically not available and must be estimated from available data sets. Therefore, data-driven adaptive beamformers (ABFs) must be implemented using sample statistic instead of ensemble ones. Performance of ABFs depends on the number of data snapshots used to estimate the SCM. When the number of snapshots is much greater than the number of variables or data dimension, ECM is replaced by the SCM. Under the assumption of Gaussian distributed data, the SCM can lead to an unbiased and asymptotically efficient estimator of the true covariance matrix. However, if we have insufficient amount of data (sample deficient), the SCM is singular (non-invertible) resulting in a poor estimate of ECM.

Generally, there are two types of approaches to solving this snapshot deficient problem. The first approach uses the technique of dimentionality reduction, also referred to as partially adaptive processing. The idea is to introduce a data transformation without too much loss of information, so that one can operate in a smaller dimensional subspace. These techniques can be classified either as reduced-dimension methods where the transformation matrix is fixed, or rank-reducing methods where the transformation matrix uses the data information.

The second type of approach is comprised of regularizing the SCM, generally by using diagonal loading (DL). The DL artificially converts the singular sample covariance matrix into an invertible (positivedefinite) covariance by the simple expedient of adding a positive diagonal matrix, or more generally, by taking a linear combination of the sample covariance and an identity matrix. One well-known drawback of the DL methods is that a universally accepted way of choosing the diagonal loading factor is still lacking. Among the methods in this broad category, there is one called DMR. Instead of projecting into a reduced-rank subspace, DMR uses the eigen-decomposition to define a subspace containing the dominant interference that it wants to reject, thereby allowing it to detect low-power signal in the presence of strong interference. The DMR weight vector takes a form similar to the adaptive MVDR, except with the SCM being replaced by the DMR-SCM.

In this chapter, we begin with a planewave beamforming problem in an insufficient amount of data scenario. Then we present three approaches mentioned above (dimension reduction, DL, and DMR) for handling rank deficient covariance matrices due to limited data snapshots. Based on these approaches, we develop an adaptive dimensionality reduction and subspace formulation technique to further facilitate our study of the performance of DMR-ABF.

2.2 Problem

Our problem begin with an insufficient amount of data scenario: a set of L statistically independent and identically distributed measurements or snapshots of an N dimensional random vector where $L < N$ is available for testing beamformer performance.

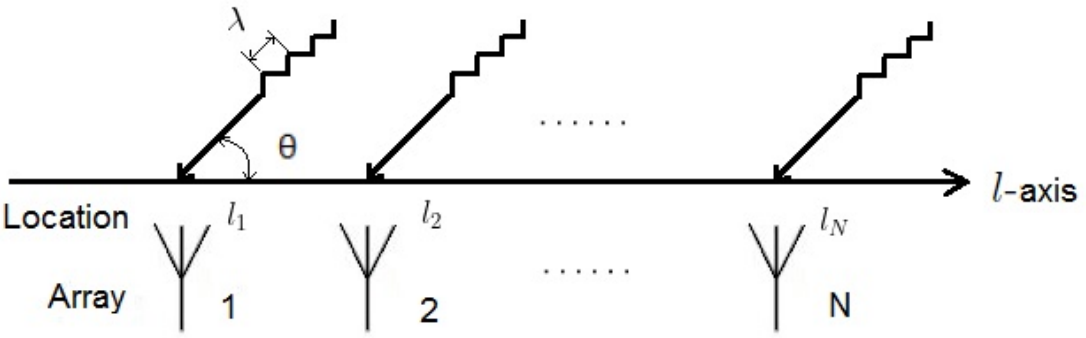

Figure 2.1 Uniform linear array with N sensors under far-field conditions.

2.2.1 Planewave beamforming problem

Planewave beamforming assumes that the data measured by an array consist of one or more planewave signals plus noise. For a sensor array receives a narrowband signal containing D planewave interference, which can be represented as

$$\mathbf{p}(l) = b_s(l)\,\mathbf{v}_s + \sum_{i=1}^{D} b_i(l)\,\mathbf{v}_i + \mathbf{n}(l) \tag{2.1}$$

where b_s is the amplitude of the signal vector $\mathbf{v}_s$, b_i is the amplitude of the ith planewave interference $\mathbf{v}_i$, $\mathbf{n}$ is a vector of complex noise samples $\mathbf{n} \sim CN(\mathbf{0}, \sigma_n^2\mathbf{I})$.

For the N element sensor array oriented along l-axis, the received signal vector and the complex exponential vector for ith planewave interference can be represented as

$$\mathbf{v}_s = \mathbf{v}(\theta_s) = \frac{1}{\sqrt{N}}\begin{bmatrix} e^{j\frac{2\pi}{\lambda}\cos(\theta_s)l_1} \\ \vdots \\ e^{j\frac{2\pi}{\lambda}\cos(\theta_s)l_N} \end{bmatrix}, \mathbf{v}_i = \mathbf{v}(\theta_i) = \frac{1}{\sqrt{N}}\begin{bmatrix} e^{j\frac{2\pi}{\lambda}\cos(\theta_i)l_1} \\ \vdots \\ e^{j\frac{2\pi}{\lambda}\cos(\theta_i)l_N} \end{bmatrix} \tag{2.2}$$

where λ is the wavelength, θ_s is the direction of the SOI, θ_i is the direction of the i-th interferer, and l_i is the location of the ith sensor. Without loss of generality, this dissertation assumes that the amplitudes b_s and b_i are i.i.d. zero-mean complex circular random variables $b_s \sim CN(\mathbf{0}, \sigma_s^2\mathbf{I})$, $b_i \sim CN(\mathbf{0}, \sigma_i^2\mathbf{I})$ and that the complex circular random noise is zero mean and spatially white. Assuming the planewave interference are independent, the ensemble covariance matrix(ECM) under H_0 is represented as

$$\mathbf{\Sigma}_{I+N} = \sum_{i=1}^{D} \sigma_i^2 \mathbf{v}_i \mathbf{v}_i^{\mathbf{H}} + \sigma_n^2 \mathbf{I} \tag{2.3}$$

while on the other hand, under H_1 is

$$\mathbf{\Sigma}_{S+I+N} = \sigma_s^2 \mathbf{v}_s \mathbf{v}_s^{\mathbf{H}} + \sum_{i=1}^{D} \sigma_i^2 \mathbf{v}_i \mathbf{v}_i^{\mathbf{H}} + \sigma_n^2 \mathbf{I} \tag{2.4}$$

where σ_s^2 is the power in the signal σ_i^2 is the power in the ith interference source, and the white noise power is σ_n^2.

In practice, the ECM is not available. Instead, the structured covariance matrix required for DMR is computed using the SCM based on L snapshots. The SCM and its eigendecomposition are defined as

$$\mathbf{S} = \frac{1}{L} \sum_{l=1}^{L} \mathbf{p}(l)\, \mathbf{p}^{\mathrm{H}}(l) \overset{EVD}{=} \sum_{n=1}^{N} \lambda_n \mathbf{e}_n \mathbf{e}_n^{\mathrm{H}} \tag{2.5}$$

where $\mathbf{p}(l)$ is the lth data snapshot, and $\mathbf{e}_n$ and λ_n are the sample eigenvectors and eigenvalues, respectively.

Thus, we are given a $N \times L$ data matrix. The columns of data matrix are consist of L independent identically distributed realizations or snapshots. We are interested

in the case where $L < N$. Consequently the sample covariance is singular with rank equal to L.

2.2.2 Metrics

The data-driven adaptive MVDR beamformer weight vector is

$$\mathbf{w} = \frac{\mathbf{S}^{-1}\mathbf{v}_s}{\mathbf{v}_s^{\mathbf{H}}\mathbf{S}^{-1}\mathbf{v}_s} \tag{2.6}$$

where $\mathbf{S}$ is the SCM based on L snapshots. The joint distribution of the elements of $\mathbf{S}$ is central complex Wishart distribution with parameters L, N. Under H_0, $\mathbf{S} \sim CW\left(L, N; \mathbf{\Sigma}_{I+N}\right)$, while under H_1, $\mathbf{S} \sim CW\left(L, N; \mathbf{\Sigma}_{S+I+N}\right)$.

We use some standard metrics to test beamformer performance: WNG, beampattern, ND, and SINR. WNG is a standard metric that quantifies the improvement in the SNR provided by a beamformer when the noise is spatially white. It is defined as

$$G_{WNG} \triangleq \frac{1}{\mathbf{w}^{\mathrm{H}}\mathbf{w}} = \frac{\left|\mathbf{v}_s^{\mathbf{H}}\mathbf{S}^{-1}\mathbf{v}_s\right|^2}{\mathbf{v}_s^{\mathbf{H}}\mathbf{S}^{-2}\mathbf{v}_s} \tag{2.7}$$

WNG is a useful indicator of how robust a beamformer is to array perturbations or mismatch.

The second metric of interest is beampattern. It is defined in terms of the angle θ:

$$B\left(\theta\right) \triangleq \mathbf{w}^{\mathrm{H}}\mathbf{v}\left(\theta\right) \tag{2.8}$$

The beampattern is analogous to the frequency response of a filter. It quantifies the beamformers response to a unity amplitude planewave from angle θ.

The third metric of interest is ND. ND is defined as the amplitude square of the beampattern in the direction of an interference. That is, in the case of a single interference $\mathbf{v}_i$,

$$G_{notch} \triangleq |B(\theta_i)|^2 = \left|\mathbf{w}^{\mathrm{H}}\mathbf{v}_i\right|^2 = \frac{\left|\mathbf{v}_s^{\mathbf{H}}\mathbf{S}^{-1}\mathbf{v}_i\right|^2}{\left|\mathbf{v}_s^{\mathbf{H}}\mathbf{S}^{-1}\mathbf{v}_s\right|^2}. \tag{2.9}$$

ND quantifies how well a beamformer can eliminate an interference. The deeper the notch, the better the interference suppression performance. Figure 2.1 shows the beampattern for the canonical single-interferer example when the INR is 40 dB. The example uses a 50-sensor ULA with half-wave-length spacing. $N = 50$, $L = 25/75/500$, $\rho_{INR} = 40dB$, $\sigma_s^2 = 10, \sigma_1^2 = 10000, \sigma_n^2 = 1$. The beampattern is plotted as a function of the directional cosine. Note that this dissertation distinguishes between a notch and a null. A null is a point where the beampattern is exactly equal to zero, whereas a notch is a partial null, which is not a zero crossing of the beampattern.

The fourth metric of interest is SINR. The SINR of a beamformer is defined as

$$SINR(\mathbf{w}) \triangleq \frac{\sigma_s^2\left|\mathbf{w}^{\mathbf{H}}\mathbf{v}_s\right|^2}{\mathbf{w}^{\mathbf{H}}\mathbf{\Sigma}_{I+N}\mathbf{w}} \tag{2.10}$$

where σ_s^2 is the desired signal power, $\mathbf{v}_s$ is the replica associated with the desired signal.

2.3 Approach One: Dimension Reduction

2.3.1 The Johnson Lindenstrauss lemma

In mathematics, A powerful result by Johnson and Lindenstrauss (JL) [19] states that a higher dimensional data set can be operated upon by a Lipschitz function and the resulting lower dimensional output data set has similar pairwise distances as the original data set. The lemma states that a set of points in a high-dimensional space

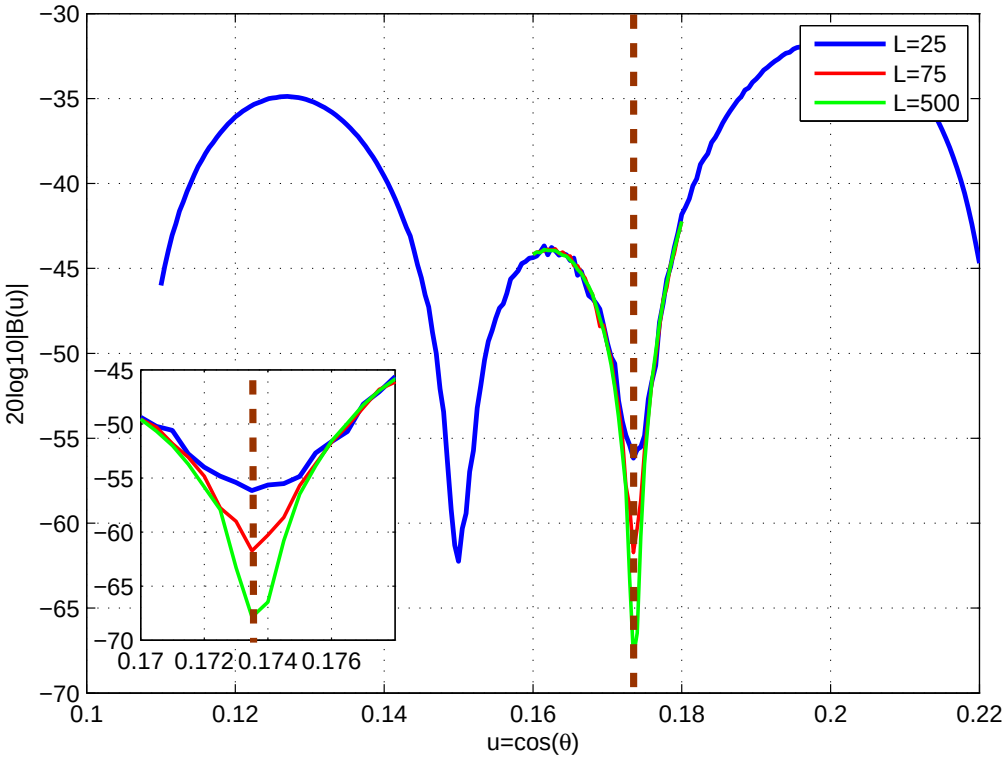

Figure 2.2 The DMR ABFs designed using 25, 75 and 500 snapshots have notches of -56, -60 and -68 dB, respectively. The SOI location is at 1.396. The interferer location is at 0.1736 (brown dash line). The example uses a 50-sensor ULA with half-wave-length spacing. $N = 50$, $INR = 40dB$, $\sigma_s^2 = 10, \sigma_1^2 = 10000, \sigma_n^2 = 1$.

can be embedded into a space of much lower dimension in such a way that distances between the points are nearly preserved. The map used for the embedding is at least Lipschitz, and can even be taken to be an orthogonal projection.

Theorem 1. (JL Lemma [19, 22]) Let $\varepsilon_o \in (0,1)$. Given any set of points $X = \{x_1, x_2, \ldots, x_n\}$ in $\mathbb{R}^N$, there exists a map A: $\mathbb{R}^N \to \mathbb{R}^d$ with $d = O\left(\frac{\log L}{\varepsilon_o^2}\right)$ such that

$$1 - \varepsilon_o \leq \frac{\|A(x_i) - A(x_j)\|_2^2}{\|x_i - x_j\|_2^2} \leq 1 + \varepsilon_o.$$

Moreover, such a map can be computed in expected $poly(L, N, 1/\varepsilon_o)$ time.

The minimum number of components to guarantees the ϵ_o-embedding is given by $d \geq O\left(\frac{\log L}{\varepsilon_o^2}\right)$. Figure 2.3 shows that with an increasing number of samples L, the minimal number of dimensions d increased logarithmically in order to guarantee an ϵ_o-embedding.

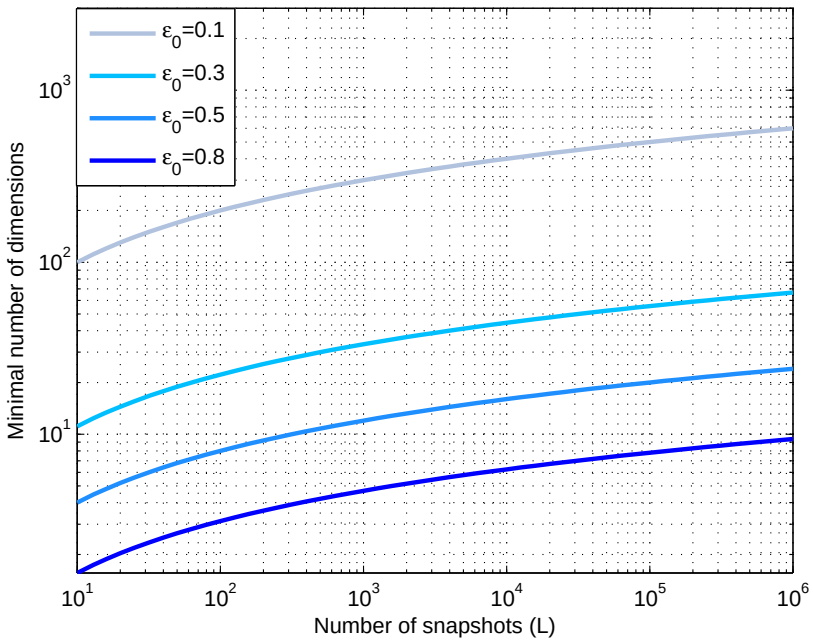

Figure 2.3 JL lemma bounds: number of samples L v.s. the minimal number of dimensions. $N = 50$.

Interestingly, new dimension d depends on the number of samples L rather than the original dimension N. The equation above can help us to know whether random projection can be used efficiently for a given dataset. Error rate is a number between 0 to 1 which determines how much error is tolerable in the transformed data. It must be kept in mind as ϵ_o goes higher, d goes lower.

The JL lemma has been discovered, proved and reproved many times, with each new proof providing a sharpened (i.e., reduced bound) and/or simplified result. However, there is one particular feature that is common to all JL embeddings: the mapping projects a vector into lower dimensions, and the length of this projection is sharply concentrated around its expectation.

In the original paper that introduced the JL lemma [19], Johnson and Lindenstrauss provide a lengthy, technical proof using geometric approximation. The first significant improvement to the JL lemma came from Frankl and Meahara [10]. They replace the random k-dimensional subspace with a collection of k random, orthonormal vectors. This approach requires a much simpler proof that attains a sharper bound. Indyk and Motwani [18] provide the next improvement by relaxing the condition of orthogonality in the projection matrix. Dasgupta and Gupta [9] provide an alternative, much simpler proof of the result of Indyk and Motwani using moment generating functions. Moreover, they provide a tighter bound than all previous versions of the JL lemma. Achlioptas [2] subsequently shows that spherical symmetry of the projection coefficients is not necessary in order to obtain a JL embedding that maintains ϵ-distortion. Instead, he shows that concentration of the projected points is sufficient. Finally, Matouek [23] improves upon the above results. Currently, researchers attempt to express the JL lemma in simple terms so that it can be better understood by the research community.

The lemma has applications in compressed sensing, manifold learning, dimension reduction, and graph embedding. Much of the data stored and manipulated

on computers, including text and images, can be represented as points in a high-dimensional space. However, the essential algorithms for working with such data tend to become bogged down very quickly as dimension increases. It is therefore desirable to reduce the dimension of the data in a way that preserves its relevant structure. The JohnsonLindenstrauss lemma is a classic result in this vein.

2.3.2 Random projection

In random projection, the original high-dimensional data is projected onto a lower-dimensional subspace using a random matrix whose columns have unit lengths. Random projection has been found to be a computationally efficient, yet sufficiently accurate method for dimension reduction of high-dimensional data sets. While this method has attracted lots of interest, empirical results are sparse.

Dimension reduction via random projection has recently received attention from the data science community. In random projection, the original N-dimensional data are projected to a d -dimensional subspace by multiplying the $d \times N$ random matrix by $N \times L$ data matrix. The random projection was motivated by the JL lemma, which asserts that a set of high-dimensional points can be projected into significantly lower dimensions, while preserving its structure within a given error tolerance and bound on the reduced dimension.

The reduced dimension d is independent of the original dimension of the problem, but is dependent on the number of snapshots L. JL Lemma provides guarantees that the newly projected data is representative of its original higher dimension counterpart. The dimension-reduced covariance matrix is now $d \times d$ and it is invertible. The inverse matrix computation required for the weight vector is reduced from $O\left(N^3\right)$ to $O\left(d^3\right)$.

The basic idea of random projection is to use a data transformation to operate in an smaller dimensional subspace (Figure 2.4). These techniques can be classified

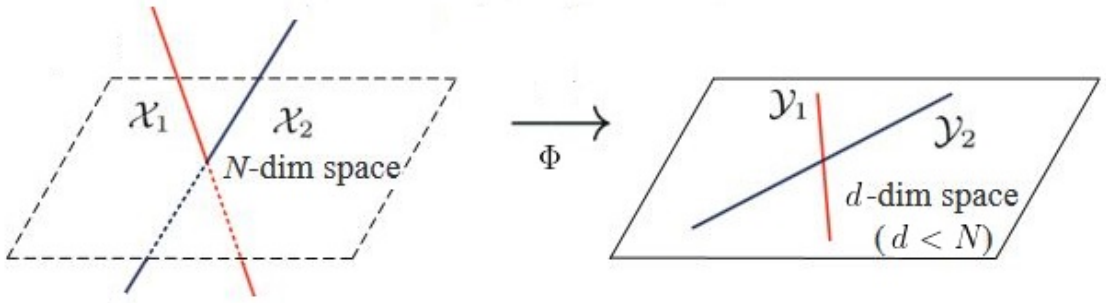

Figure 2.4 Random projections: from a high dimension to a lower dimension.

either as reduced-dimension methods which the transformation matrix is fixed, or rank-reducing methods where the transformation matrix depends on the data. In next section we will discuss these two different ways of choosing random projection matrix.

2.3.3 Data independent random projection matrix

The core idea behind random projection is given in the JL lemma, which states that if points in a vector space are of sufficiently high dimension, then they may be projected into a suitable lower-dimensional space in a way which approximately preserves the distances between the points.

In random projection, the original N-dimensional data is projected to a d-dimensional ($d < N$) subspace, using a random $d \leq N$-dimensional matrix $\mathbf{\Phi}$ whose columns have unit lengths. Using matrix notation: If $\mathbf{p}_l$ is the original N-dimensional data vector, then $\mathbf{\Phi}^H \mathbf{p}_l$ is the projection of the data onto a lower d-dimensional subspace, where $\mathbf{\Phi}$ is a $N \times d$ random matrix with $d \leq L$. Random projection is computationally simple: form the random matrix $\mathbf{\Phi}$ and project the data matrix onto d dimensions. The multiplication of the $N \times 1$ data vector $\mathbf{p}_l$ by a random matrix $\mathbf{\Phi}^H$ results in a data vector of reduced dimension $d \times 1$, which in turn produces a

statistically meaningful $d \times d$ sample covariance matrix:

$$\mathbf{\Phi}^H \frac{1}{L} \sum_{l=1}^{L} \mathbf{p}_l \mathbf{p}_l \mathbf{\Phi}^H = \mathbf{\Phi}^H \mathbf{S} \mathbf{\Phi} \tag{2.11}$$

It is important to note that dimension reduction is the transformation of data from a high-dimensional space into a low-dimensional space so that the low-dimensional representation retains some meaningful properties of the original data.

Random Permutation Matrix One possible random matrix is a random permutation matrix. The effect is to discard all but d of the N components of the data vectors.

We denote $\boldsymbol{\phi}_i, i = 1...d$ as the orthonormal vectors in $\mathbb{C}^N$. They have one thing in common: only one entry is 1, other $N-1$ entries are zeros. A permutation matrix is a $N \times d$ matrix of the form

$$\mathbf{\Phi} = \begin{bmatrix} \boldsymbol{\phi}_1 & \cdots & \boldsymbol{\phi}_d \end{bmatrix} \quad \text{where } \boldsymbol{\phi}_i \neq \boldsymbol{\phi}_j$$

For example, assume we have $N = 10$ sensors and $L = 5$ snapshots. Suppose that we randomly select $d = 3$ distinct sensors: sensors 2, 3 and 7. Formally; the dimensionality reduction of the snapshot is accomplished by multiplication by the

conjugate transpose of a 10×3 permutation matrix:

$$\mathbf{\Phi} = \begin{bmatrix} 0 & 0 & 0 \\ 1 & 0 & 0 \\ 0 & 1 & 0 \\ 0 & 0 & 0 \\ 0 & 0 & 0 \\ 0 & 0 & 0 \\ 0 & 0 & 1 \\ 0 & 0 & 0 \\ 0 & 0 & 0 \\ 0 & 0 & 0 \end{bmatrix}$$

therefore, $\mathbf{p}_l \rightarrow \mathbf{\Phi}^H \mathbf{p}_l$, and $\mathbf{S} \rightarrow \mathbf{\Phi}^H \mathbf{S} \mathbf{\Phi}$.

Figure 2.5 shows the beampattern for the canonical single-interferer example when a random permutation matrix is in use. The beampattern is plotted as a function of the direction angle.

Gaussian Distribution The random matrix $\mathbf{\Phi}$ can be generated using Gaussian distribution random variables. The first row is a random unit vector (unit norm). The second row is a random unit vector from the space orthogonal to the first row, the third row is a random unit vector from the space orthogonal to the first two rows, and so on. In this way of choosing $\mathbf{\Phi}$, and the following properties are satisfied: (1) Spherical symmetry: For any orthogonal matrix $\mathbf{A}$, $\mathbf{\Phi}^H \mathbf{A}$ and $\mathbf{\Phi}^H$ have the same distribution. (2) Orthogonality: The columns of $\mathbf{\Phi}$ are orthogonal to each other. (3) Normality: The columns of $\mathbf{\Phi}$ are unit-length vectors.

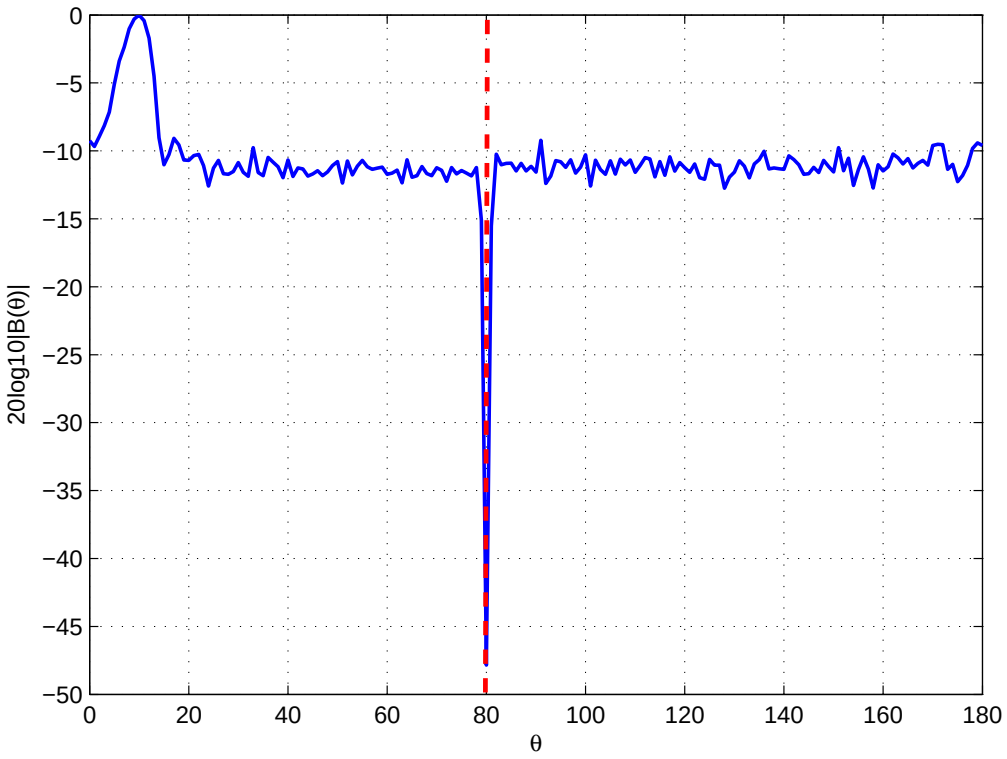

Figure 2.5 Beampattern $|B(\theta)|^2 = \left|\mathbf{w}^{\mathrm{H}}\mathbf{v}(\theta)\right|^2$ (in dB) for the single interferer example when a random permutation matrix is in use. The example uses a 50-sensor ULA with half-wave-length spacing. $N = 50$, $L = 25$, $d = 10$. $\rho_{INR} = 40dB$, $\sigma_s^2 = 10, \sigma_1^2 = 10000, \sigma_n^2 = 1$. $\theta_s = 10°$, $\theta_1 = 80°$. The red line shows location of the interference.

For a Gaussian distribution random projection matirx $\mathbf{\Phi} = \begin{bmatrix} \boldsymbol{\phi}_1 & \cdots & \boldsymbol{\phi}_d \end{bmatrix}$, $\boldsymbol{\phi}_i (i = 1 \cdots d)$ are chosen from $\mathcal{N}(\mathbf{0}, \mathbf{I})$. Figure 2.6 shows the beampattern for the canonical single-interferer example when a Gaussian distributed random projection matrix is in use.

Bernoulli Distribution Another frequently used random projection is produced using the Bernoulli distribution random variables. In this case, all the elements in $\boldsymbol{\phi}_i (i = 1 \cdots d)$ are $+1$ or -1 with equal probabilities. Thus, all of the elements in $\mathbf{\Phi}$ has zero mean and unit variance. Figure 2.7 shows the beampattern for the canonical

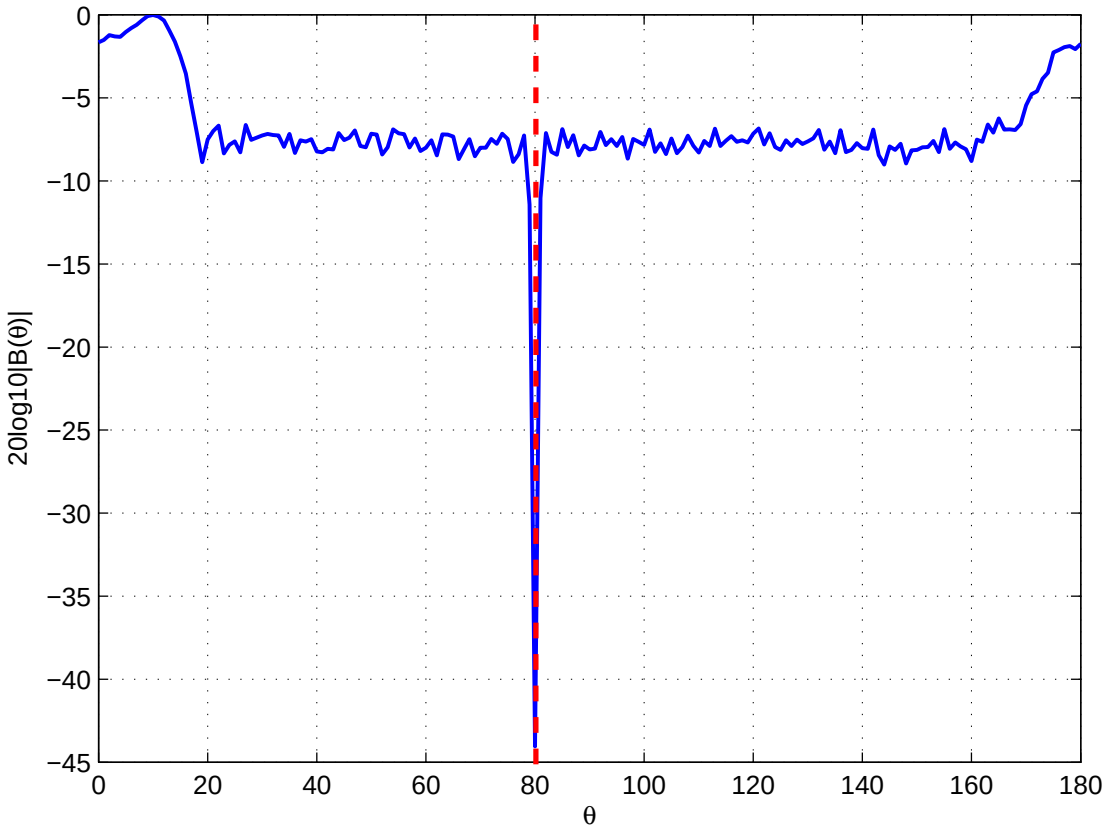

Figure 2.6 Beampattern $|B(\theta)|^2 = \left|\mathbf{w}^{\mathrm{H}}\mathbf{v}(\theta)\right|^2$ (in dB) for the single-interferer example when a Gaussian distributed random projection matrix is in use. The example uses a 50-sensor ULA with half-wave-length spacing. $N = 50$, $L = 25$, $d = 10$. $\rho_{INR} = 40dB$, $\sigma_s^2 = 10, \sigma_1^2 = 10000, \sigma_n^2 = 1$. $\theta_s = 10°$, $\theta_1 = 80°$. The red line shows location of the interference.

single-interferer example when a Bernoulli distributed random projection matrix is in use.

2.3.4 Data dependent random projection matrix

The random matrix $\mathbf{\Phi}$ can also be constructed from the principal eigenvectors of the SCM, see [15,20] for the most well-known methods using this principle. For detection purposes, this results in a low-rank adaptive matched filter where the inverse of

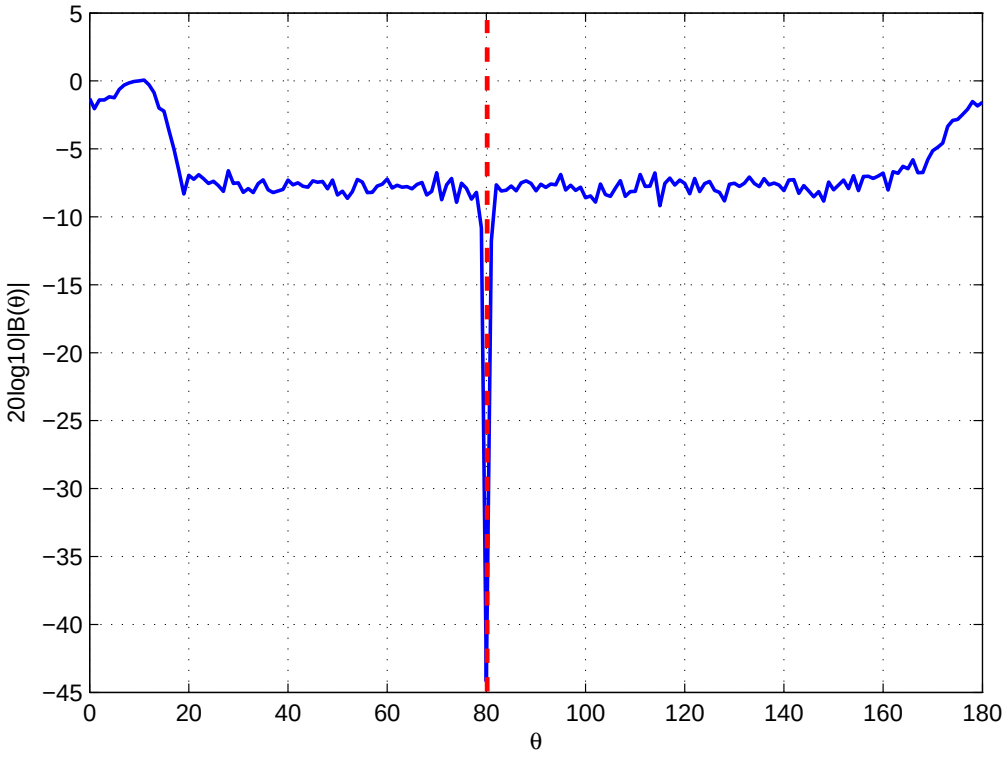

Figure 2.7 Beampattern $|B(\theta)|^2 = \left|\mathbf{w}^{\mathrm{H}}\mathbf{v}(\theta)\right|^2$ (in dB) for the single-interferer example when a Bernoulli distributed random projection matrix is in use. The example uses a 50-sensor ULA with half-wave-length spacing. $N = 50$, $L = 25$, $d = 10$. $\rho_{INR} = 40dB$, $\sigma_s^2 = 10, \sigma_1^2 = 10000, \sigma_n^2 = 1$. $\theta_s = 10°$, $\theta_1 = 80°$. The red line shows location of the interference.

the SCM is replaced by the projector onto the subspace orthogonal to the principal eigenvectors.

In [35, 36], Tucci, Marzetta, Simon and Ren proposed a beautiful and original idea where dimensionality reduction is achieved through an ensemble of isotropically random unitary matrices. More precisely, a column of $\mathbf{\Phi}$ is aligned with $\mathbf{v}_s$ (which guarantees that the signal of interest goes through the data transformation), while the other columns are drawn at random in the subspace orthogonal to $\mathbf{v}_s$. Processing is done in the reduced-dimension space and the outputs are subsequently combined. The authors provided a theoretical analysis of such technique, provided insightful results

about its relation with shrinkage of the SCM eigenvalues, and applied it successfully to direction of arrival estimation and covariance matrix estimation.

Follow the idea in [35, 36], we consider a random $N \times d$ matrix $\mathbf{\Phi}$, where $d \leq rank\,(\mathbf{S})$, $\mathbf{\Phi}^H\mathbf{\Phi} = \mathbf{I_d}$. Note it can preserve the energy of the steering vector, $\left(\mathbf{\Phi}^H\mathbf{v}_s\right)^H\left(\mathbf{\Phi}^H\mathbf{v}_s\right) = \mathbf{v}_s^H\mathbf{v}_s$. The conventional spectral estimate is $\mathbf{v}_s^H\mathbf{S}\mathbf{v_s}$, it is still obtainable from the reduced-dimension snapshots and steering vector,

$$\left(\mathbf{\Phi}^H\mathbf{v}_s\right)^H\left(\mathbf{\Phi}^H\mathbf{S}\mathbf{\Phi}\right)\left(\mathbf{\Phi}^H\mathbf{v}_s\right) = \mathbf{v}_s^H\mathbf{S}\mathbf{v_s}$$

All that matters is the subspace that is spanned by the columns of $\mathbf{\Phi}$. Without loss of generality we can make the first column of $\mathbf{\Phi}$ equal to the steering vector,

$$\mathbf{\Phi} = [\mathbf{v}_s \;\; \boldsymbol{\phi}_2 \cdots \boldsymbol{\phi}_d] \tag{2.12}$$

From the discussion in the two subsections above, we can see that choosing an appropriate $\mathbf{\Phi}$ is the key to dealing with quadratic form expression (e.g., the conventional spectral estimate is $\mathbf{v}_s^H\mathbf{S}\mathbf{v_s}$). This reminds me of the thoughts by Reed et al. [32]. By substituting several appropriate random projection matrices, they keep the quadratic form expression in the distribution of the normalized signal-to-noise ratio to be a central complex Wishart distribution. This makes sure that the subsequent derivation of the simplification process can be completed successfully.

2.4 Approach Two: Diagonal Loading

Diagonal loading is one form of Tikhonov regularization [34]. It is used to solve the problem of insufficient snapshots. The approach consists of adding a small regularization matrix, usually a scaled identity matrix, to the estimated spatial

correlation matrix (Figure 2.11). Cox et al. [14] have showed that the diagonal loading approach reduces the sensitivity to the model mismatch caused by the insufficient snapshots. Gilbert and Morgan [11] show that the diagonal loading improves the beamformers robustness when the array elements are displaced with zero-mean, independent and identically distributed random perturbations.

The number of snapshots that can be collected in the interval might be insufficient to accurately estimate of SCM, which leads to one type of model mismatch. To combat the sensitivity to mismatch and/or to improve the condition number of the SCM, a diagonally loaded SCM is introduced as:

$$\mathbf{S}_\delta = \mathbf{S} + \delta\mathbf{I} \tag{2.13}$$

where δ is the diagonal loading factor.

Figure 2.12 shows eigenvalues histogram of DL SCM. Red zone are diagonal loading factor δ. Figure 2.13 shows the diagonal loading factor determines the gain into the direction of the desired user ($\theta_s = 10°$) and also the null depth in the direction of the interference $\theta_1 = 80°$.

2.4.1 The bounds for diagonal loading factor

In order to get an optimal diagonal loading factor, or the bounds for δ, we assume the SCM can be rewritten as

$$\mathbf{S} = \begin{bmatrix} s_{11} & s_{12} & \cdots & s_{1N} \\ s_{21} & \ddots & & \vdots \\ \vdots & & \ddots & \vdots \\ s_{N1} & \cdots & \cdots & s_{NN} \end{bmatrix} = \mathbf{\Sigma}_{I+N} + \mathbf{\Sigma}_\varepsilon = \mathbf{V}\mathbf{\Lambda}_s\mathbf{V}^H + \sigma_n^2\mathbf{I} + \mathbf{\Sigma}_\varepsilon \tag{2.14}$$

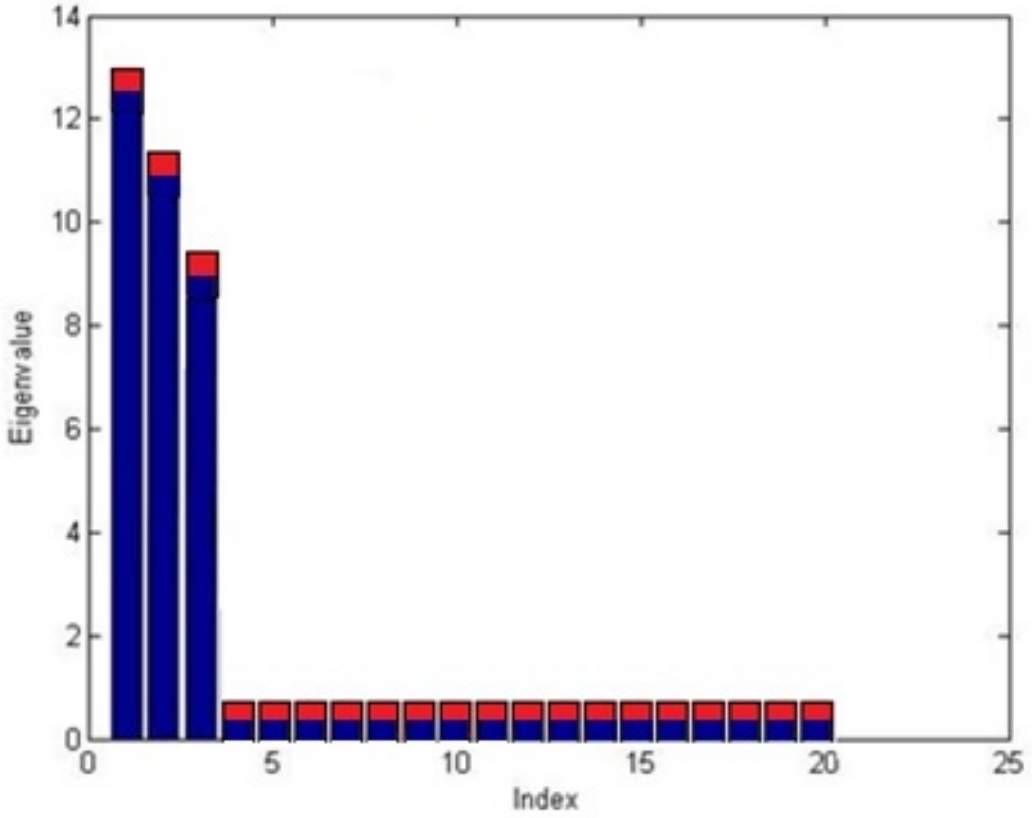

Figure 2.8 Eigenvalues histogram of DL SCM. Red zone are diagonal loading factor.

where $\mathbf{V} = [\boldsymbol{\xi}_1 \cdots \boldsymbol{\xi}_D]$, $\boldsymbol{\Lambda}_s = diag\{\sigma_1^2 \cdots \sigma_D^2\}$, and $\boldsymbol{\Sigma}_\varepsilon$ is the inaccuracy term of covariance matrix of sampling data. It is a zero mean random matrix with the standard deviation equals to $std(diag(\mathbf{S}))$. Therefore, the inverse of the diagonal loaded covariance matrix $\mathbf{S}_\delta$ can he approximately expressed as: bounds for δ, we assume the SCM can be rewritten as

$$\mathbf{S}_\delta^{-1} = (\boldsymbol{\Sigma}_{I+N} + \delta\mathbf{I})^{-1} \left[\mathbf{I} + \boldsymbol{\Sigma}_\varepsilon (\boldsymbol{\Sigma}_{I+N} + \delta\mathbf{I})^{-1}\right]^{-1} \tag{2.15}$$

As

$$\left[\mathbf{I} + \boldsymbol{\Sigma}_\varepsilon (\boldsymbol{\Sigma}_{I+N} + \delta\mathbf{I})^{-1}\right] \left[\mathbf{I} - \boldsymbol{\Sigma}_\varepsilon (\boldsymbol{\Sigma}_{I+N} + \delta\mathbf{I})^{-1}\right] \approx \mathbf{I}$$

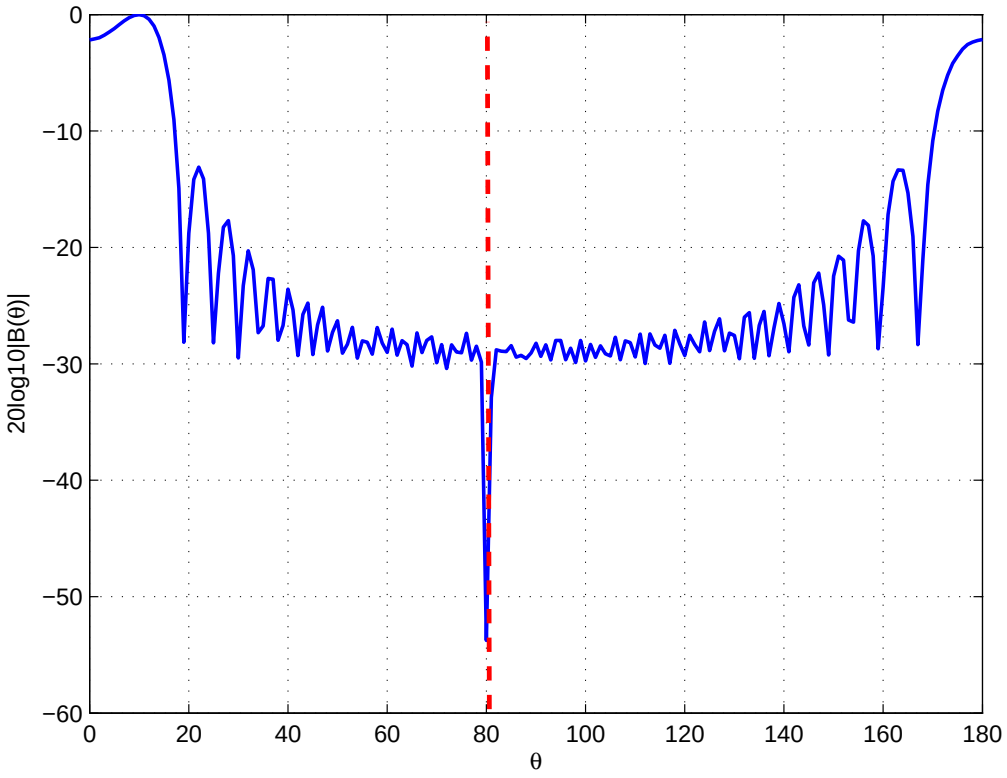

Figure 2.9 Beampattern $|B(\theta)|^2 = \left|\mathbf{w}^{\mathrm{H}}\mathbf{v}(\theta)\right|^2$ (in dB) of MVDR ABF for the single-interferer example. $\delta_{opt} = std(diag(\mathbf{S}))$. The example uses a 50-sensor ULA with half-wave-length spacing. $N = 50$, $L = 25$. $\rho_{INR} = 40dB$, $\sigma_s^2 = 10, \sigma_1^2 = 10000, \sigma_n^2 = 1$. $\theta_s = 10°$, $\theta_1 = 80°$. The red line shows location of the interference.

we have

$$\left[\mathbf{I} + \mathbf{\Sigma}_{\varepsilon}\left(\mathbf{\Sigma}_{I+N} + \delta\mathbf{I}\right)^{-1}\right]^{-1} \approx \mathbf{I} - \mathbf{\Sigma}_{\varepsilon}\left(\mathbf{\Sigma}_{I+N} + \delta\mathbf{I}\right)^{-1}$$

Therefore,

$$\begin{aligned}
\mathbf{S}_{\delta}^{-1} &= \left(\mathbf{\Sigma}_{I+N} + \delta\mathbf{I}\right)^{-1}\left[\mathbf{I} + \mathbf{\Sigma}_{\varepsilon}\left(\mathbf{\Sigma}_{I+N} + \delta\mathbf{I}\right)^{-1}\right]^{-1} \\
&= \left(\mathbf{\Sigma}_{I+N} + \delta\mathbf{I}\right)^{-1}\left[\mathbf{I} - \mathbf{\Sigma}_{\varepsilon}\left(\mathbf{\Sigma}_{I+N} + \delta\mathbf{I}\right)^{-1}\right] \\
&= \left(\mathbf{\Sigma}_{I+N} + \delta\mathbf{I}\right)^{-1}\left[\mathbf{I} - \frac{1}{\delta + \sigma_n^2}\mathbf{\Sigma}_{\varepsilon}\left[\mathbf{I} - \mathbf{V}\left(\mathbf{V}^H\mathbf{V} + \left(\delta + \sigma_n^2\right)\mathbf{\Lambda}_s^{-1}\right)^{-1}\mathbf{V}^H\right]\right]
\end{aligned} \tag{2.16}$$

The value of first bracket $\mathbf{\Sigma}_{I+N} + \delta\mathbf{I}$ is close to the covariance matrix $\mathbf{\Sigma}_{I+N}$, thus the diagonal loading value should be far less than the diagonal elements. the diagonal element value of the true covariance matrix can be estimated by the average of SCM diagonal element values:

$$\delta \ll \frac{1}{N} tr\left(\mathbf{S}\right) \tag{2.17}$$

Also, the beamformer performance degradation is caused by the second term $\mathbf{I} - \left(\delta + \sigma_n^2\right)^{-1} \mathbf{\Sigma}_{\varepsilon} \left[\mathbf{I} - \mathbf{V}\left(\mathbf{V}^H\mathbf{V} + \left(\delta + \sigma_n^2\right)\mathbf{\Lambda}_s^{-1}\right)^{-1}\mathbf{V}^H\right]$ thus it is desirable to have:

$$\sqrt{\frac{1}{N}\sum_{i=1}^{N}\left(s_{ii} - \frac{\sum_{n=1}^{N} s_{nn}}{N}\right)} < \delta + \sigma_n^2 \tag{2.18}$$

Threfore, we have

$$\sqrt{\frac{1}{N}\sum_{i=1}^{N}\left(s_{ii} - \frac{\sum_{n=1}^{N} s_{nn}}{N}\right)} - \sigma_n^2 < \delta \ll \frac{1}{N} tr\left(\mathbf{S}\right) = \frac{1}{N}\sum_{i=1}^{N} s_{ii} \tag{2.19}$$

2.4.2 Optimization and estimation of diagonal loading factor

It can be observed that the diagonal loading value has been limited to an interval. In this part, with the value δ increasing gradually in the interval, we try to observe the performance of MVDR on diagonal loading beamformer with the output SINR as the index.

The ratio with output power of the desired signals to the interference adding noise signals is defined as the output SINR:

$$SINR\left(\delta\right) = \frac{\sigma_s^2}{\mathbf{w^H}\left(\delta\right)\mathbf{\Sigma}_{I+N}\mathbf{w}\left(\delta\right)} = \frac{\sigma_s^2\left|\mathbf{v}_s^H\mathbf{S}_{\delta}^{-\mathbf{1}}\mathbf{v_s}\right|^2}{\left|\mathbf{v}_s^H\mathbf{S}_{\delta}^{-\mathbf{1}}\mathbf{\Sigma_{I+N}}\mathbf{S}_{\delta}^{-\mathbf{1}}\mathbf{v_s}\right|} \tag{2.20}$$

the ensemble output SINR is: $SINR_{ens} = \sigma_s^2 \left| \mathbf{v}_s^H \mathbf{\Sigma}_{I+N}^{-1} \mathbf{v}_s \right|$.

The performance of the estimator (2.23) is measured via estimation mean square error (MSE). Given a steering direction, the MSE of the estimator (2.23) is viewed as a function of the loading factor δ and represented via the bias-variance decomposition as,

$$\mathbf{MSE}\left(\delta\right) = \mathbf{E^2}\left[\mathbf{SINR}\left(\delta\right) - \mathbf{SINR_{ens}}\right] + \mathbf{var}\left(\mathbf{SINR}\left(\delta\right)\right) \tag{2.21}$$

The optimal diagonal loading opt is defined as

$$\delta_{opt} = \arg\min_{\delta} \mathbf{MSE}\left(\delta\right) \tag{2.22}$$

In the following simulation, we employ a 16-element ULA. The distance of elements is half of the wavelength, the direction of the desired signal is 0 degrees, and the direction of the interference signal is 40 degrees. We select the power of desired signal is far less than the noise and the power of interference signal is greater than the noise. At this point, the input SNR is 5 dB and the input INR is 10 dB. From Equation(2.22), 10 points are selected in the interval. Here we optimize the diagonal loading factor δ by using the output SINR. Figure 2.14 shows when δ equals to the standard deviation of the diagonal elements of $\mathbf{S}$, the output SINR gets the maximum value, and the performance gets the best.

Therefore, we choose the optimum DL factor as

$$\delta_{opt} = \sqrt{\frac{1}{N}\sum_{i=1}^{N}\left(s_{ii} - \frac{\sum_{n=1}^{N} s_{nn}}{N}\right)} \tag{2.23}$$

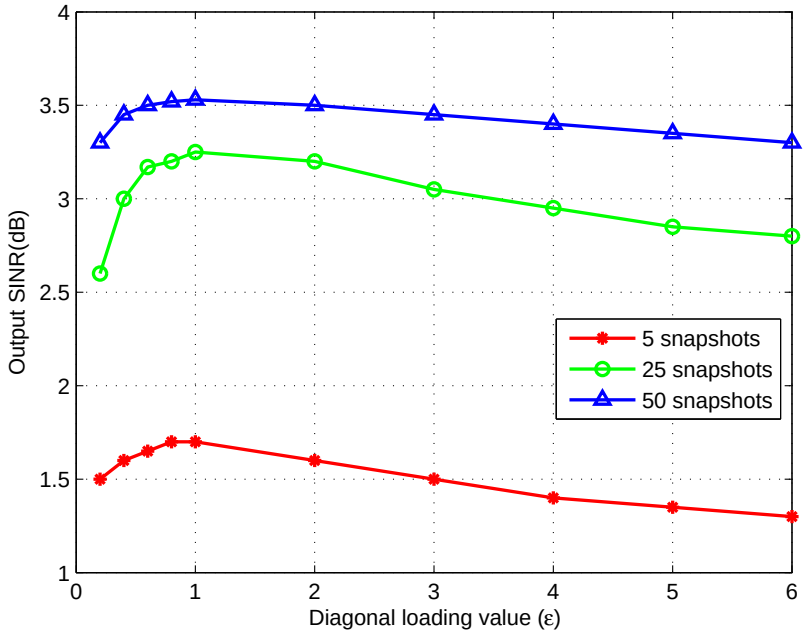

Figure 2.10 The relations between diagonal loading value and output SINR in different snapshots (SNR = -5 dB, INR = 10 dB).

2.5 Approach Three: Dominant Mode Rejection (DMR)

We assume that there are D strong planewave signals (interference) that need to be attenuated to facilitate detection of a weaker desired planewave signal. With this assumption, the SCM can be partitioned into a dominant interference subpace and a noise subspace; the latter includes the weaker signals and the noise. DMR assumes that the large eigenvalues are all associated with interference to be rejected and that the small eigenvalues are due to weak signals and noise. Sorting the eigenvalues in descending order leads to the following expression for the eigendecomposition of the ECM:

$$\Sigma = \Xi\Gamma\Xi^{\mathrm{H}} = \underbrace{\sum_{n=1}^{D} \gamma_n \xi_n \xi_n^{\mathrm{H}}}_{\text{large eigenvalues}} + \underbrace{\sum_{n=D+1}^{N} \gamma_n \xi_n \xi_n^{\mathrm{H}}}_{\text{small eigenvalues}} \tag{2.24}$$

where γ_n is the nth eigenvalue and ξ_n is the corresponding eigenvector. The eigenvectors corresponding to the D largest eigenvalues define the dominant subspace. The DMR ABF forms a structured approximation by using the dominant subspace plus an orthogonal noise subspace with equal power in each noise direction, i.e.,

$$\mathbf{S}_{\text{DMR}} = \underbrace{\sum_{n=1}^{D} \lambda_n \mathbf{e}_n \mathbf{e}_n^{\text{H}}}_{\text{large eigenvalues}} + \underbrace{\sum_{n=D+1}^{N} s_w^2 \mathbf{e}_n \mathbf{e}_n^{\text{H}}}_{\text{small eigenvalues}} \tag{2.25}$$

where s_w^2 is the estimated noise power defined as average of the remaining eigenvalues, $s_w^2 = \left(\frac{1}{N-D}\right) \sum_{n=D+1}^{N} \lambda_n$. The advantage of using the estimated noise power when computing $\mathbf{S}_{\text{DMR}}$ is that it eliminates the small eigenvalues, which cause problems with inverting the SCM to compute the MVDR weight vector.

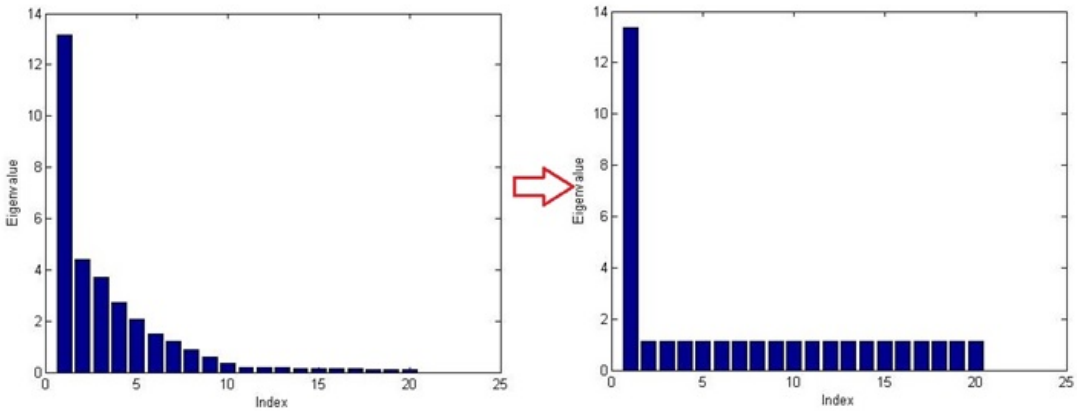

Figure 2.11 Eigenvalues histogram of DMR SCM. LHS is the orignal eigenvalues histogram while RHS is the DMR SCM eigenvalues histogram.

Figure 2.16 shows the beampattern of DMR ABF. The DMR beampattern has a notch near the interferer location. Note that while the ensemble beampattern has a minimum at the interferer angle, the sample beampatterns have minima at slightly

different angles due to the mismatch in the sample statistics. Referring to Figure 2.2 we can also learn that the more the snapshots, the deeper the notch.

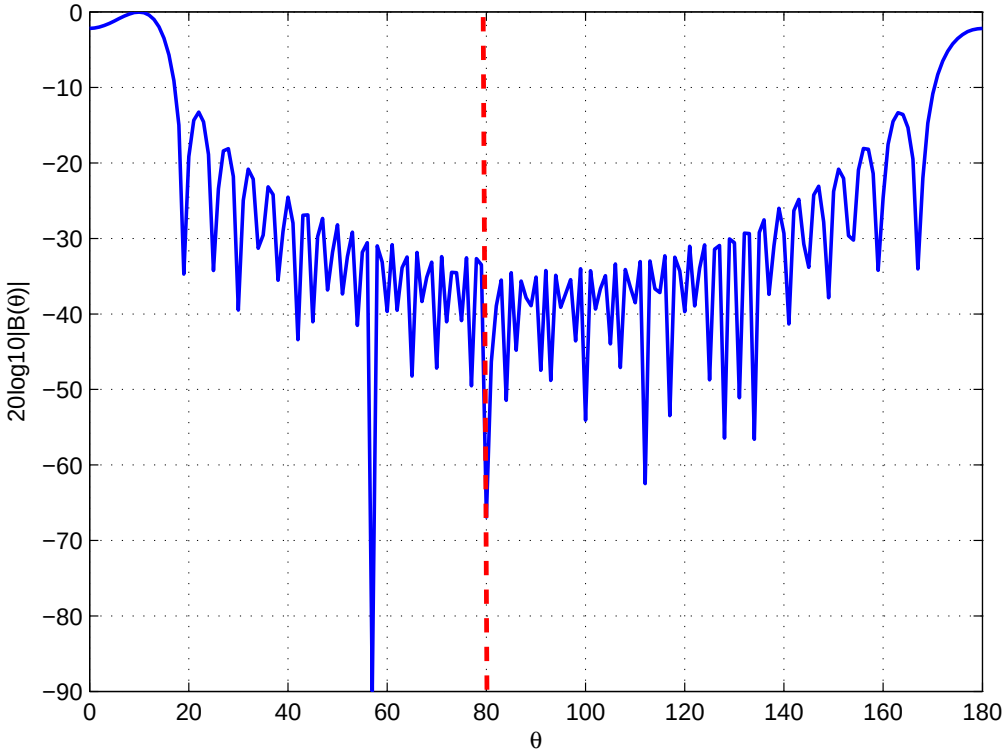

Figure 2.12 Beampattern $|B(\theta)|^2 = \left|\mathbf{w}^{\mathrm{H}}\mathbf{v}(\theta)\right|^2$ (in dB) of DMR ABF for the single-interferer example. The example uses a 50-sensor ULA with half-wave-length spacing. $N = 50$, $L = 25$. $\rho_{INR} = 40dB$, $\sigma_s^2 = 10, \sigma_1^2 = 10000, \sigma_n^2 = 1$. $\theta_s = 10°$, $\theta_1 = 80°$. The red line shows location of the interference.

2.6 Comparison

For the case of insufficient amount of data, all three approaches focus on the rank deficient SCM S. Each of the three approaches has its own advantages and disadvantages.

Dimension reduction uses a random matrix to project the original $N-dim$ space data set into a smaller $d-dim$ subspace data set to make sure the SCM is invertible. These techniques can be classified either as reduced-dimension methods (in this case $\mathbf{\Phi}$

is fixed) or rank-reducing methods where $\mathbf{\Phi}$ depends on the data. Through the display of beampatterns and colormaps, we find the matrix $\mathbf{\Phi}$ constructed from the principal eigenvectors of the ECM and SOI is more helpful for the subsequent simplification steps. We will continue to refer to this technique in subsequent chapters.

The diagonal loading factor can significantly affect the achievable mean squared error (MSE) and must be carefully chosen. Ad hoc choices can result in very conservative performance.

DMR algorithm, applied to low SNR signal circumstance, is a typical eigenspace-based algorithm which has small computational load and fast convergence speed. DMR requires at least two snapshots for the single interferer example since it needs an estimate of the dominant subspace and an estimate of the power in the noise subspace. This is DMR's biggest advantage.

2.7 Simulations

In our simulation, we compare the performance of different approaches through the value of ND. We use a uniform linear array (ULA) of $N = 50$ sensors with half-wavelength spacing. The histograms of $G = -10\log_{10}(G_{notch})$ in dB are shown in Figures 2.15-2.20. The more the histogram is to the right hand side, the deeper the notch, which means the higher the accuracy of the estimation.

2.7.1 Histogram results

Figures 2.13-2.15 present probability density function overlaid on the notch depth histogram(in dB) for the single interference case using random permutation matrix/ Normal distributed matrix/ Bernoulli distributed matrix. The results show the constrained random transformation matrix with the first column is aligned with the SOI have best performance.

Figures 2.16-2.17 show the diagonal loading/DMR SCM results. DMR has a higher speed of convergence with the increase of number of snapshots. It is important to note that the basic idea of DMR is to estimate only the large eigenvalues and corresponding eigenvectors of SCM, and use these eigenvectors to null the strong interference that they represent. The advantage is that less averaging (fewer snapshots) is required. This permits rapid convergence.

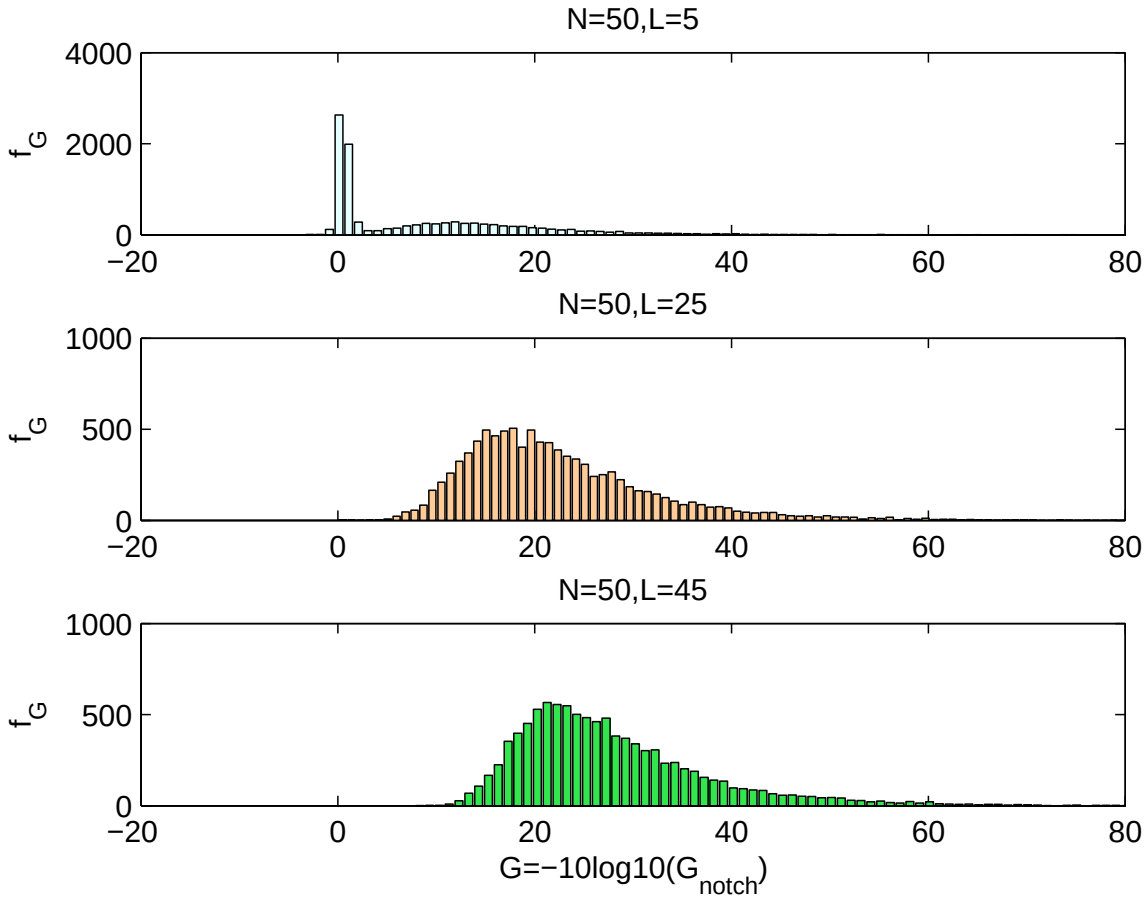

Figure 2.13 Probability density function overlaid on the notch depth histogram(in dB) for the single interference case using random permutation matrix. The example uses a 50-sensor ULA with half-wave-length spacing. $N = 50$, $L = 5/25/45$, $d = 2$, $\rho_{INR} = 10dB$, $\sigma_s^2 = 10, \sigma_1^2 = 10, \sigma_n^2 = 1$. $\theta_s = 10°$, $\theta_1 = 80°$.

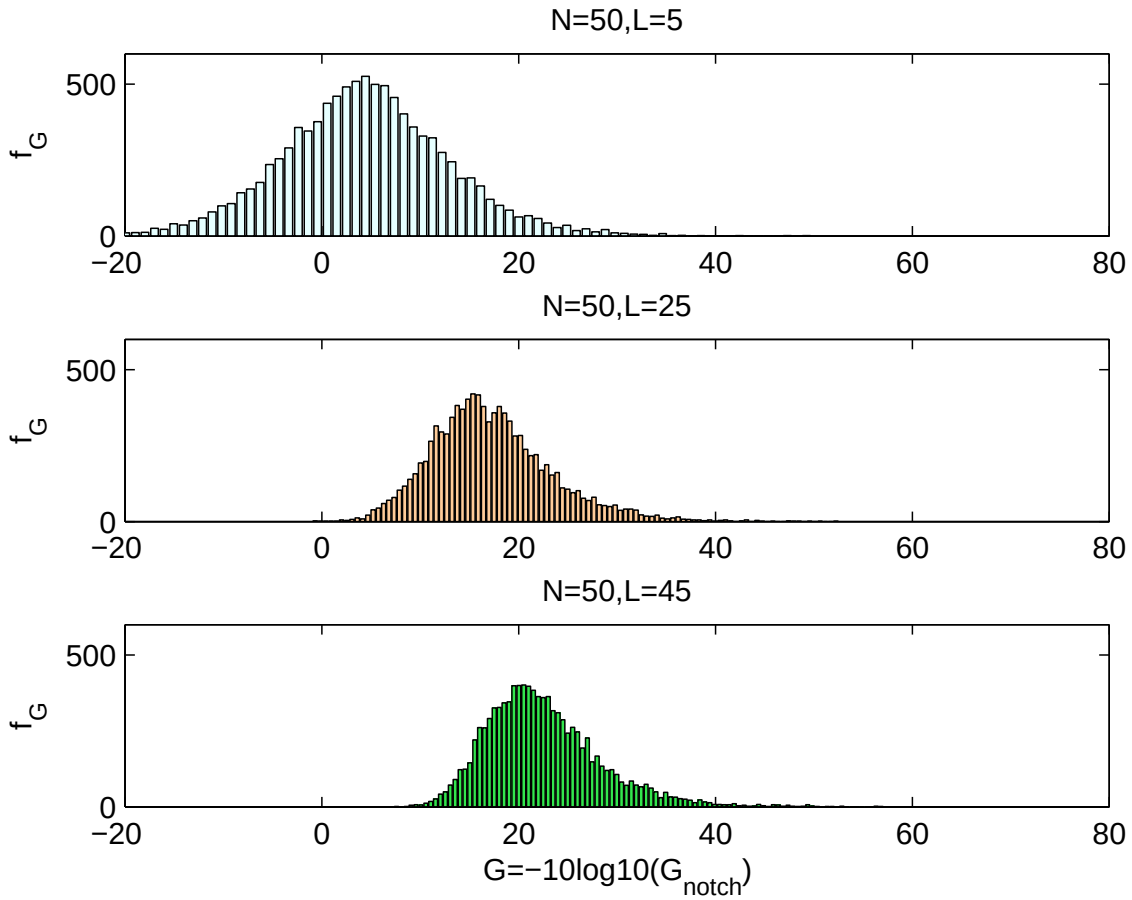

Figure 2.14 Probability density function overlaid on the notch depth histogram(in dB) for the single interference case using a Normal distributed random matrix. The example uses a 50-sensor ULA with half-wave-length spacing. $N = 50$, $L = 5/25/45$, $d = 2$, $\rho_{INR} = 10dB$,$\sigma_s^2 = 10, \sigma_1^2 = 10, \sigma_n^2 = 1$. $\theta_s = 10°$, $\theta_1 = 80°$.

2.7.2 Snapshot performance for the single interferer example

This section characterizes the variability of the DMR WNG, ND and SINR for the single-interferer example using a large set of Monte Carlo trials.

White Noise Gain Statistics Figure 2.18 and Figure 2.19 illustrates how WNG varies with different number of snapshots L and INR for the canonical single-interferer example. The mean ND versus INR plots for these cases are very similar to the

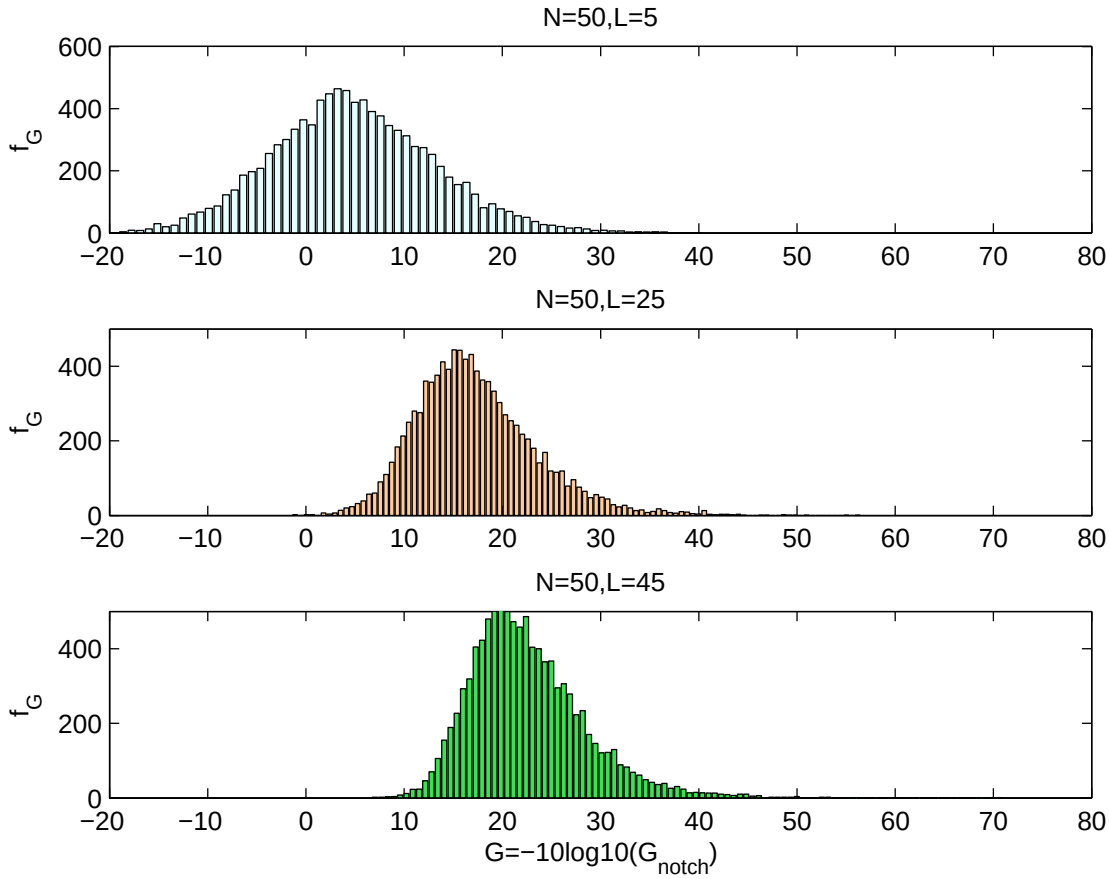

Figure 2.15 Probability density function overlaid on the notch depth histogram(in dB) for the single interference case using a Bernoulli distributed random matrix. The example uses a 50-sensor ULA with half-wave-length spacing. $N = 50$, $L = 5/25/45$, $d = 2$, $\rho_{INR} = 10dB$, $\sigma_s^2 = 10, \sigma_1^2 = 10, \sigma_n^2 = 1$. $\theta_s = 10°$, $\theta_1 = 80°$.

ensemble result. The WNG for small L or low INR is a function of INR or L, while for larger L or high INR, WNG is closer to the optimal value.

Figure 2.18 and Figure 2.19 also illustrate the variability of the WNG. Note that the WNG variability is quite small. Most of the WNG values lie within 0.15 dB of the asymptotic optimal value. For large INRs or L, WNG is concentrated around the asymptotic optimal value.

Notch Depth Statistics Figure 2.20 and Figure 2.21 show how ND varies with different number of snapshots L and INRs. Each curve represents a different number

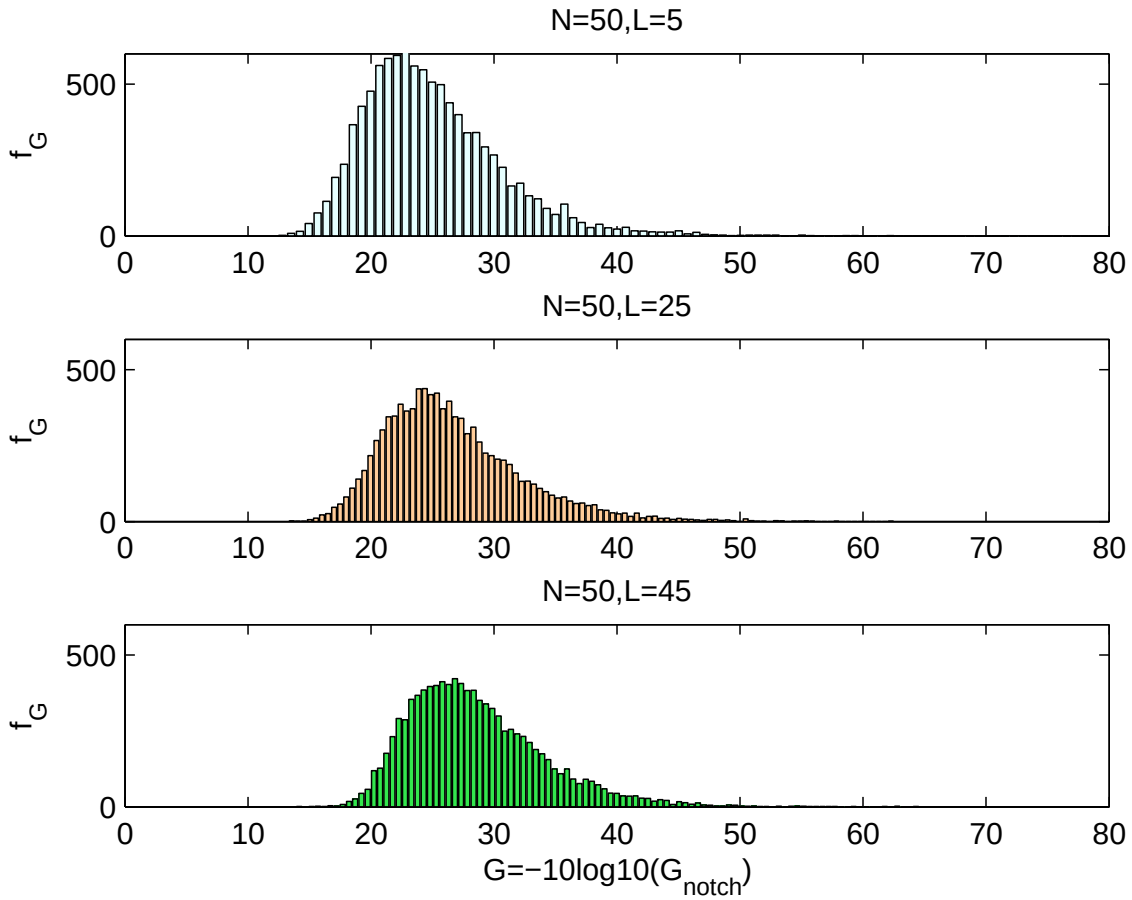

Figure 2.16 Probability density function overlaid on the notch depth histogram(in dB) for the single interference case using diagonal loading with the diagonal loading. The example uses a 50-sensor ULA with half-wave-length spacing. $N = 50$, $L = 5/25/45$, $\rho_{INR} = 10dB$, $\sigma_s^2 = 10, \sigma_1^2 = 10, \sigma_n^2 = 1$. $\theta_s = 10°$, $\theta_1 = 80°$.

of snapshots. The symbols denote the mean ND and the error bars indicate the spread of the distribution between the 10th and 90th percentiles. The error bars are asymmetric around the mean, as expected from the histogramm. Both figures illustrate there is an approximate linear relationship between ND and L and INR in dB.

The error bars in Figure 2.20 and Figure 2.21 indicate the variability of DMR ND around the mean. As the ND decreases, the error bars maintain approximately

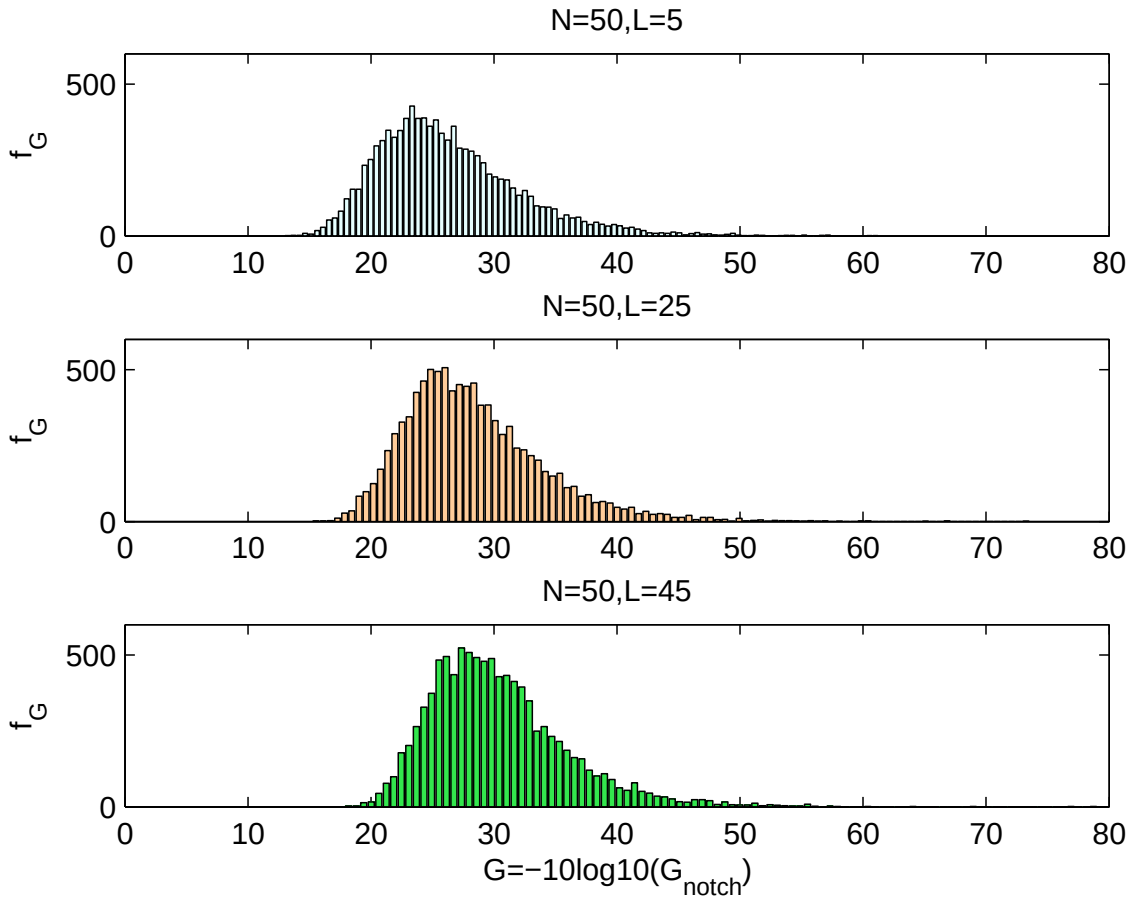

Figure 2.17 Probability density function overlaid on the notch depth histogram(in dB) for the single interference case using DMR SCM. The example uses a 50-sensor ULA with half-wave-length spacing. $N = 50$, $L = 5/25/45$, $\rho_{INR} = 10dB$, $\sigma_s^2 = 10, \sigma_1^2 = 10, \sigma_n^2 = 1$. $\theta_s = 10°$, $\theta_1 = 80°$.

constant spread for INRs above 15 dB. Since a log scale is used in these figures, this implies that the variability decreases with increasing ND.

SINR Statistics Recall that for the single-interferer example, SINR is simply the ratio of the SNR to the sum of the interferer and noise powers.

Figure 2.22 and Figure 2.23 show SINR and WNG have similar variability. Most of the SINR values lie within 0.2 dB of the asymptotic optimal value. For large INRs or L, SINR is concentrated around the asymptotic optimal value.

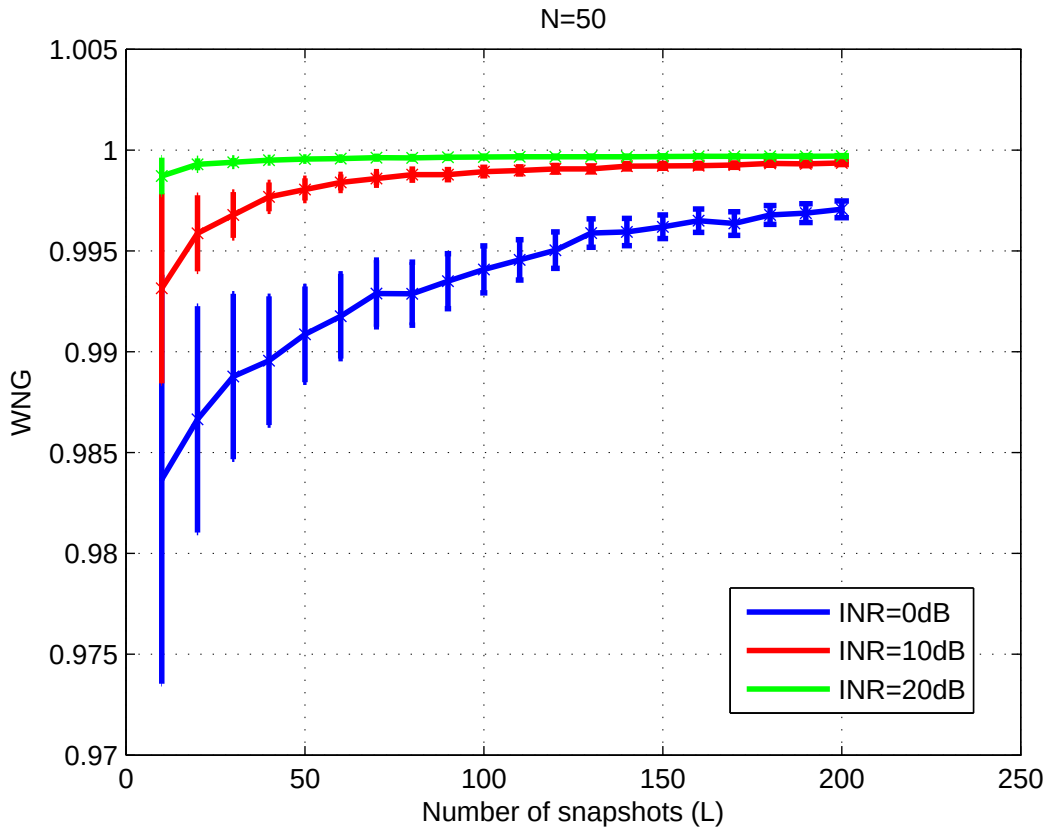

Figure 2.18 Mean DMR WNG as a function of number of snapshots L for the single interference case. The symbols denote the mean WNG and the error bars mark the span between the 10th and 90th percentiles of the data. Results are shown for ABFs generated using INR=0dB, 10dB and 20dB. $N = 50$, $\sigma_s^2 = 10, \sigma_1^2 = 1/10/100, \sigma_n^2 = 1$, $\theta_s = 10°$, $\theta_1 = 80°$.

2.8 How to Design A Proper $\mathbf{\Phi}$

From the previous sections, we can see that there is no one absolutely perfect methos to choose a random projection matrix $\mathbf{\Phi}$. We must choose a proper $\mathbf{\Phi}$ according to the actual problem. In the following, we will discuss how to choose a random projection matrix $\mathbf{\Phi}$ that is appropriate for the problem we are currently studying— DMR ABF.

Since our current interest is DMR ABF, and we will use several different metircs to test their performance, therefore, the expressions of metircs are well worth to look into.

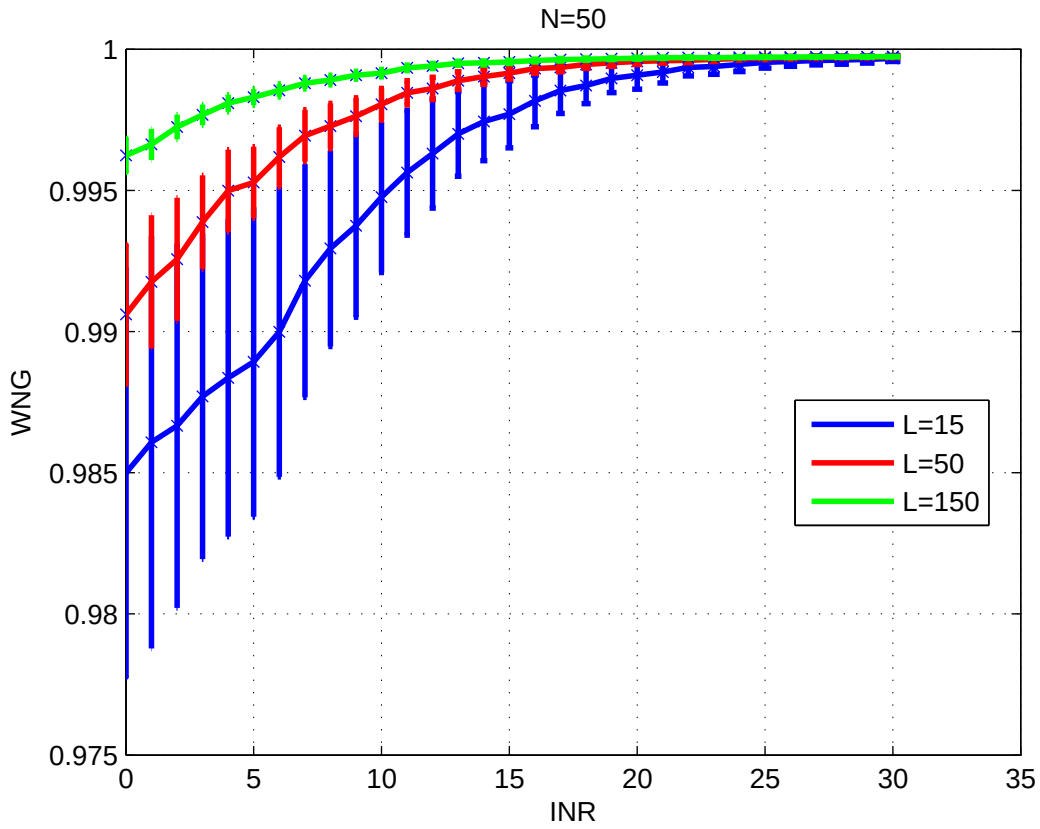

Figure 2.19 Mean DMR WNG as a function of INR for the single interference case. The symbols denote the mean WNG and the error bars mark the span between the 10th and 90th percentiles of the data. Results are shown for ABFs generated using 15, 50, 150 snapshots. $N = 50$, $\sigma_s^2 = 10, \sigma_n^2 = 1, L = 15/50/150$, $\theta_s = 10°$, $\theta_1 = 80°$.

2.8.1 DMR-SCM and the Inverse of DMR-SCM

The $N \times N$ SCM and its eigendecomposition are defined as

$$\mathbf{S} = \frac{1}{L}\sum_{l=1}^{L} \mathbf{p}\left(l\right)\mathbf{p}\left(l\right)^{\mathrm{H}} = \sum_{n=1}^{N} \lambda_n \mathbf{e}_n \mathbf{e}_n^{\mathrm{H}} \tag{2.26}$$

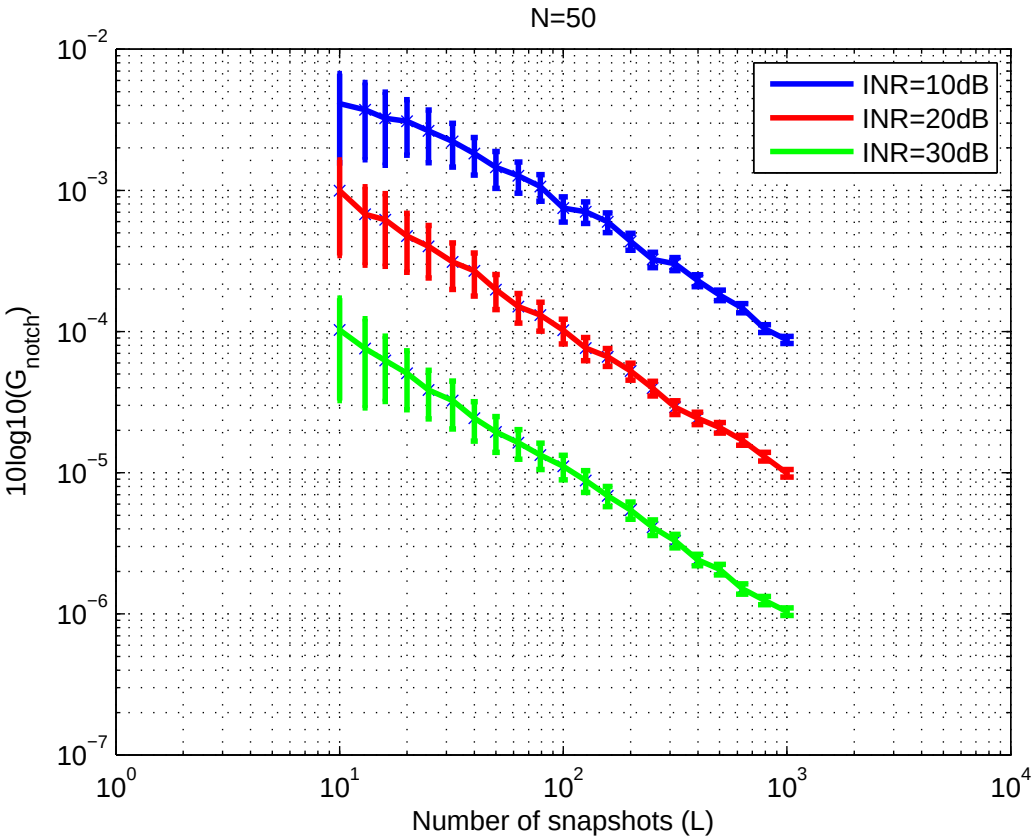

Figure 2.20 Mean DMR ND as a function of number of snapshots L for the single interference case. The symbols denote the mean ND and the error bars mark the span between the 10th and 90th percentiles of the data. Results are shown for ABFs generated using INR=10dB, 20dB and 30dB. $N = 50$, $\sigma_s^2 = 10, \sigma_1^2 = 10/100/1000, \sigma_n^2 = 1$, $\theta_s = 10°$, $\theta_1 = 80°$.

where $\mathbf{e}_i$ and λ_i are the sample eigenvectors and eigenvalues of $\mathbf{S}$, respectively. Thus, the $N \times N$ DMR-SCM is constructed as,

$$\mathbf{S}_{\text{DMR}} = \lambda_i \mathbf{e}_1 \mathbf{e}_1^{\text{H}} + \sum_{i=2}^{N} s_w^2 \mathbf{e}_i \mathbf{e}_i^{\text{H}} \tag{2.27}$$

where $s_w^2 = \left(\frac{1}{N-1}\right) \sum_{i=2}^{N} \lambda_i$ is the average of the scaled lowest eigenvalues.

The spectral decomposition of the $N \times N$ sample covariance matrix can be broken into two parts: one for the D largest eigenvalues and one for the $N - D$

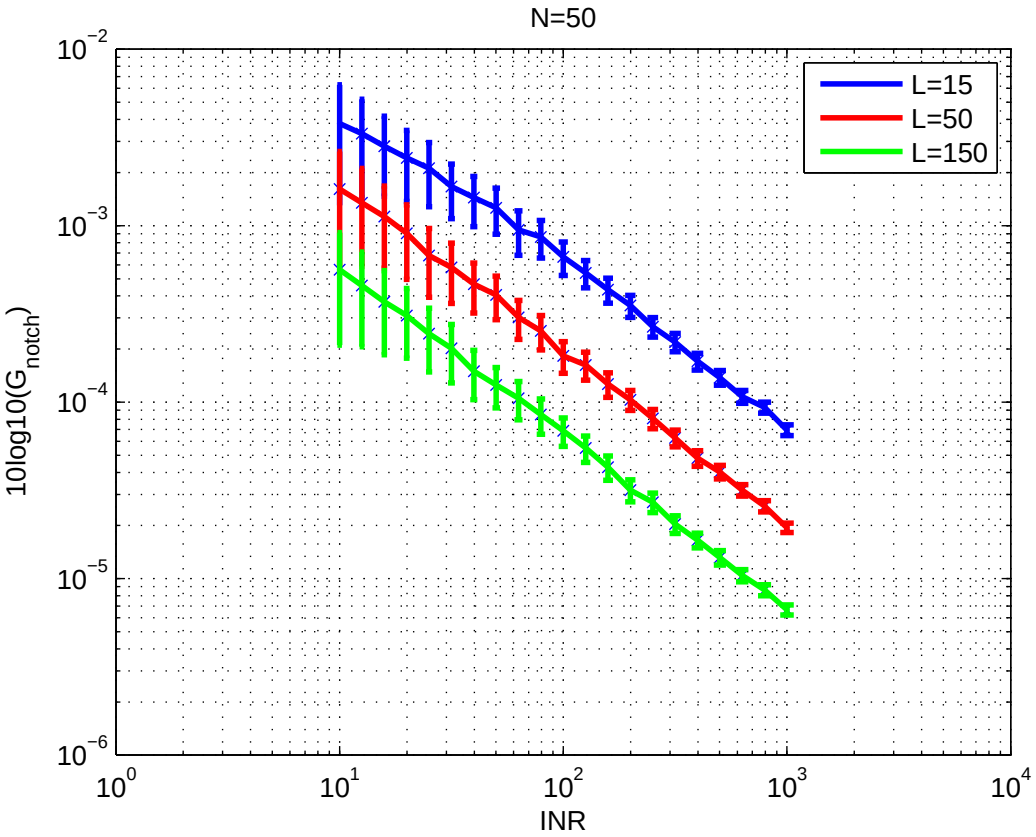

Figure 2.21 Mean DMR ND as a function of INR for the single interference case. The symbols denote the mean ND and the error bars mark the span between the 10th and 90th percentiles of the data. Results are shown for ABFs generated using 15, 50, 150 snapshots. $N = 50$, $\sigma_s^2 = 10, \sigma_n^2 = 1, L = 15/50/150$, $\theta_s = 10°$, $\theta_1 = 80°$.

smaller eigenvalues. Thus the inverse of DMR-SCM is

$$\mathbf{S}_{\text{DMR}}^{-1} = \sum_{i=1}^{D} \lambda_i^{-1} \mathbf{e}_i \mathbf{e}_i^{\text{H}} + \sum_{i=D+1}^{N} s_w^{-2} \mathbf{e}_i \mathbf{e}_i^{\text{H}} = \frac{1}{s_w^2} \left[\mathbf{I} - \sum_{i=1}^{D} \frac{\lambda_i - s_w^2}{\lambda_i} \mathbf{e}_i \mathbf{e}_i^{\text{H}} \right] \tag{2.28}$$

where s_w^2 is the estimated noise power $s_w^2 = \left(\frac{1}{N-D} \right) \sum_{n=D+1}^{N} \lambda_n$.

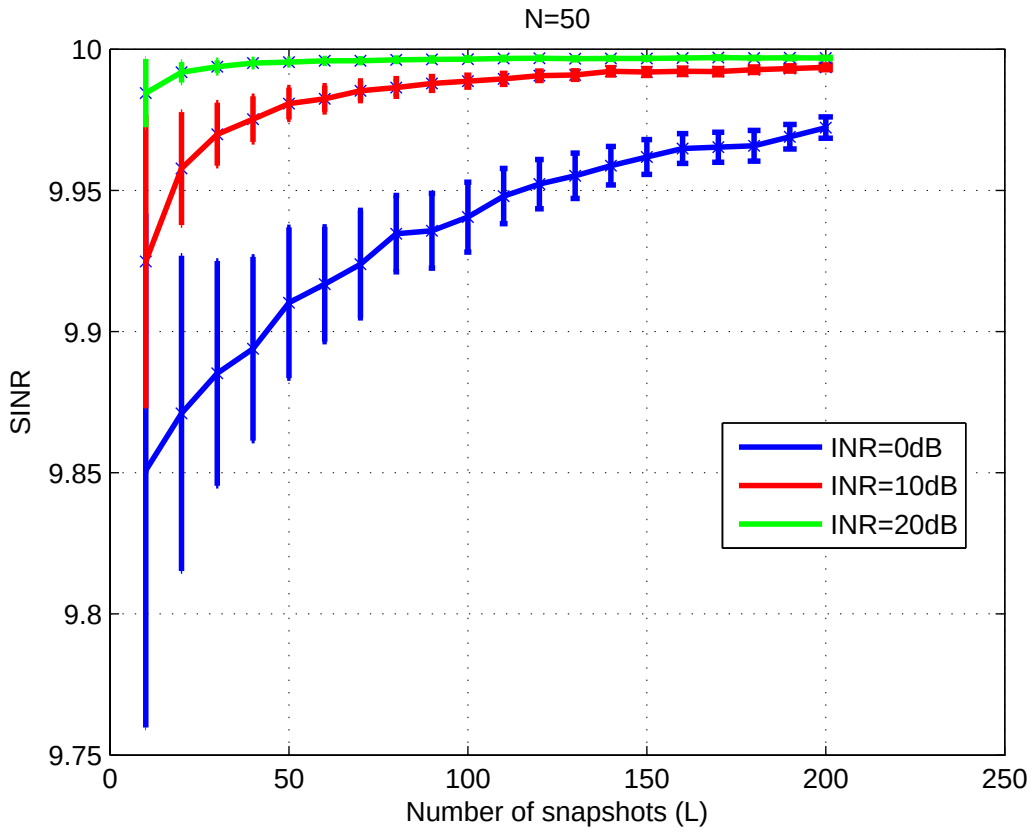

Figure 2.22 Mean DMR SINR as a function of number of snapshots L for the single interference case. The symbols denote the mean SINR and the error bars mark the span between the 10th and 90th percentiles of the data. Results are shown for ABFs generated using INR=0dB, 10dB and 20dB. $N = 50$, $\sigma_s^2 = 10, \sigma_1^2 = 1/10/100, \sigma_n^2 = 1$, $\theta_s = 10°$, $\theta_1 = 80°$.

Let $\mathbf{E_D} = [\mathbf{e_1} \cdots \mathbf{e_D}]$ and $\mathbf{\Lambda} = diag\left(\frac{s_w^2}{\lambda_1}, \cdots, \frac{s_w^2}{\lambda_D}\right)$, the matrix form of DMR SCM can be written as

$$\mathbf{S}_{\text{DMR}}^{-1} = \left(\frac{1}{s_w^2}\right)\left(\mathbf{I} - \mathbf{E_D}\mathbf{E_D^H} + \mathbf{E_D}\mathbf{\Lambda}\mathbf{E_D}^{\mathbf{H}}\right) = \left(\frac{1}{s_w^2}\right)\left(\mathbf{P}_{\mathbf{E_D}}^{\perp} + \mathbf{E_D}\mathbf{\Lambda}\mathbf{E_D}^{\mathbf{H}}\right) \tag{2.29}$$

$$\mathbf{S}_{\text{DMR}}^{-2} = \left(\frac{1}{s_w^2}\right)^2\left(\mathbf{P}_{\mathbf{E_D}}^{\perp} + \mathbf{E_D}\mathbf{\Lambda^2}\mathbf{E_D}^{\mathbf{H}}\right) \tag{2.30}$$

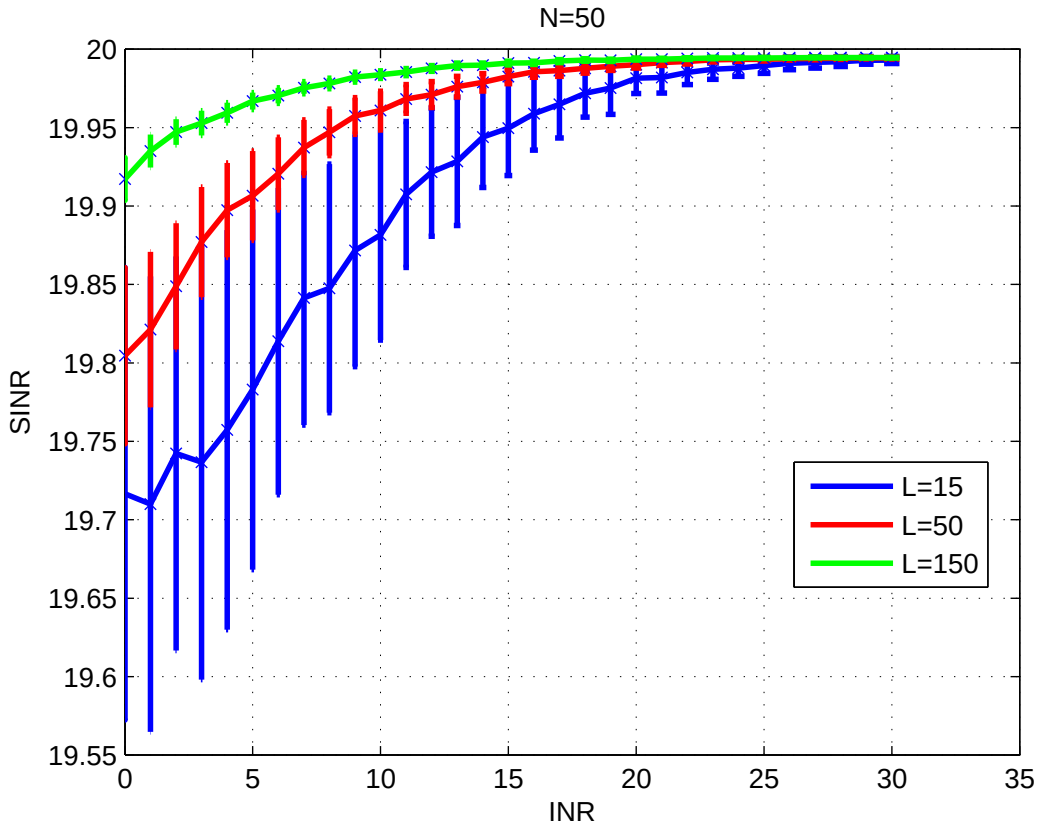

Figure 2.23 Mean DMR SINR as a function of INR for the single interference case. The symbols denote the mean SINR and the error bars mark the span between the 10th and 90th percentiles of the data. Results are shown for ABFs generated using 15, 50, 150 snapshots. $N = 50$, $\sigma_s^2 = 10, \sigma_n^2 = 1, L = 15/50/150$, $\theta_s = 10°$, $\theta_1 = 80°$.

where $\mathbf{P}_{\mathbf{E_D}}^{\perp} = \mathbf{I} - \mathbf{E_D}\mathbf{E_D}^{\mathbf{H}}$.

From the expression of the inverse matrix $\mathbf{S}_{\text{DMR}}^{-1}$, we find that the inverse matrix can be expressed using the first D sampled eigenvalues and sampled eigenvectors, plus esitmated noise power s_w^2. Although the problem we face may be the case of snapshot defient, the special feature of the DMR-SCM can make sure it is full rank, since the DMR-SCM replaces all eigenvalues with small values of its average value (esitmated noise power), so the DMR-SCM is always full rank. The advantage of this is that we don't need to look for a lower dimmention d, or an $N \times d$ matrix, we can directly choose an $N \times N$ matrix as random projection matrix $\mathbf{\Phi}$. To do this, we can start with a matrix of random Gaussian distribution (notice that a random Gaussian

distribution matrix is data independent, while we need a data dependent matrix to improve performance).

So, as the first step we can start with a matrix of random Gaussian distribution:

(1) $\mathbf{\Phi}$ is an unitary matrix, each column is orthogonal with unit-norm.

2.8.2 The dependence of Φ on SOI

We consider a random $N \times N$ matrix $\mathbf{\Phi}$, where $\mathbf{\Phi}^H\mathbf{\Phi} = \mathbf{I_d}$. Note it can preserve the energy of the steering vector, $\left(\mathbf{\Phi}^H\mathbf{v}_s\right)^H\left(\mathbf{\Phi}^H\mathbf{v}_s\right) = \mathbf{v}_s^H\mathbf{v}_s$. The conventional spectral estimate is $\mathbf{v}_s^H\mathbf{S}\mathbf{v_s}$, it is still obtainable from the reduced-dimension snapshots and steering vector,

$$\left(\mathbf{\Phi}^H\mathbf{v}_s\right)^H\left(\mathbf{\Phi}^H\mathbf{S}\mathbf{\Phi}\right)\left(\mathbf{\Phi}^H\mathbf{v}_s\right) = \mathbf{v}_s^H\mathbf{S}\mathbf{v_s}$$

All that matters is the subspace that is spanned by the columns of $\mathbf{\Phi}$ [30]. Without loss of generality we can make the first column of $\mathbf{\Phi}$ equal to the steering vector,

$$\mathbf{\Phi} = [\mathbf{v}_s \;\; \boldsymbol{\phi}_2 \cdots \boldsymbol{\phi}_d] \tag{2.31}$$

Note all the columns of $\mathbf{\Phi}$ are orthogonal with each other. Then we introduce a $N \times N$ Householder unitary matrix $\mathbf{Q}$, which collapses the steering vector into the first entry:

$$\mathbf{Q^H v_s} = [\mathbf{1} \;\; \mathbf{0} \cdots \mathbf{0}]^\mathbf{T} \equiv \mathbf{e_1} \tag{2.32}$$

where $\mathbf{Q} = \mathbf{I_N} - (\mathbf{e_1} - \mathbf{v_s})(\mathbf{e_1} - \mathbf{v_s})^{\mathbf{H}} / (\mathbf{1} - \mathbf{v_s}(\mathbf{1}))^{\mathbf{H}}$, $\mathbf{v}_s(1)$ denotes the first element of $\mathbf{v}_s$. Finally, $\mathbf{\Phi}$ s structured as follows:

$$\mathbf{\Phi} = \mathbf{Q} \begin{bmatrix} 1 & \underline{0}_{d-1}^T \\ \underline{0}_{N-1} & \mathbf{G}\left(\mathbf{G^H G}\right)^{\mathbf{-1/2}} \end{bmatrix} \tag{2.33}$$

where the entries of the $(N-1) \times (N-1)$ random matrix $\mathbf{G}$ are i.i.d. zero-mean complex Gaussian.

The key is to make sure the first column of the transformation matrix is aligned with the SOI vector (which guarantees that the SOI goes through the data transformation), while the other columns are drawn at random in the subspace orthogonal to the SOI vector.

In Equations (2.7)-(2.9), there is a common item: $\mathbf{v}_s^H \mathbf{S^{-1}} \mathbf{v_s}$. It is still obtainable from the reduced-dimension snapshots and steering vector,

$$\mathbf{v}_s^H \mathbf{S^{-1}} \mathbf{v_s} = \left(\mathbf{\Phi^H v_s}\right)^{\mathbf{H}} \left(\mathbf{\Phi^H S^{-1} \Phi}\right) \left(\mathbf{\Phi^H v_s}\right) = \boldsymbol{v}_{\mathbf{s}}^{\mathbf{H}} \left(\mathbf{\Phi^H S^{-1} \Phi}\right) \boldsymbol{v}_{\mathbf{s}}$$

where $\boldsymbol{v}_s = \mathbf{\Phi}^H \mathbf{v}_s$. Due to $|\mathbf{v}_s| = 1$, the projected steering vector becomes $\boldsymbol{v}_s = [1 \;\; 0 \cdots 0]^T$. Figure 2.24 displays the data in vector $\boldsymbol{v}_s = \mathbf{\Phi}^H \mathbf{v}_s$ as an image that uses the full range of colors in the colormap. If we don't include SOI $\mathbf{v}_s$ in the first column of $\mathbf{\Phi}$, then $\mathbf{\Phi} = [\boldsymbol{\phi}_1 \cdots \boldsymbol{\phi}_d]$, this is actually the same as that of the Gaussian distribution case. Figure 2.25 displays the data in vector $\boldsymbol{v}_s = \mathbf{\Phi}^H \mathbf{v}_s$ as an image that uses the full range of colors in the colormap. The colormap shows $\boldsymbol{\nu}_s$ have a non-zero structure. This makes it impossible to simplify expressions of WNG, ND or SINR. In this dissertationon, we propose to use and to adapt this technique in the framework of simplification.

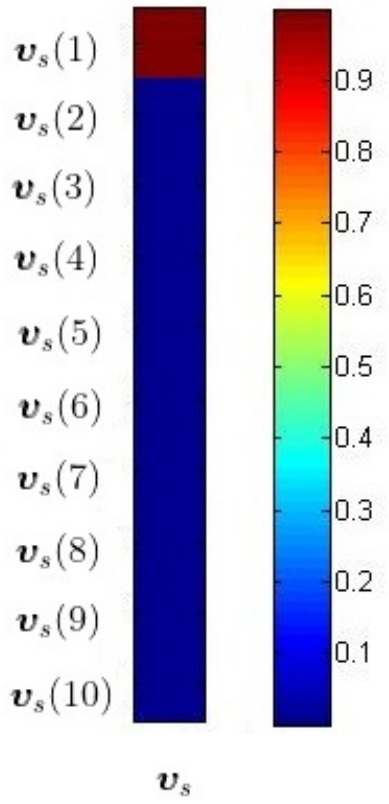

Figure 2.24 The colormap of the 10×1 vector $\boldsymbol{v}_s = \mathbf{\Phi}^H \mathbf{v}_s$ with $\mathbf{\Phi} = [\mathbf{v}_s \;\; \boldsymbol{\phi}_2 \cdots \boldsymbol{\phi}_d]$. RHS is the colorbar.

Therefore, as the second step we can add the SOI into $\mathbf{\Phi}$:

(1) $\mathbf{\Phi}$ is an unitary matrix, each column is orthogonal and norm is one.

(2) Let SOI $\mathbf{v}_s$ be the 1st column of $\mathbf{\Phi}$: $\mathbf{\Phi} = [\mathbf{v}_s \;\; \boldsymbol{\phi}_2 \cdots \boldsymbol{\phi}_d]$.

2.8.3 The dependence of $\mathbf{\Phi}$ on ensemble eigenvectors

Let's return the metric expressions. The DMR WNG is given by

$$G_{WNG} \triangleq \frac{1}{\mathbf{w}_{\mathrm{DMR}}^{\mathrm{H}} \mathbf{w}_{\mathrm{DMR}}} = \frac{\left|\mathbf{v}_s^{\mathbf{H}} \mathbf{S}_{\mathrm{DMR}}^{-1} \mathbf{v}_s\right|^2}{\mathbf{v}_s^{\mathbf{H}} \mathbf{S}_{\mathrm{DMR}}^{-2} \mathbf{v}_s} = \frac{\left|\mathbf{v}_s^{\mathbf{H}} \mathbf{\Phi}\mathbf{\Phi}^H \mathbf{S}_{\mathrm{DMR}}^{-1} \mathbf{\Phi}\mathbf{\Phi}^H \mathbf{v}_s\right|^2}{\mathbf{v}_s^{\mathbf{H}} \mathbf{\Phi}\mathbf{\Phi}^H \mathbf{S}_{\mathrm{DMR}}^{-2} \mathbf{\Phi}\mathbf{\Phi}^H \mathbf{v}_s} \tag{2.34}$$

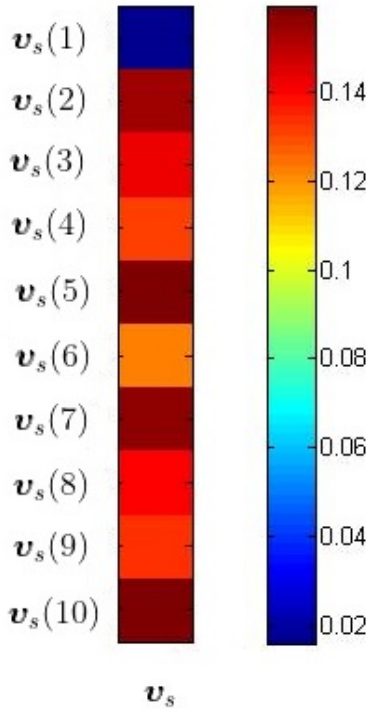

Figure 2.25 The colormap of the 10×1 vector $\boldsymbol{v}_s = \boldsymbol{\Phi}^H \mathbf{v}_s$ with $\boldsymbol{\Phi} = [\boldsymbol{\phi}_1 \;\; \boldsymbol{\phi}_2 \cdots \boldsymbol{\phi}_d]$. RHS is the colorbar.

The DMR ND for the ith interference is given by

$$G_{notch}^{(i)} \triangleq \left|\mathbf{w}_{\mathrm{DMR}}^{\mathrm{H}} \mathbf{v}_i\right|^2 = \frac{\left|\mathbf{v}_s^{\mathbf{H}} \mathbf{S}_{\mathrm{DMR}}^{-1} \mathbf{v}_i\right|^2}{\left|\mathbf{v}_s^{\mathbf{H}} \mathbf{S}_{\mathrm{DMR}}^{-1} \mathbf{v}_s\right|^2} = \frac{\left|\mathbf{v}_s^{\mathbf{H}} \boldsymbol{\Phi}\boldsymbol{\Phi}^H \mathbf{S}_{\mathrm{DMR}}^{-1} \boldsymbol{\Phi}\boldsymbol{\Phi}^H \mathbf{v}_i\right|^2}{\left|\mathbf{v}_s^{\mathbf{H}} \boldsymbol{\Phi}\boldsymbol{\Phi}^H \mathbf{S}_{\mathrm{DMR}}^{-2} \boldsymbol{\Phi}\boldsymbol{\Phi}^H \mathbf{v}_s\right|^2}, \qquad i = 1...D \quad (2.35)$$

Substituting the DMR covariance into the expression, we have

$$\boldsymbol{\Phi}^H \mathbf{S}_{\mathrm{DMR}}^{-1} \boldsymbol{\Phi} = \frac{1}{s_w^2} \boldsymbol{\Phi}^H \left(\mathbf{P}_{\mathbf{E_D}}^{\perp} + \mathbf{E_D} \boldsymbol{\Lambda} \mathbf{E_D}^{\mathbf{H}}\right) \boldsymbol{\Phi} \quad (2.36)$$

$$\boldsymbol{\Phi}^H \mathbf{S}_{\mathrm{DMR}}^{-1} \boldsymbol{\Phi} = \frac{1}{s_w^2} \boldsymbol{\Phi}^H \left(\mathbf{P}_{\mathbf{E_D}}^{\perp} + \mathbf{E_D} \boldsymbol{\Lambda}^{\mathbf{2}} \mathbf{E_D}^{\mathbf{H}}\right) \boldsymbol{\Phi} \quad (2.37)$$

They have a common term: $(D+1)\times(D+1)$ matrices,

$$\mathbf{\Delta}_k = \mathbf{\Phi}^H \mathbf{E_D} \mathbf{\Lambda}^k \mathbf{E_D}^H \mathbf{\Phi}, k = 0, 1, 2 \tag{2.38}$$

where $\mathbf{E_D} = [\mathbf{e_1} \cdots \mathbf{e_D}]$ and $\mathbf{\Lambda} = diag\left(\frac{s_w^2}{\lambda_1}, \cdots, \frac{s_w^2}{\lambda_D}\right)$. As the middle part contains the sample eigenvectors, this raises the idea that we can add the ensemble eigenvectors into the random projection matrix $\mathbf{\Phi}$, so that the following quadratic form can appear: $\boldsymbol{\xi}_i^H \sum_{k=1}^{D} \mathbf{e}_k \mathbf{e}_k^H \boldsymbol{\xi}_j$. These quadratic form values can be estimated from RMT literature.

Adaptive Dimensionality Reduction and Subspace Formulation Technique

In summary, combining the above two techniques, we propose the following adaptive dimensionality reduction and subspace formulation technique.

The eigen-decomposition of ECM is

$$\mathbf{\Sigma}_{I+N} = \sum_{i=1}^{D} \sigma_i^2 \mathbf{v}_i \mathbf{v_i^H} + \sigma_n^2 \mathbf{I} = \mathbf{\Xi \Gamma \Xi}^H \tag{2.39}$$

where $\mathbf{\Gamma} = \text{diag}\,(\gamma_1, \ldots, \gamma_D, \sigma_n^2, \ldots, \sigma_n^2)$ is a diagonal matrix of eigenvalues with descend order such that $\gamma_1 \geq \cdots \gamma_D > \sigma_n^2$. The corresponding eigenvectors are $\mathbf{\Xi} = [\boldsymbol{\xi}_1, \cdots, \boldsymbol{\xi}_N]$.

We will construct an unitary tranformation matrix $\mathbf{\Phi}$. The principle is makes sure the first column of $\mathbf{\Phi}$ is aligned with the SOI, and other D columns equal to the first D ensemble eigenvectors $[\boldsymbol{\xi}_1, \cdots, \boldsymbol{\xi}_D]$.

Let the $N \times N$ unitary tranformation matrix $\mathbf{\Phi}$ be constructed as a complete and orthonormal basis:

$$\mathbf{\Phi} = [\boldsymbol{\phi}_s \;\; \boldsymbol{\xi}_1 \cdots \boldsymbol{\xi}_D \;\; \mathbf{\Phi}_\perp] \tag{2.40}$$

where $\boldsymbol{\phi}_s$ is the array manifold for the desired look direction,

$$\boldsymbol{\phi}_s = \frac{\mathbf{v}_s - \sum_{i=1}^{D} \boldsymbol{\xi}_i \boldsymbol{\xi}_i^H \mathbf{v}_s}{\left| \mathbf{v}_s - \sum_{i=1}^{D} \boldsymbol{\xi}_i \boldsymbol{\xi}_i^H \mathbf{v}_s \right|} \tag{2.41}$$

The advantage of this technique is that it contains all the information in the data sets. Furthermore, we will illustrate this approach in performance analysis of DMR for multiple interferers case in Chapter 5.

So, as the third step we can add the ensemble eigenvectors into $\boldsymbol{\Phi}$. Note that in order to comply with the first step, we have to do some orthogonalization.

(1) $\boldsymbol{\Phi}$ is an unitary matrix, each column is orthogonal and norm is one.

(2) Let the ensemble eigenvectors $[\boldsymbol{\xi}_1 \cdots \boldsymbol{\xi}_D]$ to be the 2nd to $(D+1)$st columns of $\boldsymbol{\Phi}$.

(3) Let $\boldsymbol{\phi}_s = \frac{\mathbf{v}_s - \sum_{i=1}^{D} \boldsymbol{\xi}_i \boldsymbol{\xi}_i^H \mathbf{v}_s}{\left| \mathbf{v}_s - \sum_{i=1}^{D} \boldsymbol{\xi}_i \boldsymbol{\xi}_i^H \mathbf{v}_s \right|}$ the array manifold for the desired look direction to be the 1st column of $\boldsymbol{\Phi}$.

(4) Make sure the remaining columns are orthogonal to each other.

Therefore, the $N \times N$ unitary tranformation matrix $\boldsymbol{\Phi}$ is constructed as a complete and orthonormal basis:

$$\boldsymbol{\Phi} = [\boldsymbol{\phi}_s \;\; \boldsymbol{\xi}_1 \cdots \boldsymbol{\xi}_D \;\; \boldsymbol{\Phi}_\perp] \tag{2.42}$$

where $\boldsymbol{\phi}_s$ is the array manifold for the desired look direction,

$$\boldsymbol{\phi}_s = \frac{\mathbf{v}_s - \sum_{i=1}^{D} \boldsymbol{\xi}_i \boldsymbol{\xi}_i^H \mathbf{v}_s}{\left| \mathbf{v}_s - \sum_{i=1}^{D} \boldsymbol{\xi}_i \boldsymbol{\xi}_i^H \mathbf{v}_s \right|} \tag{2.43}$$

2.9 Summary and Conclusion

In this chapter, we investigate the way to deal with the estimation of a covariance matrix from an insufficient amount of data. We present three approaches: dimension reduction, DL, and DMR. Among the dimension reduction methods, we find the adaptive dimensionality reduction and subspace formulation technique can lead to a significant improvement for our further simplification steps. Furthermore, we use simulations of histograms of WND, ND and SINR to show the underlying performance. The results show DMR have a good performance compare with other approaches. Finally, histogram results are explained and connected to system parameters such as number of snapshots L, INR and interference's spatial distribution (DoA). The results show that there are some relationships between these metics and the system parameters. In the next chapters, we will try to find the mathematical analytical expression for these relation functions.

CHAPTER 3

DISTRIBUTION OF SINR LOSS OF THE DMR ABF

In this chapter, a closed-form derivation of the PDF for the SINR loss ratio of the DMR ABF is proposed. Maximum likelihood estimation (MLE) is used to estimate the parameters of distribution function.

3.1 Background

The narrowband planewave beamforming assumes that the lth snapshot of data measured by an ULA consist of a SOI component, a single interference, and noise, which can be represented as

$$\mathbf{p}(l) = b_s(l)\,\mathbf{v}_s + b_1(l)\,\mathbf{v}_1 + \mathbf{n}(l) \tag{3.1}$$

where b_s is the random amplitude of the signal vector $\mathbf{v}_s$ with the power σ_s^2, b_1 is the random amplitude of the planewave interference $\mathbf{v}_1$ with the power σ_1^2, $\mathbf{n}$ is a vector of complex noise samples with the power σ_n^2.

For the N element sensor array oriented along l-axis, the received signal vector and the complex exponential vector for ith planewave interference can be represented as

$$\mathbf{v}_s = \mathbf{v}(\theta_s) = \frac{1}{\sqrt{N}}\begin{bmatrix} e^{j\frac{2\pi}{\lambda}\cos(\theta_s)l_1} \\ \vdots \\ e^{j\frac{2\pi}{\lambda}\cos(\theta_s)l_N} \end{bmatrix}, \mathbf{v}_i = \mathbf{v}(\theta_i) = \frac{1}{\sqrt{N}}\begin{bmatrix} e^{j\frac{2\pi}{\lambda}\cos(\theta_i)l_1} \\ \vdots \\ e^{j\frac{2\pi}{\lambda}\cos(\theta_i)l_N} \end{bmatrix}$$

where λ is the wavelength, θ_s is the direction of the SOI, θ_i is the direction of the i-th interferer, and l_i is the location of the ith sensor. Without loss of generality, this

dissertation assumes that the amplitudes b_s and b_i are zero-mean complex circular random variables and that the complex circular random noise is zero mean and spatially white. The ECM under H_0 is represented as

$$\mathbf{\Sigma}_{I+N} = \sigma_1^2 \mathbf{v}_1 \mathbf{v}_1^{\mathbf{H}} + \sigma_n^2 \mathbf{I}_N.$$

Let us define the eigendecomposition of the SCM as

$$\mathbf{S} = \frac{1}{L} \sum_{l=1}^{L} \mathbf{p}\left(l\right) \mathbf{p}^{\mathrm{H}}\left(l\right) = \sum_{n=1}^{N} \lambda_n \mathbf{e}_n \mathbf{e}_n^{\mathrm{H}} \tag{3.2}$$

where $\mathbf{e}_i$ and λ_i are the sample eigenvectors and eigenvalues of $\mathbf{S}$, respectively. Thus, the $N \times N$ DMR-SCM is constructed as,

$$\mathbf{S}_{\mathrm{DMR}} = \lambda_i \mathbf{e}_1 \mathbf{e}_1^{\mathrm{H}} + \sum_{i=2}^{N} s_w^2 \mathbf{e}_i \mathbf{e}_i^{\mathrm{H}} \tag{3.3}$$

where $s_w^2 = \left(\frac{1}{N-1}\right) \sum_{i=2}^{N} \lambda_i$ is the average of the scaled lowest eigenvalues.

The DMR ABF weight vector has a similar form as the adaptive MVDR weight vector, expect the SCM being replaced by $\mathbf{S}_{\mathrm{DMR}}$:

$$\mathbf{w}_{\mathrm{DMR}} = \left(\mathbf{v}_s^{\mathrm{H}} \mathbf{S}_{\mathrm{DMR}}^{-1} \mathbf{v}_s\right)^{-1} \mathbf{S}_{\mathrm{DMR}}^{-1} \mathbf{v}_s. \tag{3.4}$$

The SINR of a DMR ABF is defined as

$$\mathrm{SINR} \triangleq \frac{\sigma_s^2 \left|\mathbf{w}_{\mathrm{DMR}}^{\mathrm{H}} \mathbf{v}_s\right|^2}{\mathbf{w}_{\mathrm{DMR}}^{\mathrm{H}} \mathbf{\Sigma}_{\mathrm{I+N}} \mathbf{w}_{\mathrm{DMR}}} \tag{3.5}$$

The metric of interest is the SINR loss, which is defined as the ratio of the SINR obtained using sample statistics to the SINR obtained with ensemble statistics. That is,

$$\rho_{DMR} \triangleq \frac{SINR}{SINR(\mathbf{w}_{ens})} = \frac{\sigma_s^2}{SINR(\mathbf{w}_{ens})} \frac{\left|\mathbf{v}_s^{\mathbf{H}} \mathbf{S}_{\mathrm{DMR}}^{-1} \mathbf{v}_s\right|^2}{\mathbf{v}_s^{\mathbf{H}} \mathbf{S}_{\mathrm{DMR}}^{-1} \boldsymbol{\Sigma}_{I+N} \mathbf{S}_{\mathrm{DMR}}^{-1} \mathbf{v}_s} \tag{3.6}$$

3.2 SINR Loss Using Sample Covariance Matrix

To derive the SINR loss, we focus on an illustrative example of a single planewave interference present in spatially white noise. The following theorem which stated by Capon and Goodman [7] is used in the process.

Theorem: If $N \times N$ matrix $\mathbf{A}$ is complex wishart distributed, i.e. $\mathbf{A} \sim CW\left(L, N; \mathbf{M}\right)$, with parameters L, N and covariance matrix $\mathbf{M}$, and $\mathbf{B}$ is a nonsingular $N \times N$ matrix, then $\mathbf{BAB^H}$ is $CW\left(L, N; \mathbf{CMC^H}\right)$.

For a single interference under signal absent case, the expression for the ECM simplifies to $\boldsymbol{\Sigma}_{I+N} = \sigma_1^2 \mathbf{v}_1 \mathbf{v}_1^{\mathbf{H}} + \sigma_n^2 \mathbf{I}_N$, which means $\mathbf{S} \sim CW\left(L, N; \boldsymbol{\Sigma}_{I+N}\right)$. As the ensemble result is $SINR(\mathbf{w}_{ens}) = \sigma_s^2 \mathbf{v}_s^{\mathbf{H}} \boldsymbol{\Sigma}_{I+N}^{-1} \mathbf{v}_s$, we have the p.d.f

$$\begin{aligned} \rho_{SCM} &= \frac{\sigma_s^2}{SINR(\mathbf{w}_{ens})} \left(\frac{\mathbf{v}_s^{\mathbf{H}} \mathbf{S}^{-1}}{\mathbf{v}_s^{\mathbf{H}} \mathbf{S}^{-1} \mathbf{v}_s} \boldsymbol{\Sigma}_{I+N} \frac{\mathbf{S}^{-1} \mathbf{v}_s}{\mathbf{v}_s^{\mathbf{H}} \mathbf{S}^{-1} \mathbf{v}_s} \right)^{-1} \\ &= \frac{\left|\mathbf{v}_s^{\mathbf{H}} \mathbf{S}^{-1} \mathbf{v}_s\right|^2}{\left(\mathbf{v}_s^{\mathbf{H}} \boldsymbol{\Sigma}_{I+N}^{-1} \mathbf{v}_s\right) \left(\mathbf{v}_s^{\mathbf{H}} \mathbf{S}^{-1} \boldsymbol{\Sigma}_{I+N} \mathbf{S}^{-1} \mathbf{v}_s\right)} \end{aligned} .$$

It has been found [7] ρ_{SCM} is likewise a beta function distribution, so

$$f_{\rho_{SCM}}\left(\rho\right) = \frac{L!}{\left[(N-2)!\left(L+1-N\right)!\right]} \cdot \left(1-\rho\right)^{N-2} \left(\rho\right)^{L+1-N}$$

3.3 SINR Loss Using Dominant Mode Rejection

The expression for the ECM is $\mathbf{\Sigma}_{I+N} = \sigma_1^2 \mathbf{v}_1 \mathbf{v}_1^{\mathbf{H}} + \sigma_n^2 \mathbf{I}_N$. The maximum eigenvalue of the covariance matrix is $\lambda_1 = \sigma_1^2 + \sigma_n^2$, and the rest of the eigenvalues are $\lambda_{n\neq 1} = \sigma_n^2$. The eigenvector associated with the maximum eigenvalue is $\mathbf{v}_1$. We then have $\mathbf{S}_{\text{DMR}} = \lambda_1 \mathbf{e}_1 \mathbf{e}_1^{\text{H}} + \sum_{n=2}^{N} s_w^2 \mathbf{e}_n \mathbf{e}_n^{\text{H}}$ and

$$\begin{aligned} \mathbf{S}_{\text{DMR}}^{-1} &= \lambda_1^{-1} \mathbf{e}_1 \mathbf{e}_1^{\text{H}} + \sum_{n=2}^{N} \left(s_w\right)^{-1} \mathbf{e}_n \mathbf{e}_n^{\text{H}} \\ &= \left(s_w^2\right)^{-1} \left[\mathbf{I}_N - \left(1 - \frac{s_w^2}{\lambda_1}\right) \mathbf{e}_1 \mathbf{e}_1^{\text{H}} \right] \end{aligned} \tag{3.7}$$

(3.6) can be written as,

$$\frac{\sigma_s^2}{\rho_{DMR} SINR(\mathbf{w}_{ens})} = \frac{\mathbf{v}_s^{\mathbf{H}} \mathbf{S}_{\text{DMR}}^{-1} \mathbf{\Sigma}_{I+N} \mathbf{S}_{\text{DMR}}^{-1} \mathbf{v}_s}{\left| \mathbf{v}_s^{\mathbf{H}} \mathbf{S}_{\text{DMR}}^{-1} \mathbf{v}_s \right|^2} \tag{3.8}$$

We decompose the right-hand side into,

$$\begin{aligned} &\frac{\mathbf{v}_s^{\mathbf{H}} \mathbf{S}_{\text{DMR}}^{-1} \mathbf{\Sigma}_{I+N} \mathbf{S}_{\text{DMR}}^{-1} \mathbf{v}_s}{\left| \mathbf{v}_s^{\mathbf{H}} \mathbf{S}_{\text{DMR}}^{-1} \mathbf{v}_s \right|^2} \\ &= \frac{\mathbf{v}_s^{\mathbf{H}} \mathbf{S}_{\text{DMR}}^{-1} \left(\sigma_1^2 \mathbf{v}_1 \mathbf{v}_1^{\mathbf{H}} + \sigma_n^2 \mathbf{I}_N \right) \mathbf{S}_{\text{DMR}}^{-1} \mathbf{v}_s}{\left| \mathbf{v}_s^{\mathbf{H}} \mathbf{S}_{\text{DMR}}^{-1} \mathbf{v}_s \right|^2} \\ &= \sigma_1^2 \frac{\left| \mathbf{v}_s^{\mathbf{H}} \mathbf{S}_{\text{DMR}}^{-1} \mathbf{v}_1 \right|^2}{\left| \mathbf{v}_s^{\mathbf{H}} \mathbf{S}_{\text{DMR}}^{-1} \mathbf{v}_s \right|^2} + \sigma_n^2 \frac{\mathbf{v}_s^{\mathbf{H}} \mathbf{S}_{\text{DMR}}^{-1} \mathbf{S}_{\text{DMR}}^{-1} \mathbf{v}_s}{\left| \mathbf{v}_s^{\mathbf{H}} \mathbf{S}_{\text{DMR}}^{-1} \mathbf{v}_s \right|^2} \\ &= \sigma_1^2 \cdot G_{notch} + \sigma_n^2 \cdot \frac{1}{G_{WNG}} \end{aligned} \tag{3.9}$$

Here $G_{notch} = \left| \mathbf{v}_s^{\mathbf{H}} \mathbf{S}_{\text{DMR}}^{-1} \mathbf{v}_1 \right|^2 / \left| \mathbf{v}_s^{\mathbf{H}} \mathbf{S}_{\text{DMR}}^{-1} \mathbf{v}_s \right|^2 = \left| \mathbf{w}_{DMR}^{\mathbf{H}} \mathbf{v}_1 \right|^2$ is the ND, which can be represented as the absolute value squared of the beampattern in the direction of the interference; $G_{WNG} = \left| \mathbf{v}_s^{\mathbf{H}} \mathbf{S}_{\text{DMR}}^{-1} \mathbf{v}_s \right|^2 / \mathbf{v}_s^{\mathbf{H}} \mathbf{S}_{\text{DMR}}^{-1} \mathbf{S}_{\text{DMR}}^{-1} \mathbf{v}_s = 1 / \mathbf{w}_{DMR}^{\mathbf{H}} \mathbf{w}_{DMR}$ is

the WNG, which can be represented as the improvement in SNR provided by the beamformer when the noise is spatially white.

3.3.1 Simplification under high INR

Since the emsemble result of s_w^2/λ_1 is $\sigma_n^2/\left(\sigma_1^2+\sigma_n^2\right) = 1/\left(\rho_{INR}+1\right)$, it is a small number under high INR. Equation (3.1) can be rewritten as,

$$\mathbf{S}_{\mathrm{DMR}}^{-1} \approx \left(s_w^2\right)^{-1}\left[\mathbf{I}_N - \mathbf{e}_1\mathbf{e}_1^{\mathrm{H}}\right] = \left(s_w^2\right)^{-1}\mathbf{P}_{\mathbf{e}_1}^{\perp} \tag{3.10}$$

where $\mathbf{P}_{\mathbf{e}_1}^{\perp} = \mathbf{I}_N - \mathbf{e}_1\mathbf{e}_1^{\mathrm{H}}$ is the projection matrix.

In [38], white noise gain statistics indicate that it will have very low variability under high INR, and concentrated to the value of $\|\mathbf{v}_s\|^2$, that is $G_{WNG} \approx 1$. Then,

$$\frac{\mathbf{v}_s^{\mathbf{H}}\mathbf{S}_{\mathrm{DMR}}^{-1}\mathbf{S}_{\mathrm{DMR}}^{-1}\mathbf{v}_s}{\left|\mathbf{v}_s^{\mathbf{H}}\mathbf{S}_{\mathrm{DMR}}^{-1}\mathbf{v}_s\right|^2} = \frac{1}{\mathbf{v}_s^{\mathbf{H}}\mathbf{P}_{\mathbf{e}_1}^{\perp}\mathbf{v}_s} = 1$$

so $\left|\mathbf{v}_s^{\mathbf{H}}\mathbf{S}_{\mathrm{DMR}}^{-1}\mathbf{v}_s\right| = 1$.

3.3.2 Approximating principal eigenvector

We can use the power iteration method to estimate the principal eigenvector of the sample covariance matrix. Make an initial guess for the eigenvector, $\mathbf{e}_0 = [1\cdots 1]^T$, and normalize it by assigning $\mathbf{e}_0 = \dfrac{\mathbf{e}_0}{\|\mathbf{e}_0\|}$. Compute $\hat{\mathbf{e}}_1 = \mathbf{S}\cdot\mathbf{e_0}$, and then normalize $\hat{\mathbf{e}}_1$. Repeat this process until satisfying a convergence criterion.

$$\mathbf{e}_1 = \frac{\mathbf{S}\mathbf{v_1}}{\|\mathbf{S}\mathbf{v_1}\|} \tag{3.11}$$

For the low rank case, which means limited number of snapshots, it will have enough accuracy to estimate the principal eigenvector.

3.3.3 Whitening the sample covariance matrix

Let $\mathbf{U} = [\mathbf{u}_1, \mathbf{u}_2, ..., \mathbf{u}_N]$ be an unitary matrix [30], such that $\mathbf{u}_i = \mathbf{U}\boldsymbol{\delta}_i$, where $\boldsymbol{\delta}_i = [0, \cdots, 1, \cdots, 0]^T$. Set $\mathbf{u}_1 = \boldsymbol{\Sigma}_{I+N}^{1/2}\mathbf{v}_1$, $\mathbf{u}_s = \boldsymbol{\Sigma}_{I+N}^{1/2}\mathbf{v}_s = \sum_{i=1}^{N}\alpha_i\mathbf{u}_i$, $\gamma = \|\mathbf{S}\mathbf{v_1}\|$.

Replacing the DMR covariance matrix with the projection matrix $\mathbf{P}_{\mathbf{e}_1}^{\perp}$:

$$\begin{aligned}
&\mathbf{v}_s^{\mathbf{H}}\mathbf{S}_{\mathrm{DMR}}^{-1}\mathbf{v}_1 = \mathbf{v}_s^{\mathbf{H}}\mathbf{P}_{\mathbf{e}_1}^{\perp}\mathbf{v}_1 = \mathbf{v}_s^{\mathbf{H}}\mathbf{v}_1 - \frac{1}{\gamma^2}\mathbf{v}_s^{\mathbf{H}}\mathbf{S}\mathbf{v}_1\mathbf{v}_1^{\mathrm{H}}\mathbf{S}\mathbf{v}_1 \\
&= \mathbf{u}_s^{\mathbf{H}}\boldsymbol{\Sigma}_{I+N}^{-1}\mathbf{u}_1 - \frac{1}{\gamma^2}\mathbf{u}_s^{\mathbf{H}}\boldsymbol{\Sigma}_{I+N}^{-1/2}\mathbf{S}\boldsymbol{\Sigma}_{I+N}^{-1/2}\mathbf{u}_1\mathbf{u}_1^{\mathrm{H}}\boldsymbol{\Sigma}_{I+N}^{-1/2}\mathbf{S}\boldsymbol{\Sigma}_{I+N}^{-1/2}\mathbf{u}_1 \\
&= \mathbf{u}_s^{\mathbf{H}}\boldsymbol{\Sigma}_{I+N}^{-1}\mathbf{u}_1 - \frac{1}{\gamma^2}\mathbf{u}_s^{\mathbf{H}}\mathbf{S}_0\mathbf{u}_1\mathbf{u}_1^{\mathrm{H}}\mathbf{S}_0\mathbf{u}_1 \\
&= \mathbf{u}_s^{\mathbf{H}}\boldsymbol{\Sigma}_{I+N}^{-1}\mathbf{u}_1 - \frac{1}{\gamma^2}\sum_{i=1}^{N}\alpha_i\mathbf{u}_i^{\mathbf{H}}\mathbf{S}_0\mathbf{u}_1\mathbf{u}_1^{\mathrm{H}}\mathbf{S}_0\mathbf{u}_1
\end{aligned}$$

where $\mathbf{S}_0 = \boldsymbol{\Sigma}_{I+N}^{-1/2}\mathbf{S}\boldsymbol{\Sigma}_{I+N}^{-1/2}$ follows a $CW(L, N; \mathbf{I}_N)$ wishart distribution.

Let us define $k = \mathbf{u}_s^{\mathbf{H}}\boldsymbol{\Sigma}_{I+N}^{-1}\mathbf{u}_1$, $c_{i1} = \mathbf{u}_i^{\mathbf{H}}\mathbf{S}_0\mathbf{u}_1 = \boldsymbol{\delta}_i^{\mathbf{H}}\mathbf{U}^{\mathbf{H}}\mathbf{S}_0\mathbf{U}\boldsymbol{\delta}_1 = \boldsymbol{\delta}_i^{\mathbf{H}}\mathbf{C}\boldsymbol{\delta}_1$, where $\mathbf{C} = \mathbf{U}^{\mathbf{H}}\mathbf{S}_0\mathbf{U}$ still follows a $CW(L, N; \mathbf{I}_N)$ complex wishart distribution, we have

$$\left|\mathbf{v}_s^{\mathbf{H}}\mathbf{S}_{\mathrm{DMR}}^{-1}\mathbf{v}_1\right|^2 = \left|\sum_{i=1}^{N}\frac{\alpha_i}{\gamma^2}c_{11}c_{i1} - k\right|^2. \tag{3.12}$$

Here c_{i1} is the element of ith row, first column of $\mathbf{C}$. As the off-diagnol elements $c_{21}, \cdots, c_{N1}$ have the same distribution, we can rewrite (3.12) as

$$\left|\mathbf{v}_s^{\mathbf{H}}\mathbf{S}_{\mathrm{DMR}}^{-1}\mathbf{v}_1\right|^2 = \left|\beta_1 c_{11}^2 + \beta_2 c_{11}c_{21} - k\right|^2 \tag{3.13}$$

where $\beta_1 = \alpha_1/\gamma^2$, $\beta_2 = \sum_{i=2}^{N} \alpha_i/\gamma^2$.

3.3.4 Finding the distribution function

Let's parition matrix $\mathbf{C} = \mathbf{U^H S}_0\mathbf{U}$ into:

$$\mathbf{C} = \begin{pmatrix} c_{11} & \mathbf{c}_{12} \\ \mathbf{c}_{21} & \mathbf{C}_{22} \end{pmatrix}$$

Since the off-diagonal element $c_{21}, ..., c_{2N}$ have the same distribution, we have

$$\left|\mathbf{v}_s^{\mathbf{H}}\mathbf{S}_{\mathrm{DMR}}^{-1}\mathbf{v}_1\right|^2 = \frac{1}{N-1}\left|\left(\beta_1 \cdot \mathbf{1} + \beta_2 c_{11}^{-1}\mathbf{c}_{21}\right) c_{11}^2 - k \cdot \mathbf{1}\right|^2 \tag{3.14}$$

The p.d.f of $\mathbf{e}_{21} = c_{11}^{-1}\mathbf{c}_{21}$ is

$$f\left(\mathbf{e}_{12}\right) = \frac{\Gamma\left(L+1\right)}{\Gamma\left(L-N+2\right)\Gamma\left(N-1\right)} \frac{1}{\left|1+\mathbf{e}_{12}^H\mathbf{e}_{12}\right|^{L+1}}. \tag{3.15}$$

An outline of the derivation of (3.15) is included in the Appendix.

c_{11} follows a χ_L^2 distribution, so the p.d.f of $y = (c_{11})^2$ is

$$f_Y(y) = \frac{1}{2^{\frac{L}{2}+1}\Gamma(\frac{L}{2}))} y^{\frac{L}{4}-1} e^{-\frac{\sqrt{y}}{2}} \tag{3.16}$$

Since the distribution of $\mathbf{e}_{21}$ will be a decreasing power law distribution of the norm and under low rank case, y is approximated to a decreasing power law distribution, it is reasonable to assume the norm of $\mathbf{x} = \left(\beta_1 \cdot \mathbf{1} + \beta_2 c_{11}^{-1}\mathbf{c}_{21}\right) c_{11}^2 - k \cdot \mathbf{1}$,

which is $G_{notch} = \mathbf{x^H x}/\left(N-1\right)$, will have a distribution of

$$f_{G_{notch}}\left(g\right) = \frac{L \cdot K}{\left(1 + K \cdot g\right)^{L+1}}. \tag{3.17}$$

Note $\int_0^\infty f_{G_{notch}}\left(g\right) dg = 1$. In the next, we will show the maximum likelihood (ML) estimates of the parameter K.

3.3.5 Finding the parameter K

Figure 3.1 shows the ML estimates of the parameter K. The plots show that for the number of snapshots L ranges from 5 to 45, the parameter K is approximately equal the INR ρ_{INR}. Thus, the approximated p.d.f. of notch depth is

$$f_{G_{notch}}\left(g\right) = \frac{L \cdot \rho_{INR}}{\left(1 + \rho_{INR} \cdot g\right)^{L+1}} \tag{3.18}$$

The histogram in Figure 3.4 shows that the beta-prime distribution fits the simulated notch depth data well.

Figures 3.2-3.3 display notch depth G_{ND} as a function of number of snapshots L and ρ_{INR}. The symbols denote the mean ND and the error bars indicate the spread of the distribution between the 10th and 90th percentiles. Note here the error bars are asymmetric around the mean, as the notch depth distribution is asymmetric. The mean notch depth on a log-log scale has a predictable slope as a function of INR and snapshots. The log-linear relationship in Figure 3.2 and Figure 3.3 give us inspiration. In Chapter 5, we will find the the analytical results of the sample means of ND.

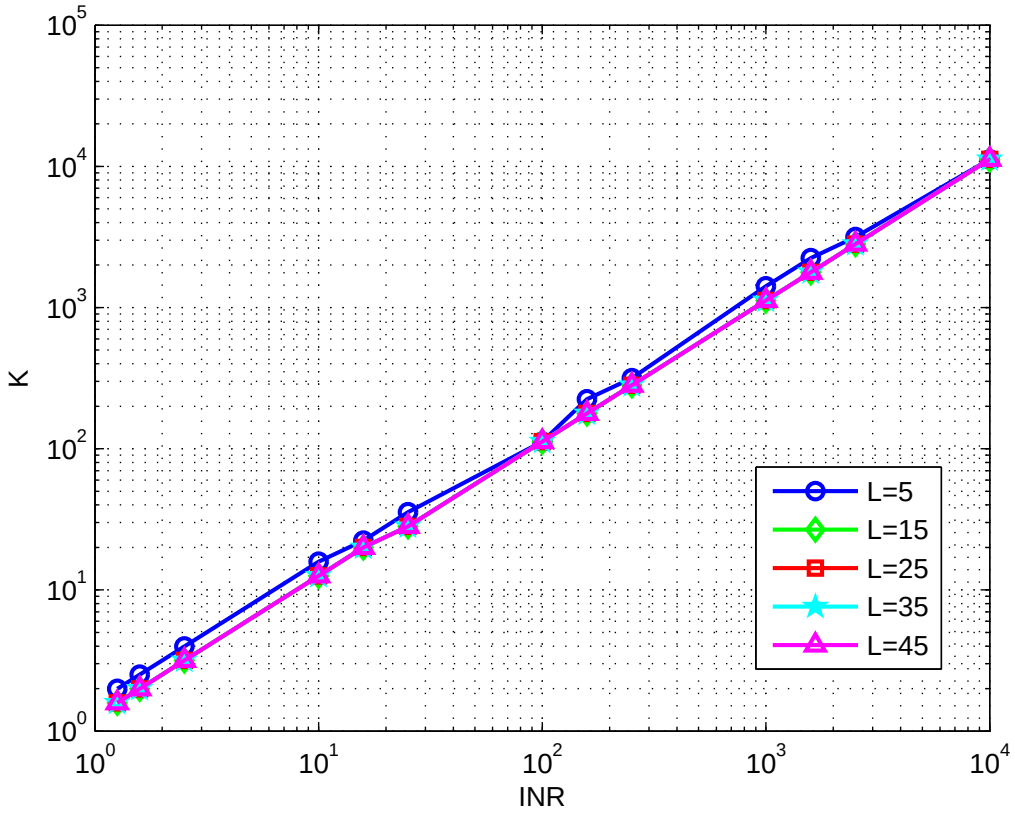

Figure 3.1 ML estimates of the parameters of the beta distribution for simulated ND data. The environment consists of one interferer located near the peak sidelobe of the conventional beamformer(CBF) and spatially white noise.

3.3.6 The distribution function of SINR loss

Combining with previous results, we have

$$\frac{1}{\rho_{DMR} SINR(\mathbf{w}_{ens})} = \frac{\rho_{INR}}{\rho_{SNR}} \cdot G_{notch} + \frac{1}{\rho_{SNR}} \cdot \frac{1}{G_{WNG}}$$

where $\rho_{SNR} = \sigma_s^2/\sigma_n^2$.

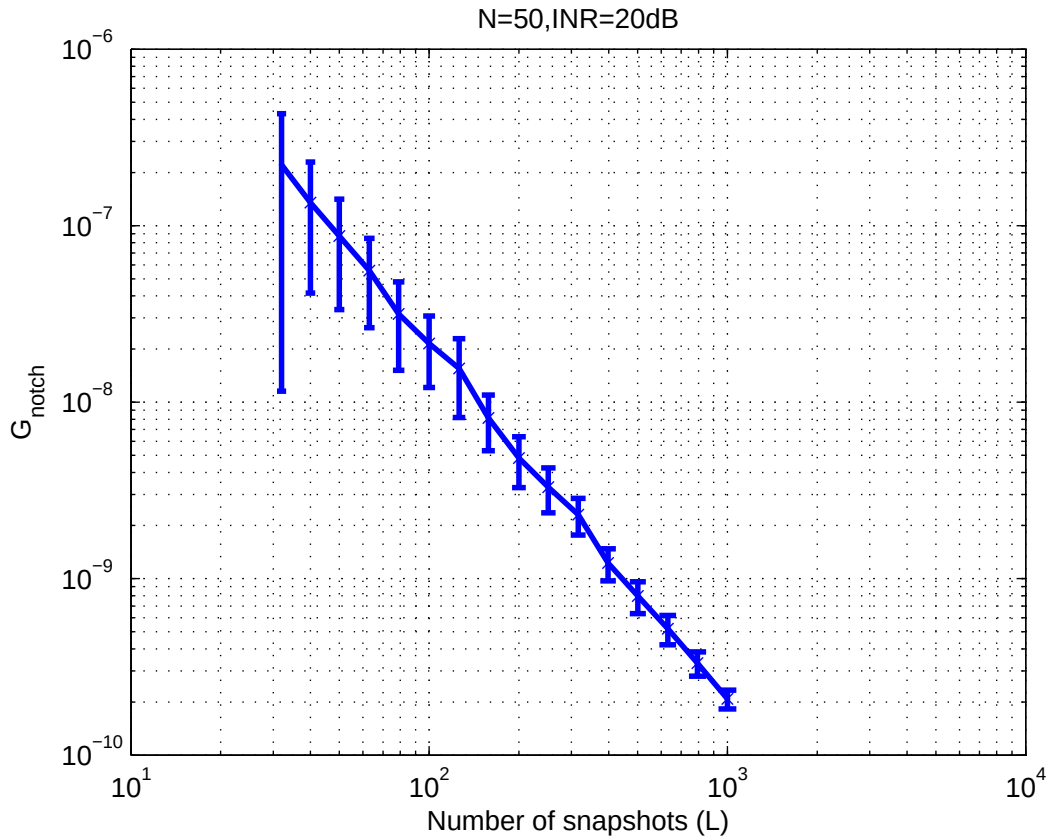

Figure 3.2 DMR notch depth g_{ND} as a function of number of snapshots L. The example uses a 50-sensor ULA with half-wave-length spacing. Here $N = 50$, $\rho_{INR} = 20dB$, $\sigma_s^2 = 10, \sigma_1^2 = 100, \sigma_n^2 = 1$, $\theta_s = 10°$, $\theta_1 = 80°$. Results are shown for DMR ABFs generated using 1000 trials for each L. The solid line denotes the mean and the error bars mark the span between the 10th and 90th percentiles of the data.

Using the approximations for $SINR(\mathbf{w}_{ens})$ and g_{WNG} discussed in [38], we have $SINR(\mathbf{w}_{ens}) \approx N \cdot \rho_{SNR}$. Finally the p.d.f. of ρ_{DMR} is

$$f_{\rho_{DMR}}(\rho) = L \cdot \rho^{L-1}, \quad 0 \leq \rho \leq 1 \tag{3.19}$$

Figure 3.5 shows the beta distribution with parameters $a = L$ and $b = 1$ is an excellent fit for the SINR loss of the DMR ABF in the case of a single interference.

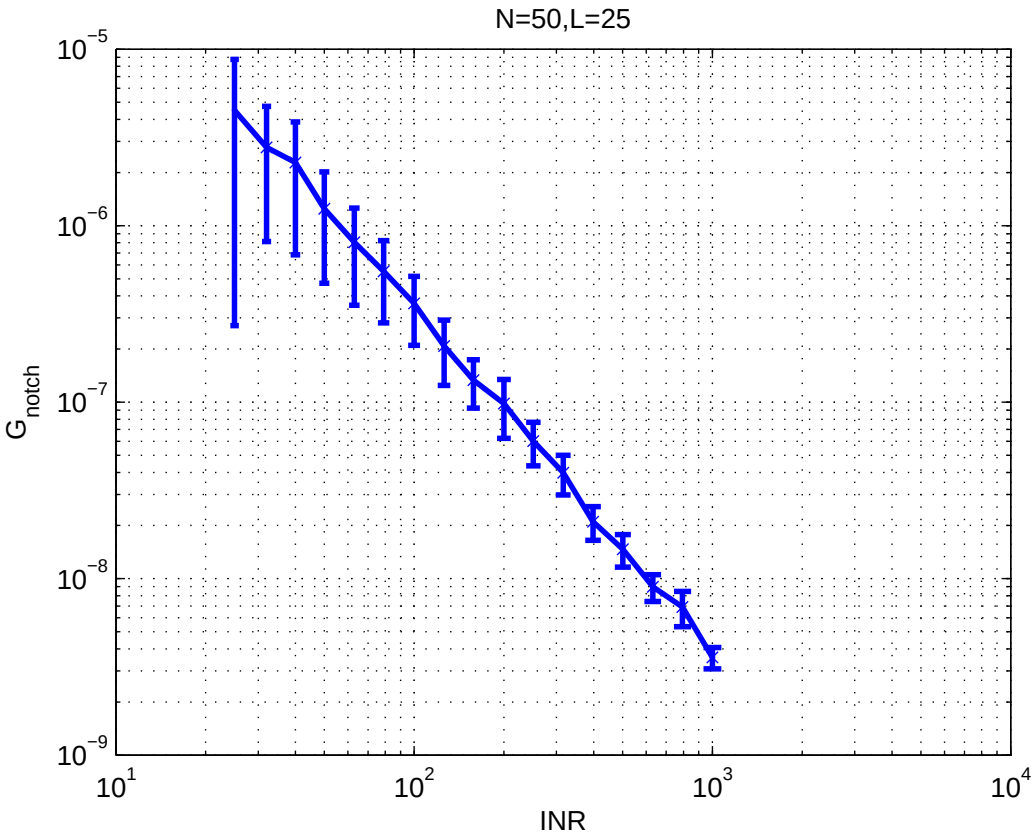

Figure 3.3 DMR notch depth g_{ND} as a function of INR ρ_{INR}. The example uses a 50-sensor ULA with half-wave-length spacing. Here $N = 50$, $L = 25$, $\sigma_s^2 = 10, \sigma_n^2 = 1$, $\theta_s = 10°$, $\theta_1 = 80°$. Results are shown for DMR ABFs generated using 1000 trials for each INR value. The solid line denotes the mean and the error bars mark the span between the 10th and 90th percentiles of the data.

3.4 Summary and Conclusion

We have shown that the distribution of SINR loss ratio of the DMR beamformer for single interference can be used a beta-distributed function to express it [16]. Numerical simulations support the beta-distributed function has a good performance. The results presented suggest several possible further research directions, such as multiple interference and signal present case, which will be more realistic.

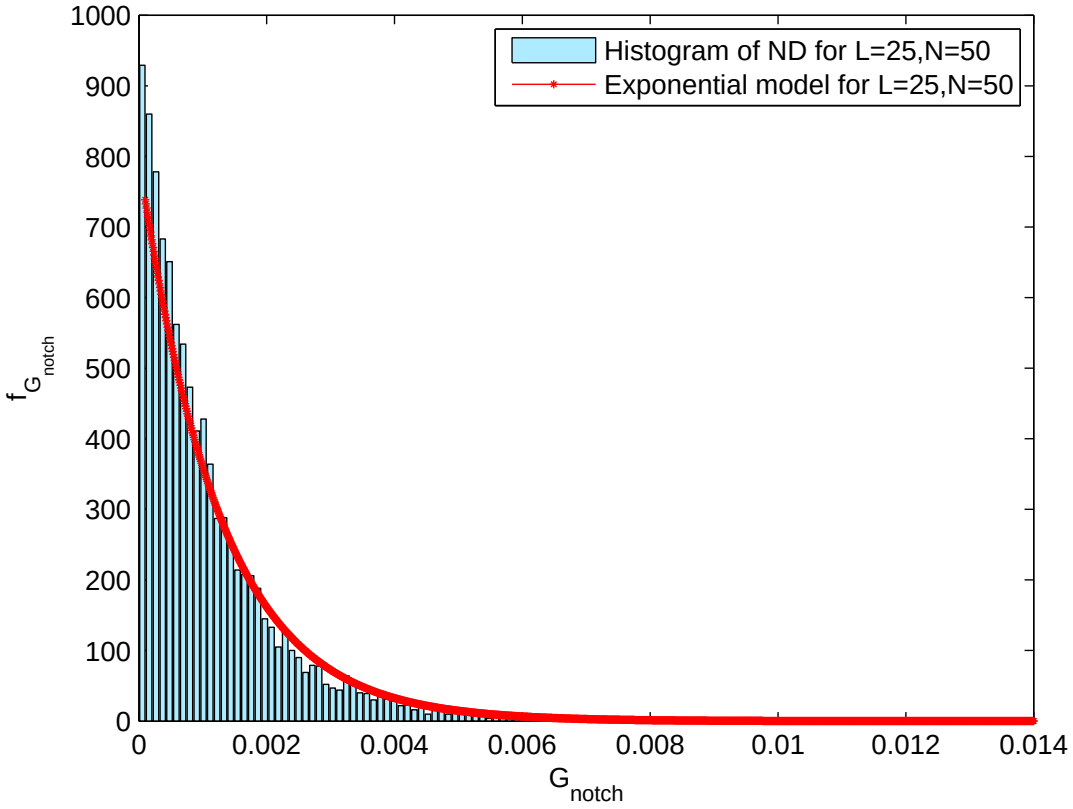

Figure 3.4 Probability density function overlaid on the notch depth histogram for the single interference case. The example uses a 50-sensor ULA with half-wave-length spacing. Here $N = 50$, $L = 2$, $\rho_{INR} = 15dB$, $\sigma_s^2 = 10, \sigma_1^2 = 32, \sigma_n^2 = 1$, $\theta_s = 10°$, $\theta_1 = 80°$.

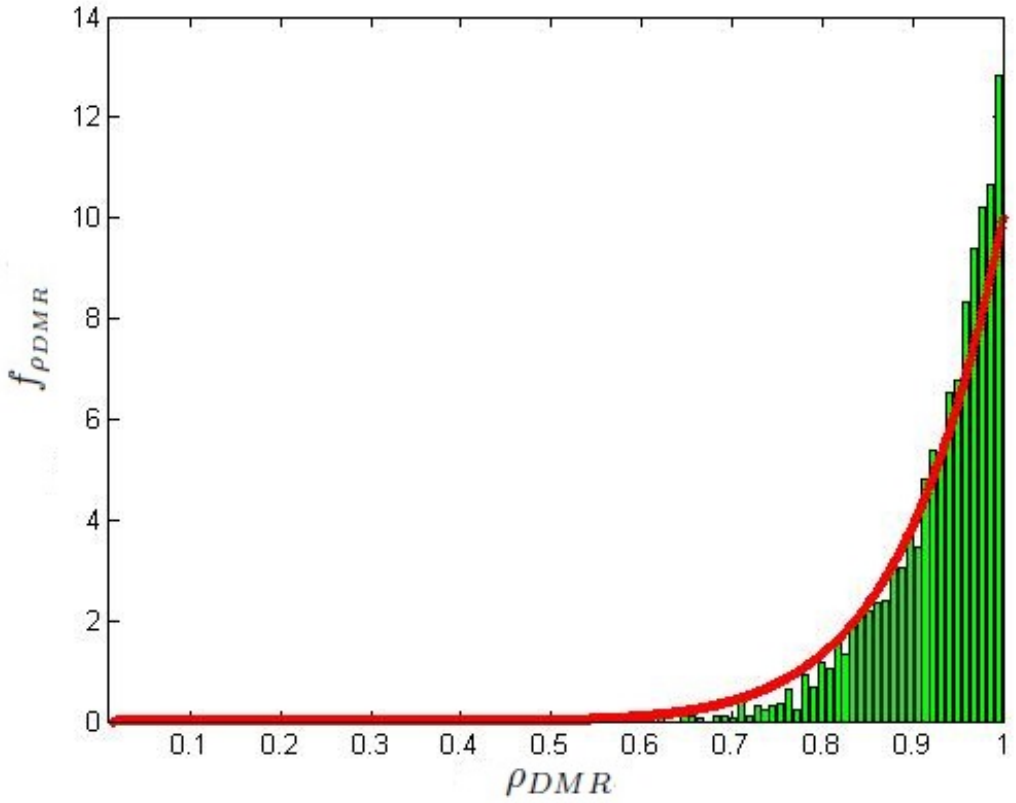

Figure 3.5 Probability density function overlaid on the SINR loss histogram for the single interference case. The example uses a 50-sensor ULA with half-wave-length spacing. Here $N = 20$, $L = 10$, $\rho_{INR} = 10dB$, $\sigma_s^2 = 10, \sigma_1^2 = 10, \sigma_n^2 = 1$, $\theta_s = 10°$, $\theta_1 = 80°$.

CHAPTER 4

DISTRIBUTION OF DMR NOTCH DEPTH FOR A SINGLE INTERFERENCE CASE

In this Chapter, a closed-form derivation of the PDF for the ND of the DMR ABF is proposed. It was conjectured that the ND is a beta distribution [40]. Based on Chapter 3's result, another analytical derivation combined with simulations is presented.

4.1 Background

The narrowband planewave beamforming assumes that the lth data measured by an array consist of SOI plus a single planewave interference and noise, which can be represented as

$$\mathbf{p}(l) = b_s(l)\,\mathbf{v}_s + b_1(l)\,\mathbf{v}_1 + \mathbf{n}(l) \tag{4.1}$$

where b_s is the amplitude of the signal vector $\mathbf{v}_s$, b_1 is the amplitude of the planewave interference $\mathbf{v}_1$, $\mathbf{n}$ is a vector of complex noise samples.

For the N element sensor array oriented along z-axis, the normalized modes for signal and planewave interference can be represented as

$$\mathbf{v}_s = \frac{1}{\sqrt{N}}\begin{bmatrix} e^{j\frac{2\pi}{\lambda}cos(\theta_s)z_1} \\ \vdots \\ e^{j\frac{2\pi}{\lambda}cos(\theta_s)z_N} \end{bmatrix}, \mathbf{v}_1 = \frac{1}{\sqrt{N}}\begin{bmatrix} e^{j\frac{2\pi}{\lambda}cos(\theta_1)z_1} \\ \vdots \\ e^{j\frac{2\pi}{\lambda}cos(\theta_1)z_N} \end{bmatrix}$$

where λ is the wavelength, θ_1 is the plavewave angle, and z_i is the location of the ith sensor. Without loss of generality, this paper assumes that the amplitudes b_s and

b_1 are zero-mean complex circular random variables and that the complex circular random noise is zero mean and spatially white. Assuming the planewave interference are independent, the ECM under signal absent case is represented as

$$\mathbf{\Sigma}_{I+N} = \sigma_1^2 \mathbf{v}_1 \mathbf{v}_1^{\mathbf{H}} + \sigma_n^2 \mathbf{I}_N$$

where σ_1^2 is the interference power, and the white noise power is σ_n^2.

The $N \times N$ SCM and its eigendecomposition are defined as

$$\mathbf{S} = \frac{1}{L} \sum_{l=1}^{L} \mathbf{p}\left(l\right) \mathbf{p}^{\mathrm{H}}\left(l\right) = \sum_{n=1}^{N} \lambda_n \mathbf{e}_n \mathbf{e}_n^{\mathrm{H}} \tag{4.2}$$

where $\mathbf{e}_i$ and λ_i are the sample eigenvectors and eigenvalues of $\mathbf{S}$, respectively. Thus, the $N \times N$ DMR-SCM is constructed as,

$$\mathbf{S}_{\mathrm{DMR}} = \lambda_i \mathbf{e}_1 \mathbf{e}_1^{\mathrm{H}} + \sum_{i=2}^{N} s_w^2 \mathbf{e}_i \mathbf{e}_i^{\mathrm{H}} \tag{4.3}$$

where $s_w^2 = \left(\frac{L}{L-1}\right)\left(\frac{1}{N-1}\right)\sum_{i=2}^{N} \lambda_i$ is the average of the scaled lowest eigenvalues.

The DMR ABF weight vector has the same form as the adaptive MVDR weight vector, with SCM replaced by $\mathbf{S}_{\mathrm{DMR}}$:

$$\mathbf{w}_{\mathrm{DMR}} = \left(\mathbf{v}_s^{\mathrm{H}} \mathbf{S}_{\mathrm{DMR}}^{-1} \mathbf{v}_s\right)^{-1} \mathbf{S}_{\mathrm{DMR}}^{-1} \mathbf{v}_s. \tag{4.4}$$

The ND is defined as the amplitude square of the beampattern in the direction of an interference. That is, in the case of interference $\mathbf{v}_1$,

$$G_{notch} \triangleq \left|\mathbf{w}_{\mathrm{DMR}}^{\mathrm{H}}\mathbf{v}_1\right|^2 = \frac{\left|\mathbf{v}_s^{\mathbf{H}}\mathbf{S}_{\mathrm{DMR}}^{-1}\mathbf{v}_1\right|^2}{\left|\mathbf{v}_s^{\mathbf{H}}\mathbf{S}_{\mathrm{DMR}}^{-1}\mathbf{v}_s\right|^2}. \tag{4.5}$$

4.2 Derivation of Distribution for the ND of the DMR ABF

4.2.1 Simplification of $\mathbf{S}_{\mathrm{DMR}}^{-1}$

The DMR covariance matrix depends on the eigendecomposition of the SCM. In [1], the relative influence of the sample eigenvalues and eigenvectors on ND had been investigated. Two alternative DMR implementations were proposed: the first alternative beamformer used ensemble eigenvectors and sample eigenvalues to generate a structured covariance matrix, while the second used ensemble eigenvalues and sample eigenvectors. The result showed that the sample eigenvector alternative beamformer was indistinguishable from the standard DMR, while the result of sample eigenvalue alternative beamformer was centered on the ensemble ND. Therefore the sample eigenvectors determined the ND of the DMR ABF.

Combined with sample eigenvectors and ensemble eigenvalues, the DMR matrix $\mathbf{S}_{\mathrm{DMR}}$ at a high level of INR is

$$\mathbf{S}_{\mathrm{DMR}}^{-1} \approx \left(s_w^2\right)^{-1}\left[\mathbf{I}_N - \mathbf{e}_1\mathbf{e}_1^{\mathrm{H}}\right] = \left(s_w^2\right)^{-1}\mathbf{P}_{\mathbf{e}_1}^{\perp} \tag{4.6}$$

where $\mathbf{P}_{\mathbf{e}_1}^{\perp} = \mathbf{I}_N - \mathbf{e}_1\mathbf{e}_1^{\mathrm{H}}$, $\mathbf{e}_1$ is the sample eigenvector corresponding to the largest eigenvalue. Then, we have,

$$G_{notch} = \frac{\left|\mathbf{v}_s^{\mathbf{H}}\mathbf{S}_{\mathrm{DMR}}^{-1}\mathbf{v}_1\right|^2}{\left|\mathbf{v}_s^{\mathbf{H}}\mathbf{S}_{\mathrm{DMR}}^{-1}\mathbf{v}_s\right|^2} \approx \frac{\left|\mathbf{v}_s^{\mathbf{H}}\mathbf{P}_{\mathbf{e}_1}^{\perp}\mathbf{v}_1\right|^2}{\left|\mathbf{v}_s^{\mathbf{H}}\mathbf{P}_{\mathbf{e}_1}^{\perp}\mathbf{v}_s\right|^2}. \tag{4.7}$$

4.2.2 Unitary transformation to simplify G_{notch} expression

As $\mathbf{v}_s$ is a unit vector ($\mathbf{v}_s^{\mathbf{H}}\mathbf{v}_s = 1$), we can design a unitary transformation matrix $\mathbf{\Phi} = [\boldsymbol{\phi}_1, \cdots, \boldsymbol{\phi}_N]$ such that $\boldsymbol{\phi}_1 = \mathbf{\Phi}\boldsymbol{\delta}_1 = \mathbf{v}_s$, where $\boldsymbol{\delta}_1 = [1, 0, \cdots, 0]^T$. Define $\mathbf{T} = \mathbf{\Phi}^H \mathbf{v}_s \mathbf{v}_s^{\mathbf{H}} \mathbf{\Phi} = \boldsymbol{\delta}_1 \boldsymbol{\delta}_1^{\mathbf{H}}$, and $\mathbf{Q} = \mathbf{\Phi}^{\mathbf{H}} \mathbf{P}_{\mathbf{e}_1}^{\perp} \mathbf{\Phi} = (q_{ij}) \in \mathbb{C}^{N \times N}$. Then the scalar in the denominator of (4.3) becomes

$$\begin{aligned} \mathbf{v}_s^{\mathbf{H}} \mathbf{P}_{\mathbf{e}_1}^{\perp} \mathbf{v}_s &= tr\left(\mathbf{v}_s^{\mathbf{H}} \mathbf{P}_{\mathbf{e}_1}^{\perp} \mathbf{v}_s\right) = tr\left(\mathbf{v}_s^{\mathbf{H}} \mathbf{\Phi}\mathbf{\Phi}^{\mathbf{H}} \mathbf{P}_{\mathbf{e}_1}^{\perp} \mathbf{\Phi}\mathbf{\Phi}^{\mathbf{H}} \mathbf{v}_s\right) \\ &= tr\left(\mathbf{\Phi}^{\mathbf{H}} \mathbf{v}_s \mathbf{v}_s^{\mathbf{H}} \mathbf{\Phi} \cdot \mathbf{\Phi}^{\mathbf{H}} \mathbf{P}_{\mathbf{e}_1}^{\perp} \mathbf{\Phi}\right) = tr\left(\mathbf{TQ}\right) = q_{11}. \end{aligned}$$

Note also there exists a unitary transformation matrix $\mathbf{M} = (m_{ij}) \in \mathbb{C}^{N \times N}$ such that $\mathbf{\Phi M \Phi^H} \mathbf{v}_s = \mathbf{v}_1$. As $\mathbf{M}\boldsymbol{\delta}_1 = \mathbf{\Phi}^{\mathbf{H}} \mathbf{v}_1$, the elements of the first column are $m_{i1} = \boldsymbol{\phi}_i^{\mathbf{H}} \mathbf{v}_1$, $(i = 1 \cdots N)$. Then the scalar in the numerator of (4.3) becomes

$$\begin{aligned} \mathbf{v}_s^{\mathbf{H}} \mathbf{P}_{\mathbf{e}_1}^{\perp} \mathbf{v}_1 &= tr\left(\mathbf{v}_s^{\mathbf{H}} \mathbf{\Phi}\mathbf{\Phi}^{\mathbf{H}} \mathbf{P}_{\mathbf{e}_1}^{\perp} \mathbf{\Phi M \Phi^H} \mathbf{v}_s\right) \\ &= tr\left(\mathbf{\Phi}^{\mathbf{H}} \mathbf{v}_s \mathbf{v}_s^{\mathbf{H}} \mathbf{\Phi} \cdot \mathbf{\Phi}^{\mathbf{H}} \mathbf{P}_{\mathbf{e}_1}^{\perp} \mathbf{\Phi} \cdot \mathbf{M}\right) = tr\left(\mathbf{TQM}\right) \\ &= \sum_{i=1}^{N} q_{1i} m_{i1} = \sum_{i=1}^{N} \left(q_{1i} \boldsymbol{\phi}_i^{\mathbf{H}} \mathbf{v}_1\right). \end{aligned}$$

To illustrate how to construct the orthogonal columns of the unitary transformation matrix $\mathbf{\Phi}$, we choose the first column $\boldsymbol{\phi}_1$ as SOI vector $\mathbf{v}_s$. Then, $\mathbf{u}_2$ is chosen from the subspace spanned by $[\mathbf{v_s}, \mathbf{v_1}]$ and it is orthogonal to $\mathbf{u}_1$:

$$\boldsymbol{\phi}_2 = \mathbf{P}_{\boldsymbol{\phi}_1}^{\perp} \mathbf{v}_1 / \left\| \mathbf{P}_{\boldsymbol{\phi}_1}^{\perp} \mathbf{v}_1 \right\|, \quad \mathbf{P}_{\boldsymbol{\phi}}^{\perp} = \mathbf{I}_N - \boldsymbol{\phi}_1 \left(\boldsymbol{\phi}_1^{\mathbf{H}} \boldsymbol{\phi}_1\right)^{-1} \boldsymbol{\phi}_1^{\mathbf{H}}.$$

The remaining column vectors $\mathbf{u}_3 \cdots \mathbf{u}_N$ are chosen orthonormal to the subspace spanned by $[\boldsymbol{\phi}_1, \boldsymbol{\phi}_2]$ *e.g.* , via use of the Gram-Schmidt method. So $\boldsymbol{\phi}_2^{\mathbf{H}} \mathbf{v}_1 = \alpha =$

$\sqrt{1-|\mathbf{v}_s^{\mathbf{H}}\mathbf{v}_1|^2}$, and $\boldsymbol{\phi}_i^{\mathbf{H}}\mathbf{v}_1 = 0\,(i = 3\cdots N)$. Consequently $\sum_{i=1}^{N}\left(q_{1i}\boldsymbol{\phi}_i^{\mathbf{H}}\mathbf{v}_1\right) = q_{11}m_{11} + q_{12}$. Then,

$$G_{notch} = \frac{\left|\mathbf{v}_s^{\mathbf{H}}\mathbf{P}_{\mathbf{e}_1}^{\perp}\mathbf{v}_1\right|^2}{\left|\mathbf{v}_s^{\mathbf{H}}\mathbf{P}_{\mathbf{e}_1}^{\perp}\mathbf{v}_s\right|^2} = \left|m_{11} + \alpha\cdot\frac{q_{12}}{q_{11}}\right|^2 \tag{4.8}$$

where $m_{11} = \mathbf{v}_s^{\mathbf{H}}\mathbf{v}_1$, $q_{11} = \boldsymbol{\phi}_1^H\mathbf{P}_{\mathbf{e}_1}^{\perp}\boldsymbol{\phi}_1 = 1 - \boldsymbol{\phi}_1^H\mathbf{e_1}\mathbf{e_1^H}\boldsymbol{\phi}_1$, $q_{12} = \boldsymbol{\phi}_1^H\mathbf{P}_{\mathbf{e}_1}^{\perp}\boldsymbol{\phi}_2 = -\boldsymbol{\phi}_1^H\mathbf{e_1}\mathbf{e_1^H}\boldsymbol{\phi}_2$, and $\alpha = \sqrt{1-|\mathbf{v}_s^{\mathbf{H}}\mathbf{v}_1|^2}$.

4.2.3 Perturbation analysis on G_{notch}

The random matrix theory predicts the sample eigenvectors have a phase transition [3,7,29]. The principal sample eigenvector $\mathbf{e_1}$ of SCM is the estimate of the ensemble eigenvector $\boldsymbol{\xi_1}$ of ECM $\boldsymbol{\Sigma}_{I+N}$ when the INR is above a threshold level, that is, $\mathbf{e_1}$ is regard as lying on a cone around $\boldsymbol{\xi_1}$. As INR and/or L/N increases, the radius of the cone decreases.

Note $\sum_{i=1}^{N}\boldsymbol{\phi}_i^H\mathbf{e_1}\mathbf{e_1^H}\boldsymbol{\phi}_i = 1$, and $span\,(\boldsymbol{\phi}_1, \boldsymbol{\phi}_2) = span\,(\mathbf{v_s}, \mathbf{v_1})$. Therefore

$$\mathbf{e_1^H}\left(\boldsymbol{\phi}_1\boldsymbol{\phi}_1^H + \boldsymbol{\phi}_2\boldsymbol{\phi}_2^H\right)\mathbf{e_1} \geq \mathbf{e_1^H}\mathbf{v_1}\mathbf{v_1^H}\mathbf{e_1} = \cos^2(\mathbf{v_1}, \mathbf{e_1})$$

Since our assumption is at a high level of INR, $N\cdot\rho_{INR}$ is above the threshold $\sqrt{N/L}$, then $\mathbf{e_1}$ is a biased esimate of $\boldsymbol{\xi_1}$ [1]. The prediction of the limiting value of the generalised cosine between the ensemble eigenvector and sample eigenvector is asymptotic to 1 . So $\sum_{i=1}^{2}\boldsymbol{\phi}_i^H\mathbf{e_1}\mathbf{e_1^H}\boldsymbol{\phi}_i \overset{a.s.}{\to} 1$, and consequently, the complex ratio q_{12}/q_{11} can be repesented as

$$\frac{q_{12}}{q_{11}} = \frac{\boldsymbol{\phi}_1^H\mathbf{e_1}\mathbf{e_1^H}\boldsymbol{\phi}_2}{\boldsymbol{\phi}_1^H\mathbf{e_1}\mathbf{e_1^H}\boldsymbol{\phi}_1 - 1} \approx -\frac{\boldsymbol{\phi}_1^H\mathbf{e_1}\mathbf{e_1^H}\boldsymbol{\phi}_2}{\boldsymbol{\phi}_2^H\mathbf{e_1}\mathbf{e_1^H}\boldsymbol{\phi}_2} = -\frac{\boldsymbol{\phi}_1^H\mathbf{e_1}}{\boldsymbol{\phi}_2^H\mathbf{e_1}}. \tag{4.9}$$

Now, let's focus on finding the PDF of $Z = \frac{X}{Y} = \frac{\boldsymbol{\phi}_1^{\mathbf{H}}\mathbf{e}_1}{\boldsymbol{\phi}_2^{\mathbf{H}}\mathbf{e}_1}$. Note $\sigma_x^2 = \boldsymbol{\phi}_1^{\mathbf{H}}\boldsymbol{\Sigma}\boldsymbol{\phi}_1$, $\sigma_y^2 = \boldsymbol{\phi}_2^{\mathbf{H}}\boldsymbol{\Sigma}\boldsymbol{\phi}_2$, and the correlation coefficient of X and Y is $\rho = \frac{\boldsymbol{\phi}_1^{\mathbf{H}}\boldsymbol{\Sigma}\boldsymbol{\phi}_2}{\sqrt{\boldsymbol{\phi}_1^{\mathbf{H}}\boldsymbol{\Sigma}\boldsymbol{\phi}_1}\sqrt{\boldsymbol{\phi}_2^{\mathbf{H}}\boldsymbol{\Sigma}\boldsymbol{\phi}_2}}$. From [7], the sample eigenvector $\mathbf{e}_1$ is asymptotically normally distributed as: $\mathbf{e}_1 \sim \mathcal{CN}(\mathbf{v}_1, \boldsymbol{\Sigma})$, with $\boldsymbol{\Sigma} \approx \frac{1}{L}\sum_{k=2}^{N} \frac{\gamma_1\gamma_k}{(\gamma_1-\gamma_k)^2}\boldsymbol{\xi}_k\boldsymbol{\xi}_k^{\mathbf{H}}$, $\gamma_i\,(i = 1, 2\cdots N)$ and $\boldsymbol{\xi}_i\,(i = 1, 2\cdots N)$ are eigenvalues and eigenvectorsof ECM $\boldsymbol{\Sigma}_{I+N}$.

Next, we will derive the PDF of ND, that is

$$G_{notch} = \left|m_{11} + \alpha \cdot \frac{q_{12}}{q_{11}}\right|^2 = \left|m_{11} - \alpha \cdot \frac{X}{Y}\right|^2 = |m_{11} - \alpha \cdot Z|^2 = |W|^2 . \tag{4.10}$$

4.2.4 PDF of G_{notch}

The ratio of complex Gaussian random variables appears in many different applications such as wireless communication systems, optics, and medical imaging. The real-valued Gaussian ratio distribution has been studied, and expressions in the form of Cauchy-Lorentz distribution have been derived. In [26], Nadimi *et al.* derived the joint (amplitude and phase) distribution of the ratio of two independent non-zero-mean complex Gaussian random variables with polar representations. In [27], Yan and Ren studied the PDFs of multivariate ratios of proper complex Gaussian random variables. We can combine their results and get the PDF of the ratio of two proper complex Gaussian random variables.

Theorem: Ratio of two non-zero mean correlated proper complex Gaussian random variables. If X and Y are two correlated proper complex Gaussian random variables having joint density

$$\begin{pmatrix} X \\ Y \end{pmatrix} \sim \mathcal{CN}\left(\begin{bmatrix} \mu_x \\ \mu_y \end{bmatrix}, \begin{bmatrix} \sigma_x^2 & \rho_{xy}\sigma_x\sigma_y \\ \rho_{xy}^*\sigma_x\sigma_y & \sigma_y^2 \end{bmatrix}\right),$$

and the correlation coefficient $\rho = r_\rho e^{j\theta_\rho}$, the joint probability distribution of the amplitude and the phase of ratio $Z = X/Y$ presented by the polar distribution is:

$$
\begin{aligned}
f_{R_z,\Theta_z}(r_z,\theta_z) &= \frac{r_z\left(1-r_\rho^2\right)\sigma_x^2\sigma_y^2}{\pi\left[\sigma_y^2 r_z^2 - 2r_\rho\sigma_x\sigma_y\cos\left(\theta_z+\theta_\rho\right)r_z+\sigma_x^2\right]^2} \\
&\times e^{\left[-\mu_y^*\sigma_x^2\mu_y-\mu_x^*\rho^*\sigma_x\sigma_y\mu_y-\mu_y^*\rho\sigma_x\sigma_y\mu_x+\mu_x^*\sigma_y^2\mu_x\right]/\left[\left(1-r_\rho^2\right)\sigma_x^2\sigma_y^2\right]} \\
&\times {}_1F_1\left(2,1;\frac{\left[\left(\mu_y^*\sigma_x^2-\mu_x^*\rho^*\sigma_x\sigma_y\right)+\left(\mu_x^*\sigma_y^2-\mu_y^*\rho\sigma_x\sigma_y\right)r_z e^{j\theta_z}\right]^2}{\left(1-r_\rho^2\right)\sigma_x^2\sigma_y^2\left[\sigma_y^2 r_z^2-2r_\rho\sigma_x\sigma_y\cos\left(\theta_z+\theta_\rho\right)r_z+\sigma_x^2\right]}\right)
\end{aligned}
\tag{4.11}
$$

The steps to find the PDF of ND are:

(1) $$f_{Z_r,Z_i}(z_r,z_i) = \left.\frac{f_{R_z,\Theta_z}(r_z,\theta_z)}{\left|\frac{\partial(z_r,z_i)}{\partial(r_z,\theta_z)}\right|}\right|_{\substack{\theta_z=\arctan(z_i/z_r)\\ r_z=\sqrt{z_r^2+z_i^2}}}$$

(2) $$f_{W_r,W_i}(w_r,w_i) = \left.\frac{f_{Z_r,Z_i}(z_r,z_i)}{\left|\frac{\partial(w_r,w_i)}{\partial(z_r,z_i)}\right|}\right|_{\substack{z_r=(m_r-w_r)/\alpha\\ z_i=(m_i-w_i)/\alpha}}$$

(3) $$f_{G,\Theta}(g,\theta) = \left.\frac{f_{W_r,W_i}(w_r,w_i)}{\left|\frac{\partial(g,\theta)}{\partial(w_r,w_i)}\right|}\right|_{\substack{w_r=\sqrt{g}\cos\theta\\ w_i=\sqrt{g}\cos\theta}}$$

(4) $$f_{G_{notch}}(g) = \int_0^{2\pi} f_{G,\Theta}(g,\theta)\,d\theta$$

Finally, we have

$$f_{G_{notch}}(g) = \int_0^{2\pi} \frac{\left(1-r_\rho^2\right)\sigma_x^2\sigma_y^2}{2\pi\alpha^2\left[\sigma_y^2 R_g^2 - 2r_\rho\sigma_x\sigma_y\cos\left(\Phi_g+\theta_\rho\right)R_g+\sigma_x^2\right]^2}$$
$$\times e^{\left[-\mu_y^*\sigma_x^2\mu_y-\mu_x^*\rho^*\sigma_x\sigma_y\mu_y-\mu_y^*\rho\sigma_x\sigma_y\mu_x+\mu_x^*\sigma_y^2\mu_x\right]/\left[\left(1-r_\rho^2\right)\sigma_x^2\sigma_y^2\right]} \tag{4.12}$$
$$\times {}_1F_1\left(2,1;\frac{\left[\left(\mu_y^*\sigma_x^2-\mu_x^*\rho^*\sigma_x\sigma_y\right)+\left(\mu_x^*\sigma_y^2-\mu_y^*\rho\sigma_x\sigma_y\right)R_g e^{j\Phi_g}\right]^2}{\left(1-r_\rho^2\right)\sigma_x^2\sigma_y^2\left[\sigma_y^2R_g^2-2r_\rho\sigma_x\sigma_y\cos\left(\Phi_g+\theta_\rho\right)R_g+\sigma_x^2\right]}\right)d\theta$$

where $R_g = R_g(\theta) = \sqrt{\left(m_r-\sqrt{g}\cos\theta\right)^2+\left(m_i-\sqrt{g}sin\theta\right)^2}/\alpha$, $\Phi_g = \Phi_g(\theta) = \arctan\dfrac{m_i-\sqrt{g}sin\theta}{m_r-\sqrt{g}\cos\theta}$, $m_r = \Re\left(\mathbf{v}_s^{\mathbf{H}}\mathbf{v}_1\right)$, $m_i = \Im\left(\mathbf{v}_s^{\mathbf{H}}\mathbf{v}_1\right)$, and $\alpha = \sqrt{1-\left|\mathbf{v}_s^{\mathbf{H}}\mathbf{v}_1\right|^2}$. Here ${}_1F_1(a,b;z)$ is the confluent hypergeometric functions of the first kind ${}_1F_1(a;b;z) = 1+\dfrac{a}{b}z+\dfrac{a(a+1)}{b(b+1)}\dfrac{z^2}{2!}+\ldots = \sum_{k=0}^{\infty}\dfrac{(a)_k}{(b)_k}\dfrac{z^k}{k!}$ where $(a)_k$ and $(b)_k$ are Pochhammer symbols.
.

4.2.5 Special case

Note when the angle difference between the SOI and the interference direction approximates to 90°, the correlation coefficient $\rho \approx 0$ and the inner product $\mathbf{v}_s^{\mathbf{H}}\mathbf{v}_1 \approx 0$, become negligible. Then the parameters in (10) can be simplified into: $\mu_x \approx 0$, $\mu_y \approx 1$, and $\rho = r_\rho e^{j\theta_\rho} \approx 0$.

To simplify the hypergeometric function, a simpler and more manageable expression for the distribution is proposed by Nadarajahet and Kwong [42]. The confluent hypergeometric function of the first kind can be represented as ${}_1F_1(2,1;z) = (z+1)e^z$. In such case, (10) can be represented as:

$$f_{G_{notch}}(g) = \frac{\sigma_x^2/\sigma_y^2}{\left(g+\sigma_x^2/\sigma_y^2\right)^2}\left(\frac{1}{\sigma_y^2}\left(\frac{\sigma_x^2/\sigma_y^2}{g+\sigma_x^2/\sigma_y^2}\right)+1\right)\exp\left(\frac{-g/\sigma_y^2}{g+\sigma_x^2/\sigma_y^2}\right). \tag{4.13}$$

For a single interference case, the ECM is $\mathbf{\Sigma}_{I+N} = \sigma_1^2 \mathbf{v}_1 \mathbf{v}_1^{\mathbf{H}} + \sigma_n^2 \mathbf{I}_N$, where σ_1^2 is the power in the interference source, and σ_n^2 is the white noise power. In such case, the maximum eigenvalue is $\gamma_1 = \sigma_1^2 + \sigma_n^2$, and the rest of the eigenvalues are $\gamma_{n\neq 1} = \sigma_n^2$. The eigenvector associated with the γ_1 is $\boldsymbol{\xi}_1 = \mathbf{v}_1$. The INR is defined as $\rho_{INR} = \sigma_1^2/\sigma_n^2$. With the assumption of high level INR, $\gamma_1 \gg \gamma_{n\neq 1}$ and $\sigma_1^2 \gg \sigma_n^2$.

$$\begin{aligned} \frac{1}{\sigma_x^2} = \frac{1}{\boldsymbol{\phi}_1^{\mathbf{H}} \mathbf{\Sigma} \boldsymbol{\phi}_1} &= \frac{L}{\boldsymbol{\phi}_1^{\mathbf{H}} \left(\sum_{k=2}^{N} \frac{\lambda_1 \lambda_k}{(\lambda_1 - \lambda_k)^2} \boldsymbol{\xi}_k \boldsymbol{\xi}_k^{\mathbf{H}} \right) \boldsymbol{\phi}_1} \\ &\approx \frac{L}{\frac{\gamma_1 \sigma_n^2}{(\gamma_1 - \sigma_n^2)^2} \boldsymbol{\phi}_1^{\mathbf{H}} \left(\mathbf{I}_N - \boldsymbol{\xi}_1 \boldsymbol{\xi}_1^{\mathbf{H}} \right) \boldsymbol{\phi}_1} \approx \frac{(\gamma_1 - \sigma_n^2)\, L}{\sigma_n^2} = \rho_{INR} \cdot \ L \end{aligned} \tag{4.14}$$

Note $\sigma_x^2, \sigma_y^2 \ll 1$, $g \ll \sigma_x^2/\sigma_y^2$ and $1/\sigma_x^2 = 1/\boldsymbol{\phi}_1^{\mathbf{H}} \mathbf{\Sigma} \boldsymbol{\phi}_1 \approx \rho_{INR} \cdot L$, therefore we can simplify (11) into:

$$f_{G_{notch}}(g) = \frac{1}{\sigma_x^2} \exp\left(-\frac{g}{\sigma_x^2} \right) \approx \rho_{INR} \cdot L \cdot e^{-\rho_{INR} \cdot L \cdot g}. \tag{4.15}$$

4.2.6 Comparison with previous study

The distribution of G_{notch} in [38, 39] is

$$f_{G_{notch}}(g) = \frac{\rho_{INR} \cdot L}{(1 + \rho_{INR} \cdot g)^{L+1}}, \tag{4.16}$$

with the mean $E_{G_{notch}}(g) = 1/(\rho_{INR} \cdot L)$ and variance $Var_{G_{notch}}(g) = 1/(\rho_{INR} \cdot L)^2$. Note (6.12) is consistent with Cox's conjecture [33] that the mean ND in dB goes like $-10\log_{10}(\rho_{INR} \cdot L)$ over a wide range.

There is a connection between our result (4.11) and the previous result (4.12):

$$\begin{aligned} &\lim_{g\to 0} \frac{\rho_{INR}\cdot L}{(1+\rho_{INR}\cdot g)^{L+1}} = \rho_{INR}\cdot L \cdot \lim_{g\to 0} (1+\rho_{INR}\cdot g)^{-(L+1)\cdot \frac{\rho_{INR}\cdot g}{\rho_{INR}\cdot g}} \\ &= \rho_{INR}\cdot L \cdot e^{-(L+1)\rho_{INR}\cdot g} \approx \rho_{INR}\cdot L \cdot e^{-\rho_{INR}\cdot L\cdot g}. \end{aligned} \tag{4.17}$$

Therefore it proves that ND is exponentially-distributed under reasonable assumptions.

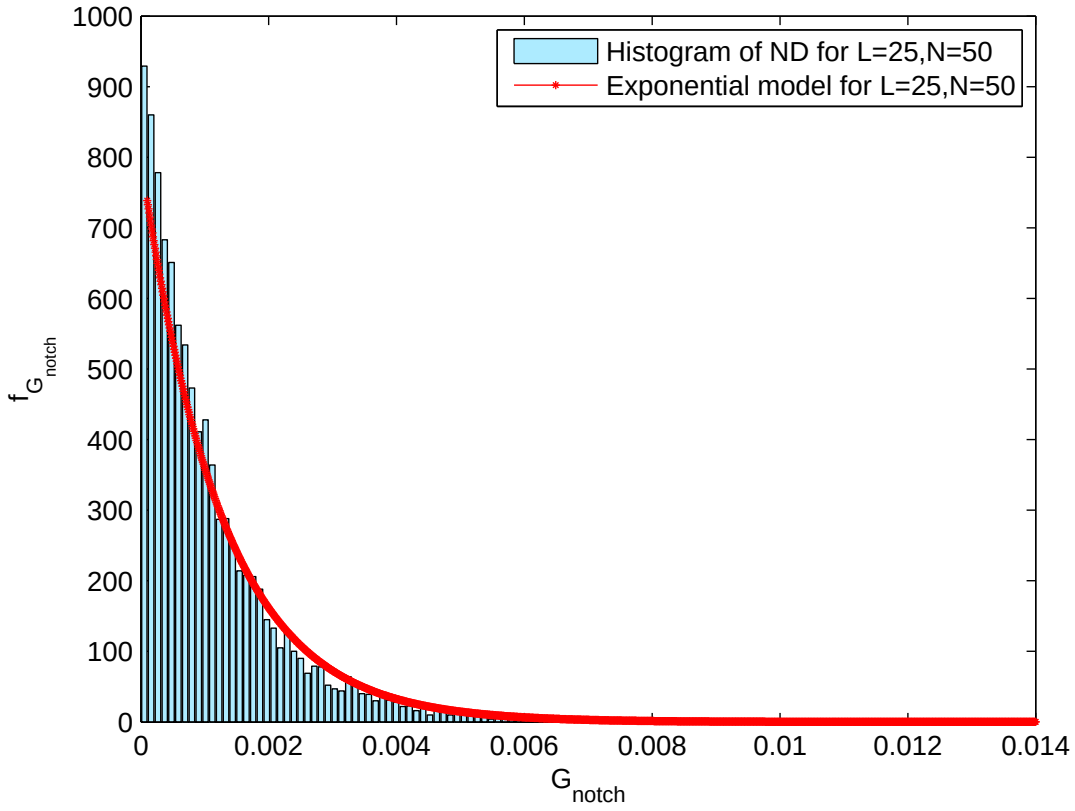

Figure 4.1 Probability density function overlaid on the notch depth histogram for the single interference case. The example uses a 50-sensor ULA with half-wave-length spacing. Here $N = 50$, $L = 25$, $\rho_{INR} = 15dB$, $\sigma_s^2 = 10, \sigma_1^2 = 32, \sigma_n^2 = 1$, $\theta_s = 10°$, $\theta_1 = 80°$.

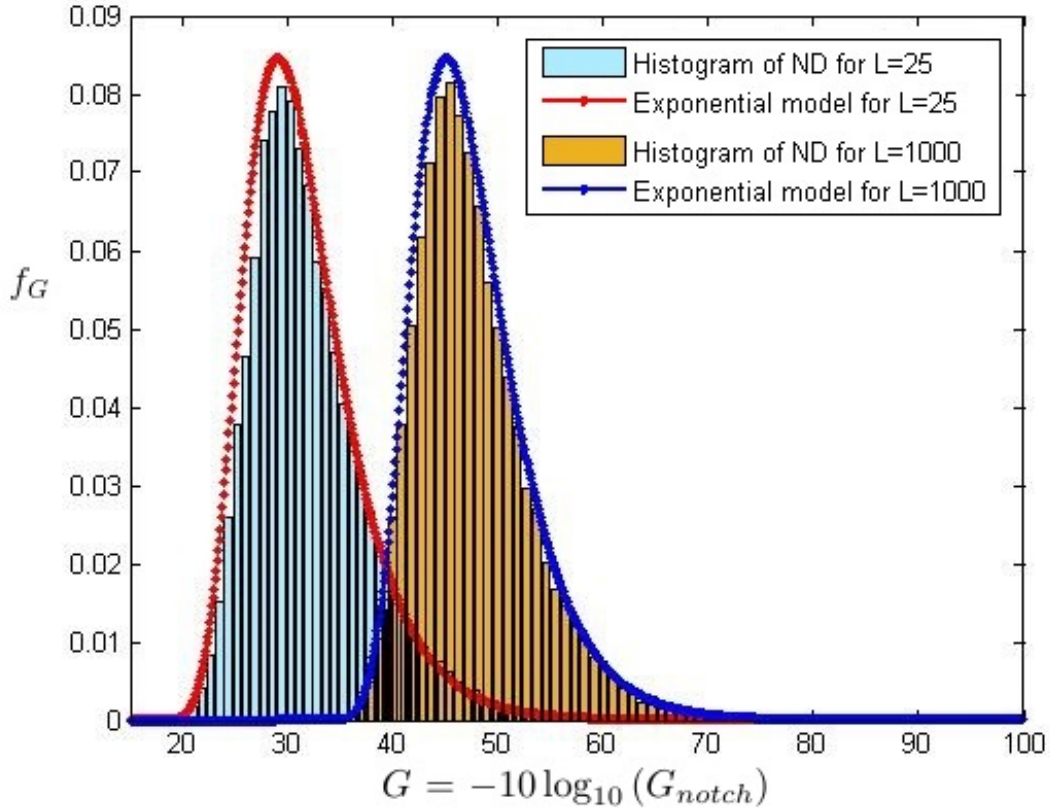

Figure 4.2 Probability density function overlaid on the notch depth histogram(in dB) for the single interference case. The example uses a 50-sensor ULA with half-wave-length spacing. Here $N = 50$, $L = 25$, $\rho_{INR} = 15dB$, $\sigma_s^2 = 10, \sigma_1^2 = 32, \sigma_n^2 = 1$, $\theta_s = 10°$, $\theta_1 = 80°$. LHS histogram uses $L = N/2 = 25$ snapshots, while the RHS uses $L = 20N = 1000$ snapshots.

4.3 Numerical Results

In our simulation, we use a ULA of 50 sensors with half-wavelength spacing. Figure 4.1 shows that the distribution function of G_{notch} fits the simulated ND data well for the single interference case. The histograms of $G = -10\log_{10}(G_{notch})$ in dB are shown in Figure 4.2 to compare the performance of our model accuracy. Inspired by the snapshot analysis of adaptive MVDR beamformer in [41], we also show the PDF and ND histogram with varying L and fixed N. The result compares the NDs of the DMR ABFs with $L = 0.5N = 25$ and $L = 20N = 1000$ snapshots. Note that the ND histograms are unimodal and asymmetric. The tail on the RHS (lower ND values) is

longer than the tail on the LHS (higher ND values). As L/N increases, simulation results approach to the ensemble value of $G = 100dB$. Note our result will fail for the snapshot severely deficient case or at a low level of INR.

4.4 Summary and Conclusion

This chapter presents a theoretical analysis for the ND of the DMR based ABF. A closed-form expression has been derived for the PDF of ND. Numerical results demonstrate the close approximation between proposed distribution function and the simulated ND histogram. Our result applies to the case of single interference with reasonable levels of INR when the angle between the SOI and interference direction satisfies Rayleigh resolution. The PDF shows the ND of the DMR based ABF is related to the number of snapshots, INR, the SOI and interference direction [17].

CHAPTER 5

PERFORMANCE ANALYSIS OF DMR FOR MULTIPLE INTERFERERS CASE

In this chapter, we focus on an illustrative example of multiple planewave interference in spatially white noise. Section one gives an overview of the multiple interference case, and presents several standard metrics. Section two derives models of the notch depth (ND), white noise gain (WNG), and signal-to-interference-and-noise ratio (SINR) for the DMR ABF through an adaptive dimensionality reduction and subspace formulation technique. Section three presents RMT models. Section four compares the analytical results to the sample means computed through Monte-Carlo based simulations.

5.1 Background

5.1.1 Model and metrics for multiple interferers case

The narrowband planewave beamforming assumes that the lth data measured by an array consist of SOI plus D planewave interference and noise, which can be represented as

$$\mathbf{p}(l) = b_s(l)\,\mathbf{v}_s + \sum_{i=1}^{D} b_i(l)\,\mathbf{v}_i + \mathbf{n}(l) \tag{5.1}$$

where b_s is the amplitude of the signal vector $\mathbf{v}_s$, b_i is the amplitude of the planewave interference $\mathbf{v}_i$, $\mathbf{n}$ is a vector of complex noise samples.

For the N element sensor array oriented along z-axis, the normalized modes for signal and planewave interference can be represented as

$$\mathbf{v}_s = \frac{1}{\sqrt{N}} \begin{bmatrix} e^{j\frac{2\pi}{\lambda}cos(\theta_s)z_1} \\ \vdots \\ e^{j\frac{2\pi}{\lambda}cos(\theta_s)z_N} \end{bmatrix}, \mathbf{v}_1 = \frac{1}{\sqrt{N}} \begin{bmatrix} e^{j\frac{2\pi}{\lambda}cos(\theta_i)z_1} \\ \vdots \\ e^{j\frac{2\pi}{\lambda}cos(\theta_i)z_N} \end{bmatrix}$$

where λ is the wavelength, θ_i is the plavewave angle, and z_i is the location of the ith sensor. Without loss of generality, this paper assumes that the amplitudes b_s and b_i are zero-mean complex circular random variables and that the complex circular random noise is zero mean and spatially white.

The $N \times N$ ECM under *signal absent* for the multiple interference case can be represented as

$$\mathbf{\Sigma}_{I+N} = \sum_{i=1}^{D} \sigma_i^2 \mathbf{v}_i \mathbf{v}_i^{\mathbf{H}} + \sigma_n^2 \mathbf{I}_N \tag{5.2}$$

where σ_i^2 is the power in the ith interference source, and σ_n^2 is the white noise power.

The $N \times N$ SCM and its eigendecomposition are defined as

$$\mathbf{S} = \frac{1}{L} \sum_{l=1}^{L} \mathbf{p}\left(l\right) \mathbf{p}^{\mathrm{H}}\left(l\right) = \sum_{n=1}^{N} \lambda_n \mathbf{e}_n \mathbf{e}_n^{\mathrm{H}} \tag{5.3}$$

where $\mathbf{e}_i$ and λ_i are the sample eigenvectors and eigenvalues of $\mathbf{S}$, respectively. Thus, the $N \times N$ DMR-SCM is constructed as,

$$\mathbf{S}_{\mathrm{DMR}} = \lambda_i \mathbf{e}_1 \mathbf{e}_1^{\mathrm{H}} + \sum_{i=2}^{N} s_w^2 \mathbf{e}_i \mathbf{e}_i^{\mathrm{H}} \tag{5.4}$$

where $s_w^2 = \left(\frac{L}{L-1}\right)\left(\frac{1}{N-1}\right)\sum_{i=2}^{N}\lambda_i$ is the average of the scaled lowest eigenvalues.

The DMR ABF weight vector has the same form as the adaptive MVDR weight vector, with ECM $\mathbf{\Sigma}_{I+N}$ replaced by $\mathbf{S}_{\text{DMR}}$:

$$\mathbf{w}_{\text{DMR}} = \left(\mathbf{v}_s^{\text{H}}\mathbf{S}_{\text{DMR}}^{-1}\mathbf{v}_s\right)^{-1}\mathbf{S}_{\text{DMR}}^{-1}\mathbf{v}_s. \tag{5.5}$$

The WNG is a standard metric that quantifies the improvement in the SNR provided by a beamformer when the noise is spatially white. It is defined as

$$G_{WNG} \triangleq \frac{1}{\mathbf{w}_{\text{DMR}}^{\text{H}}\mathbf{w}_{\text{DMR}}} = \frac{\left|\mathbf{v}_s^{\mathbf{H}}\mathbf{S}_{\text{DMR}}^{-1}\mathbf{v}_s\right|^2}{\mathbf{v}_s^{\mathbf{H}}\mathbf{S}_{\text{DMR}}^{-2}\mathbf{v}_s} \tag{5.6}$$

The ND is defined as the amplitude square of the beampattern in the direction of an interference. That is, in the case of interference $\mathbf{v}_1$,

$$G_{notch} \triangleq \left|\mathbf{w}_{\text{DMR}}^{\text{H}}\mathbf{v}_1\right|^2 = \frac{\left|\mathbf{v}_s^{\mathbf{H}}\mathbf{S}_{\text{DMR}}^{-1}\mathbf{v}_1\right|^2}{\left|\mathbf{v}_s^{\mathbf{H}}\mathbf{S}_{\text{DMR}}^{-1}\mathbf{v}_s\right|^2}. \tag{5.7}$$

The SINR of a beamformer is defined as

$$\text{SINR} \triangleq \frac{\sigma_s^2\left|\mathbf{w}_{\text{DMR}}^{\text{H}}\mathbf{v}_s\right|^2}{\mathbf{w}_{\text{DMR}}^{\text{H}}\mathbf{\Sigma}_{\text{I+N}}\mathbf{w}_{\text{DMR}}} \tag{5.8}$$

where σ_s^2 is the desired signal power, $\mathbf{v}_s$ is the replica associated with the desired signal.

5.1.2 Inverse of DMR-SCM

The spectral decomposition of the $N \times N$ sample covariance matrix can be broken into two parts: one for the D largest eigenvalues and one for the $N - D$ smaller eigenvalues. Thus the inverse of DMR-SCM is

$$\mathbf{S}_{\mathrm{DMR}}^{-1} = \sum_{i=1}^{D} \lambda_i^{-1} \mathbf{e}_i \mathbf{e}_i^{\mathrm{H}} + \sum_{i=D+1}^{N} s_w^{-2} \mathbf{e}_i \mathbf{e}_i^{\mathrm{H}} = \frac{1}{s_w^2} \left[\mathbf{I} - \sum_{i=1}^{D} \frac{\lambda_i - s_w^2}{\lambda_i} \mathbf{e}_i \mathbf{e}_i^{\mathrm{H}} \right] \tag{5.9}$$

where s_w^2 is the estimated noise power $s_w^2 = \left(\frac{1}{N-D} \right) \sum_{n=D+1}^{N} \lambda_n$.

Let $\mathbf{E_D} = [\mathbf{e_1} \cdots \mathbf{e_D}]$ and $\mathbf{\Lambda} = diag \left(\frac{s_w^2}{\lambda_1}, \cdots, \frac{s_w^2}{\lambda_D} \right)$, the matrix form of DMR SCM can be written as

$$\mathbf{S}_{\mathrm{DMR}}^{-1} = \left(\frac{1}{s_w^2} \right) \left(\mathbf{I} - \mathbf{E_D} \mathbf{E_D^H} + \mathbf{E_D} \mathbf{\Lambda} \mathbf{E_D}^{\mathbf{H}} \right) = \left(\frac{1}{s_w^2} \right) \left(\mathbf{P}_{\mathbf{E_D}}^{\perp} + \mathbf{E_D} \mathbf{\Lambda} \mathbf{E_D}^{\mathbf{H}} \right) \tag{5.10}$$

$$\mathbf{S}_{\mathrm{DMR}}^{-2} = \left(\frac{1}{s_w^2} \right)^2 \left(\mathbf{P}_{\mathbf{E_D}}^{\perp} + \mathbf{E_D} \mathbf{\Lambda^2} \mathbf{E_D}^{\mathbf{H}} \right) \tag{5.11}$$

where $\mathbf{P}_{\mathbf{E_D}}^{\perp} = \mathbf{I} - \mathbf{E_D} \mathbf{E_D}^{\mathbf{H}}$.

5.2 Adaptive Dimensionality Reduction and Subspace Formulation Technique

5.2.1 Unitary transformation matrix

The eigen-decomposition of ECM is

$$\mathbf{\Sigma}_{I+N} = \sum_{i=1}^{D} \sigma_i^2 \mathbf{v}_i \mathbf{v}_i^{\mathbf{H}} + \sigma_n^2 \mathbf{I} = \mathbf{\Xi \Gamma \Xi}^H \tag{5.12}$$

where $\mathbf{\Gamma} = \text{diag}\,(\gamma_1, \ldots, \gamma_D, \sigma_n^2, \ldots, \sigma_n^2)$ is a diagonal matrix of eigenvalues with descend order such that $\gamma_1 \geq \cdots \gamma_D > \sigma_n^2$. The corresponding eigenvectors are $\mathbf{\Xi} = [\boldsymbol{\xi}_1, \cdots, \boldsymbol{\xi}_N]$.

We will use adaptive dimensionality reduction and subspace formulation technique from Chapter 2 to construct an unitary tranformation matrix $\mathbf{\Phi}$. The principle is makes sure one column of the random unitary matrix $\mathbf{\Phi}$ is aligned with the SOI vector, and other D columns equal to the first D ensemble eigenvectors $[\boldsymbol{\xi}_1, \cdots, \boldsymbol{\xi}_D]$.

Let the $N \times N$ unitary tranformation matrix $\mathbf{\Phi}$ be constructed as a complete and orthonormal basis:

$$\mathbf{\Phi} = [\boldsymbol{\phi}_s \;\; \boldsymbol{\xi}_1 \cdots \boldsymbol{\xi}_D \;\; \mathbf{\Phi}_\perp] \tag{5.13}$$

where $\boldsymbol{\phi}_s$ is the array manifold for the desired look direction,

$$\boldsymbol{\phi}_s = \frac{\mathbf{v}_s - \sum_{i=1}^{D} \boldsymbol{\xi}_i \boldsymbol{\xi}_i^H \mathbf{v}_s}{\left| \mathbf{v}_s - \sum_{i=1}^{D} \boldsymbol{\xi}_i \boldsymbol{\xi}_i^H \mathbf{v}_s \right|} \tag{5.14}$$

Note it is orthogonal to the ensemble interference subspace.

Therefore, the multiplication of $\mathbf{v}_s$, $\mathbf{v}_1$ and $\mathbf{\Phi}$ leads to the unitary transformation as

$$\boldsymbol{\nu}_s = \mathbf{\Phi}^H \mathbf{v}_s = [\boldsymbol{\upsilon}_s \;\; 0 \cdots 0]^T = \left[\boldsymbol{\phi}_s^H \mathbf{v}_s \;\; \boldsymbol{\xi}_1^H \mathbf{v}_s \cdots \boldsymbol{\xi}_D^H \mathbf{v}_s \;\; 0 \cdots 0\right]^T \tag{5.15}$$

$$\boldsymbol{\nu}_i = \mathbf{\Phi}^H \mathbf{v}_i = \left[\boldsymbol{\upsilon}_i \;\; \mathbf{\Phi}_\perp^H \mathbf{v}_i\right]^T = \left[\boldsymbol{\phi}_s^H \mathbf{v}_i \;\; \boldsymbol{\xi}_1^H \mathbf{v}_i \cdots \boldsymbol{\xi}_D^H \mathbf{v}_i \;\; \mathbf{\Phi}_\perp^H \mathbf{v}_i\right]^T, i = 1 \ldots D \tag{5.16}$$

where $\boldsymbol{\upsilon}_s = \left[\boldsymbol{\phi}_s^H \mathbf{v}_s \;\; \boldsymbol{\xi}_1^H \mathbf{v}_s \cdots \boldsymbol{\xi}_D^H \mathbf{v}_s\right]^T$, and $\boldsymbol{\upsilon}_i = \left[\boldsymbol{\phi}_s^H \mathbf{v}_i \;\; \boldsymbol{\xi}_1^H \mathbf{v}_i \cdots \boldsymbol{\xi}_D^H \mathbf{v}_i\right]^T$.

In the next, we will expresse WNG, ND, and SINR loss in terms of random matrices containing sample and ensemble eigenvectors and eigenvalues.

5.2.2 DMR white noise gain

The DMR WNG is given by

$$G_{WNG} \triangleq \frac{1}{\mathbf{w}_{\mathrm{DMR}}^{\mathrm{H}}\mathbf{w}_{\mathrm{DMR}}} = \frac{\left|\mathbf{v}_s^{\mathbf{H}}\mathbf{S}_{\mathrm{DMR}}^{-1}\mathbf{v}_s\right|^2}{\mathbf{v}_s^{\mathbf{H}}\mathbf{S}_{\mathrm{DMR}}^{-2}\mathbf{v}_s} = \frac{\left|\mathbf{v}_s^{\mathbf{H}}\mathbf{\Phi}\mathbf{\Phi}^H\mathbf{S}_{\mathrm{DMR}}^{-1}\mathbf{\Phi}\mathbf{\Phi}^H\mathbf{v}_s\right|^2}{\mathbf{v}_s^{\mathbf{H}}\mathbf{\Phi}\mathbf{\Phi}^H\mathbf{S}_{\mathrm{DMR}}^{-2}\mathbf{\Phi}\mathbf{\Phi}^H\mathbf{v}_s} \tag{5.17}$$

Since $\nu_s = \mathbf{\Phi}^H\mathbf{v}_s$,

$$G_{WNG} = \frac{\left|\boldsymbol{\nu}_s^{\mathbf{H}}\mathbf{\Phi}^H\mathbf{S}_{\mathrm{DMR}}^{-1}\mathbf{\Phi}\boldsymbol{\nu}_s\right|^2}{\boldsymbol{\nu}_s^{\mathbf{H}}\mathbf{\Phi}^H\mathbf{S}_{\mathrm{DMR}}^{-2}\mathbf{\Phi}\boldsymbol{\nu}_s} \tag{5.18}$$

Substituting the DMR covariance into the expression, we have

$$\mathbf{\Phi}^H\mathbf{S}_{\mathrm{DMR}}^{-1}\mathbf{\Phi} = \frac{1}{s_w^2}\left[\boldsymbol{\phi}_s^H \;\; \boldsymbol{\xi}_1^H\cdots\boldsymbol{\xi}_D^H \;\; \mathbf{\Phi}_\perp^H\right]^T\left(\mathbf{P}_{\mathbf{E_D}}^{\perp} + \mathbf{E_D}\mathbf{\Lambda}\mathbf{E_D}^{\mathbf{H}}\right)\left[\boldsymbol{\phi}_s \;\; \boldsymbol{\xi}_1\cdots\boldsymbol{\xi}_D \;\; \mathbf{\Phi}_\perp\right] \tag{5.19}$$

$$\mathbf{\Phi}^H\mathbf{S}_{\mathrm{DMR}}^{-2}\mathbf{\Phi} = \left(\frac{1}{s_w^2}\right)^2\left[\boldsymbol{\phi}_s^H \;\; \boldsymbol{\xi}_1^H\cdots\boldsymbol{\xi}_D^H \;\; \mathbf{\Phi}_\perp^H\right]^T\left(\mathbf{P}_{\mathbf{E_D}}^{\perp} + \mathbf{E_D}\mathbf{\Lambda^2}\mathbf{E_D}^{\mathbf{H}}\right)\left[\boldsymbol{\phi}_s \;\; \boldsymbol{\xi}_1\cdots\boldsymbol{\xi}_D \;\; \mathbf{\Phi}_\perp\right] \tag{5.20}$$

Let us define $(D+1)\times(D+1)$ matrices,

$$\mathbf{\Delta}_k = \left[\boldsymbol{\phi}_s^H \;\; \boldsymbol{\xi}_1^H\cdots\boldsymbol{\xi}_D^H\right]^T\mathbf{E_D}\mathbf{\Lambda}^k\mathbf{E_D}^H\left[\boldsymbol{\phi}_s \;\; \boldsymbol{\xi}_1\cdots\boldsymbol{\xi}_D\right], k = 0, 1, 2 \tag{5.21}$$

Therefore, both the numerator and denominator of (5.18) are quadratic forms. Note matrix ν_s have $N - D - 1$ zeros, thus we can simplify both the numerator and

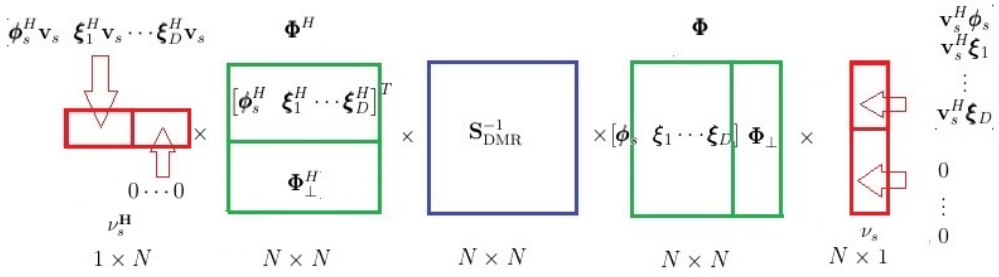

Figure 5.1 Matrix multiplication of the numerator of Equation(5.20). The number of columns in the first matrix equals N.

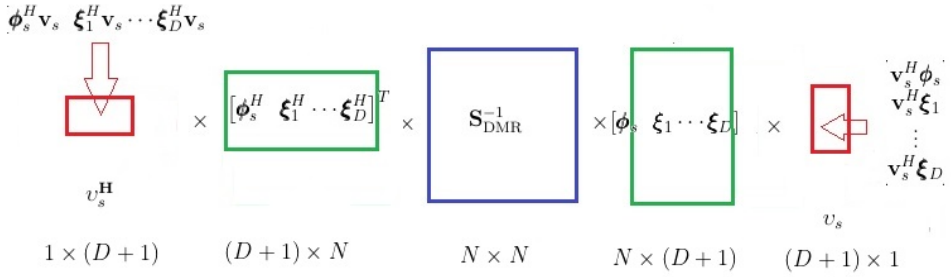

Figure 5.2 Matrix multiplication of the numerator of Equation(5.20). The number of columns in the first matrix equals $D+1$.

denominator as the multiplication of rank $D+1$ matrices (Figures 5.1-5.2). Therefore, the WNG can be computed as

$$G_{WNG} = \frac{\left(1-\boldsymbol{\upsilon}_s^{\mathbf{H}}\left(\boldsymbol{\Delta}_0-\boldsymbol{\Delta}_1\right)\boldsymbol{\upsilon}_s\right)^2}{1-\boldsymbol{\upsilon}_s^{\mathbf{H}}\left(\boldsymbol{\Delta}_0-\boldsymbol{\Delta}_2\right)\boldsymbol{\upsilon}_s} \tag{5.22}$$

where $\boldsymbol{\upsilon}_s = \left[\boldsymbol{\phi}_s^H\mathbf{v}_s \;\; \boldsymbol{\xi}_1^H\mathbf{v}_s\cdots\boldsymbol{\xi}_D^H\mathbf{v}_s\right]^T$.

5.2.3 DMR notch depth

The DMR ND for the ith interference is given by

$$G_{notch}^{(i)} \triangleq \left|\mathbf{w}_{\mathrm{DMR}}^{\mathrm{H}}\mathbf{v}_i\right|^2 = \frac{\left|\mathbf{v}_s^{\mathbf{H}}\mathbf{S}_{\mathrm{DMR}}^{-1}\mathbf{v}_i\right|^2}{\left|\mathbf{v}_s^{\mathbf{H}}\mathbf{S}_{\mathrm{DMR}}^{-1}\mathbf{v}_s\right|^2} = \frac{\left|\mathbf{v}_s^{\mathbf{H}}\mathbf{\Phi}\mathbf{\Phi}^H\mathbf{S}_{\mathrm{DMR}}^{-1}\mathbf{\Phi}\mathbf{\Phi}^H\mathbf{v}_i\right|^2}{\left|\mathbf{v}_s^{\mathbf{H}}\mathbf{\Phi}\mathbf{\Phi}^H\mathbf{S}_{\mathrm{DMR}}^{-2}\mathbf{\Phi}\mathbf{\Phi}^H\mathbf{v}_s\right|^2}, \quad i = 1...D \tag{5.23}$$

Since $\boldsymbol{\nu}_s = \mathbf{\Phi}^H\mathbf{v}_s$,

$$G_{notch}^{(i)} = \frac{\left|\boldsymbol{\nu}_s^{\mathbf{H}}\mathbf{\Phi}^H\mathbf{S}_{\mathrm{DMR}}^{-1}\mathbf{\Phi}\boldsymbol{\nu}_i\right|^2}{\left|\boldsymbol{\nu}_s^{\mathbf{H}}\mathbf{\Phi}^H\mathbf{S}_{\mathrm{DMR}}^{-2}\mathbf{\Phi}\boldsymbol{\nu}_s\right|^2}, \quad i = 1...D \tag{5.24}$$

Substituting the DMR covariance into the expression, we can also get equation (5.21) and (5.22).

Therefore, the ND can be computed as

$$G_{notch}^{(i)} = \rho_{INR}^{(i)} \cdot \frac{\left(\boldsymbol{v}_s^{\mathbf{H}}\boldsymbol{v}_i - \boldsymbol{v}_s^{\mathbf{H}}\left(\mathbf{\Delta}_0 - \mathbf{\Delta}_1\right)\boldsymbol{v}_i\right)^2}{\left(1 - \boldsymbol{v}_s^{\mathbf{H}}\left(\mathbf{\Delta}_0 - \mathbf{\Delta}_1\right)\boldsymbol{v}_s\right)^2} \tag{5.25}$$

where $\mathbf{\Delta}_k = \left[\boldsymbol{\phi}_s^H \;\; \boldsymbol{\xi}_1^H \cdots \boldsymbol{\xi}_D^H\right]^T \mathbf{E}\mathbf{\Lambda}^k\mathbf{E}^H\left[\boldsymbol{\phi}_s \;\; \boldsymbol{\xi}_1 \cdots \boldsymbol{\xi}_D\right], k = 0, 1, 2.$

5.2.4 DMR SINR

The DMR SINR is

$$\begin{aligned}\mathrm{SINR} \triangleq & \frac{\sigma_s^2\left|\mathbf{w}_{\mathrm{DMR}}^{\mathrm{H}}\mathbf{v}_s\right|^2}{\mathbf{w}_{\mathrm{DMR}}^{\mathrm{H}}\mathbf{\Sigma}_{\mathrm{I+N}}\mathbf{w}_{\mathrm{DMR}}} = \frac{\frac{\sigma_s^2}{\sigma_n^2}\left|\mathbf{w}_{DMR}^H\mathbf{v}_s\right|^2}{\sum_{i=1}^{D}\frac{\sigma_i^2}{\sigma_n^2}\left|\mathbf{w}_{DMR}^H\mathbf{v}_i\right|^2 + \mathbf{w}_{DMR}^H\mathbf{w}_{DMR}} \\ & = \frac{\rho_{SNR}}{\sum_{i=1}^{D}\left(\rho_{INR}^{(i)}\right)^2 \cdot G_{notch}^{(i)} + G_{WNG}^{-1}}\end{aligned} \tag{5.26}$$

The terms in the denominator represent the power of the interference and the power of the white noise at the output of the ABF. Note the SINR is a function of WNG, ND, SNR and INRs. Combined with $G_{notch}^{(i)}$ and G_{WNG}, we get

$$SINR = \rho_{SNR} \cdot \left(\sum_{i=1}^{D} \left(\rho_{INR}^{(i)} \right)^2 \cdot \frac{\left(\boldsymbol{v}_s^{\mathbf{H}} \boldsymbol{v}_i - \boldsymbol{v}_s^{\mathbf{H}} \left(\boldsymbol{\Delta}_0 - \boldsymbol{\Delta}_1 \right) \boldsymbol{v}_i \right)^2}{\left(1 - \boldsymbol{v}_s^{\mathbf{H}} \left(\boldsymbol{\Delta}_0 - \boldsymbol{\Delta}_1 \right) \boldsymbol{v}_s \right)^2} + \frac{1 - \boldsymbol{v}_s^{\mathbf{H}} \left(\boldsymbol{\Delta}_0 - \boldsymbol{\Delta}_2 \right) \boldsymbol{v}_s}{\left(1 - \boldsymbol{v}_s^{\mathbf{H}} \left(\boldsymbol{\Delta}_0 - \boldsymbol{\Delta}_1 \right) \boldsymbol{v}_s \right)^2} \right)^{-1} \tag{5.27}$$

5.3 RMT Models

In snapshot-deficient case, classical asymptotic results for the eigenvalues and eigenvectors do not perform well. RMT asymptotic analysis differs from the classical mthods. It characterizes the sample eigenvalues and sample eigenvectors of SCM. Recent work on RMT contains valuable insights about the behavior of the eigenvalues and eigenvectors of large random matrices. RMT predicts that the sample eigenvectors have a phase transition [6, 28, 29]. When the INR is above the threshold, the sample eigenvector is a biased estimate of the true eigenvector. The sample eigenvector lies on a cone around the true eigenvector.

As shown in [39], the sample eigenvectors have a greater impact on DMR performance than the sample eigenvalues. Paul [29], Nadler [28], and Benaych-Georges and Nadakuditi [6] describe the eigenvectors of the spiked covariance model (when some of the eigenvalues are larger than 1 and the others are 1, then the model is called spiked covariance model). This model assumes that the data consist of one or more loud signals plus white noise. The RMT analysis of the spiked covariance case is asymptotic $N, L \to \infty$ and the ratio $N/L = c$. The spiked covariance model is characterized by an ECM with eigenvalues $\gamma_1 \geq \cdots \gamma_D > 1 + \sqrt{c}$. Since the spiked covariance model ECM matches that of the DMR model, the eigenvalue and eigenvector results for spiked covariance are applicable to modeling the WNG, ND

and SINR. The spikes are consist of the D largest spectral components that exceed the phase transition threshold $1+\sqrt{c}$ can represent the interferers in the DMR model.

5.3.1 Sample eigenvalues

In [4], Baik and Silverstein consider a spiked population model whose population eigenvalues are all unit except for a few fixed eigenvalues. It shows sample eigenvalue λ_i asymptotically converges to

$$\lambda_i \to \gamma_i + \frac{\gamma_i c}{\gamma_i - 1} \tag{5.28}$$

Note that as $c \to 0$, $\lambda_i \to \gamma_i$, it will match the classical asymptotic results.

5.3.2 Sample eigenvectors

The key result related to DMR is a prediction of the limiting value of the generalized cosine between the ensemble eigenvector and the sample eigenvector [29]

$$\cos^2(\boldsymbol{\xi}_i, \mathbf{e}_i) \to \begin{cases} 0, & \text{if } N \cdot \rho_{INR} \le \sqrt{c} \\ \dfrac{1 - \frac{c}{(\gamma_i/\sigma_n^2 - 1)^2}}{1 + \frac{c}{(\gamma_i/\sigma_n^2 - 1)}}, & \text{if } N \cdot \rho_{INR} > \sqrt{c} \end{cases} \tag{5.29}$$

This describes a phase transition phenomenon. Then the scalar product of ensemble eigenvectors $\boldsymbol{\xi}_i$ and $\boldsymbol{\xi}_j$ in subspace spanned by $\{\mathbf{e}_1, \cdots, \mathbf{e}_D\}$ is approximate to

$$\boldsymbol{\xi}_i^H \sum_{k=1}^{D} \mathbf{e}_k \mathbf{e}_k^H \boldsymbol{\xi}_j \to \begin{cases} 0, & \text{if } i \neq j \\ \dfrac{1 - \frac{c}{(\gamma_i/\sigma_n^2 - 1)^2}}{1 + \frac{c}{(\gamma_i/\sigma_n^2 - 1)}} = \mu_i, & \text{if } i = j \end{cases} \tag{5.30}$$

Considering $i = j$, as $c \to 0$, $\boldsymbol{\xi}_i^H \sum_{k=1}^{D} \mathbf{e}_k \mathbf{e}_k^H \boldsymbol{\xi}_j \to 1$, this means the ensemble interference eigenvector is completely contained in the sample eigenvector subspace. Thus the accuracy of the sample outlier subspace as a prediction of the ensemble outlier subspace increases as the number of snapshots increases for a fixed dimension. The sample outlier eigenvector is unbiased in directions orthogonal to ensemble outlier eigenvector when the ensemble outliers are well separated. Thus the error component of the sample eigenvector is uniformly distributed over the ensemble bulk subspace [6, 28, 29].

5.3.3 The bound for RMT model

It is important to note that our results only have a good match for reasonable levels of INR. As the spiked covariance model is characterized by an ECM with eigenvalues $\gamma_1 \geq \cdots \gamma_D > 1 + \sqrt{c} = 1 + \sqrt{N/L}$, the minimum reasonable level of INR is $10 \log_{10} \left(1 + \sqrt{N/L}\right)$.

One more point, DMR requires at least two snapshots for the single interference example since it needs an estimate of the dominant subspace and an estimate of the power in the noise subspace. The dominant subspace is defined by the eigenvector associated with the maximum eigenvalue. With two snapshots, the noise power is simply a scaled version of the only other nonzero eigenvalue. For the multiple interference case, DMR requires at least $D + 1$ snapshots. The dominant subspace needs D largest eigenvalues and the dominant subspace needs the smallest eigenvalue.

5.3.4 Calculate matrix $\boldsymbol{\Delta}_k$

The $(D + 1) \times (D + 1)$ matrix $\boldsymbol{\Delta}_k$ is a diagonal matrix.

$$\boldsymbol{\Delta}_k = \left[\boldsymbol{\phi}_s^H \;\; \boldsymbol{\xi}_1^H \cdots \boldsymbol{\xi}_D^H\right]^T \mathbf{E_D} \boldsymbol{\Lambda}^k \mathbf{E_D}^H \left[\boldsymbol{\phi}_s \;\; \boldsymbol{\xi}_1 \cdots \boldsymbol{\xi}_D\right], k = 0, 1, 2 \tag{5.31}$$

For the element in 1st column and 1st row: $\boldsymbol{\phi}_s^H \mathbf{E_D} \boldsymbol{\Lambda}^k \mathbf{E_D}^H \boldsymbol{\phi}_s$, $\boldsymbol{\phi}_s$ is the ensemble eigenvector while $\boldsymbol{e}_i,\ i = 1 \cdots D$ are sample eigenvectors. As introduced before, the sample outlier eigenvectors are unbiased in directions orthogonal to the ensemble outlier. Then the residual outlier energy $1 - \mu_i$ will be uniformly distributed over the $N - D$ eigenvectors. Thus,

$$\boldsymbol{\phi}_s^H \mathbf{E_D} \boldsymbol{\Lambda}^k \mathbf{E_D}^H \boldsymbol{\phi}_s \to \sum_{i=1}^{D} \frac{\lambda_i^{-k}(1-\mu_i)}{N-D} \tag{5.32}$$

For the element in ist column and ist row: $\boldsymbol{\xi}_i^H \mathbf{E_D} \boldsymbol{\Lambda}^k \mathbf{E_D}^H \boldsymbol{\xi}_i \to \lambda_i^{-k} \mu_i$.

Using the RMT results for the sample eigenvectors and eigenvalues of the spiked covariance model, we have the RMT approximations of $\boldsymbol{\Delta}_k$:

$$\boldsymbol{\Delta}_k = diag\left\{ \sum_{i=1}^{D} \frac{\lambda_i^{-k}(1-\mu_i)}{N-D}, \lambda_1^{-k}\mu_1, \cdots, \lambda_D^{-k}\mu_D \right\} \tag{5.33}$$

5.3.5 RMT result for white noise gain

$$G_{WNG} = \frac{\left(1 - \boldsymbol{v}_s^{\mathbf{H}} \left(\boldsymbol{\Delta}_0 - \boldsymbol{\Delta}_1\right) \boldsymbol{v}_s\right)^2}{1 - \boldsymbol{v}_s^{\mathbf{H}} \left(\boldsymbol{\Delta}_0 - \boldsymbol{\Delta}_2\right) \boldsymbol{v}_s} \tag{5.34}$$

where $\boldsymbol{v}_s = \left[\boldsymbol{\phi}_s^H \mathbf{v}_s \ \ \boldsymbol{\xi}_1^H \mathbf{v}_s \cdots \boldsymbol{\xi}_D^H \mathbf{v}_s\right]^T$.

5.3.6 RMT result for notch depth

$$G_{notch}^{(i)} = \rho_{INR}^{(i)} \cdot \frac{\left(\boldsymbol{v}_s^{\mathbf{H}} \boldsymbol{v}_i - \boldsymbol{v}_s^{\mathbf{H}} \left(\boldsymbol{\Delta}_0 - \boldsymbol{\Delta}_1\right) \boldsymbol{v}_i\right)^2}{\left(1 - \boldsymbol{v}_s^{\mathbf{H}} \left(\boldsymbol{\Delta}_0 - \boldsymbol{\Delta}_1\right) \boldsymbol{v}_s\right)^2} \tag{5.35}$$

where $\boldsymbol{v}_s = \left[\boldsymbol{\phi}_s^H \mathbf{v}_s \ \ \boldsymbol{\xi}_1^H \mathbf{v}_s \cdots \boldsymbol{\xi}_D^H \mathbf{v}_s\right]^T$, and $\boldsymbol{v}_i = \left[\boldsymbol{\phi}_s^H \mathbf{v}_i \ \ \boldsymbol{\xi}_1^H \mathbf{v}_i \cdots \boldsymbol{\xi}_D^H \mathbf{v}_i\right]^T$.

5.3.7 RMT result for SINR

$$SINR = \rho_{SNR} \cdot \left(\sum_{i=1}^{D} \left(\rho_{INR}^{(i)} \right)^2 \cdot \frac{\left(\boldsymbol{v}_s^{\mathbf{H}} \boldsymbol{v}_i - \boldsymbol{v}_s^{\mathbf{H}} \left(\boldsymbol{\Delta}_0 - \boldsymbol{\Delta}_1 \right) \boldsymbol{v}_i \right)^2}{\left(1 - \boldsymbol{v}_s^{\mathbf{H}} \left(\boldsymbol{\Delta}_0 - \boldsymbol{\Delta}_1 \right) \boldsymbol{v}_s \right)^2} + \frac{1 - \boldsymbol{v}_s^{\mathbf{H}} \left(\boldsymbol{\Delta}_0 - \boldsymbol{\Delta}_2 \right) \boldsymbol{v}_s}{\left(1 - \boldsymbol{v}_s^{\mathbf{H}} \left(\boldsymbol{\Delta}_0 - \boldsymbol{\Delta}_1 \right) \boldsymbol{v}_s \right)^2} \right)^{-1} \tag{5.36}$$

equations (5.33-5.35) are the RMT results, the expressions contain SNR, INR, the number of sensors N, the number of snapshots L ($c = N/L$), the ensemble interference rank D, ensemble eigenvalues γ_i, SOI $\mathbf{v}_s$ and interference $\mathbf{v}_1$.

5.4 Simulation for RMT Results

In this section, we compares the RMT models to the sample means computed through Monte Carlo simulations. The comparisons are under multiple interference scenarios. We use a ULA of $N = 50$ sensors with half-wavelength spacing.

In Figures 5.3-5.8, the solid line denotes the mean and the error bars mark the span between the 10th and 90th percentiles of the data. Results are shown for WNG generated using 1000 trials for each snapshot. Figures 5.3-5.4 show the RMT based DMR ABF WNG model predictions and sample means of Monte Carlo simulations. The results show our model predictions match the sample mean, even for the snapshot deficient case.

Figures 5.5-5.6 show the RMT based DMR ABF ND model predictions and sample means of Monte Carlo simulations. The results show our model predictions match the sample mean for the snapshot deficient case. But there is a little deviation in the low INR part. The reason is equation(5.26) is derived under the assumption of $\boldsymbol{\Phi}_{\perp}^{H} \mathbf{v}_i \approx \underline{0}$, which only works under high INRs.

Figures 5.7-5.8 show the RMT based DMR ABF SINR model predictions and sample means of Monte Carlo simulations. The performance is still good under high INRs case while poor under low INRs. Similarly, the results show well for the snapshot deficient case.

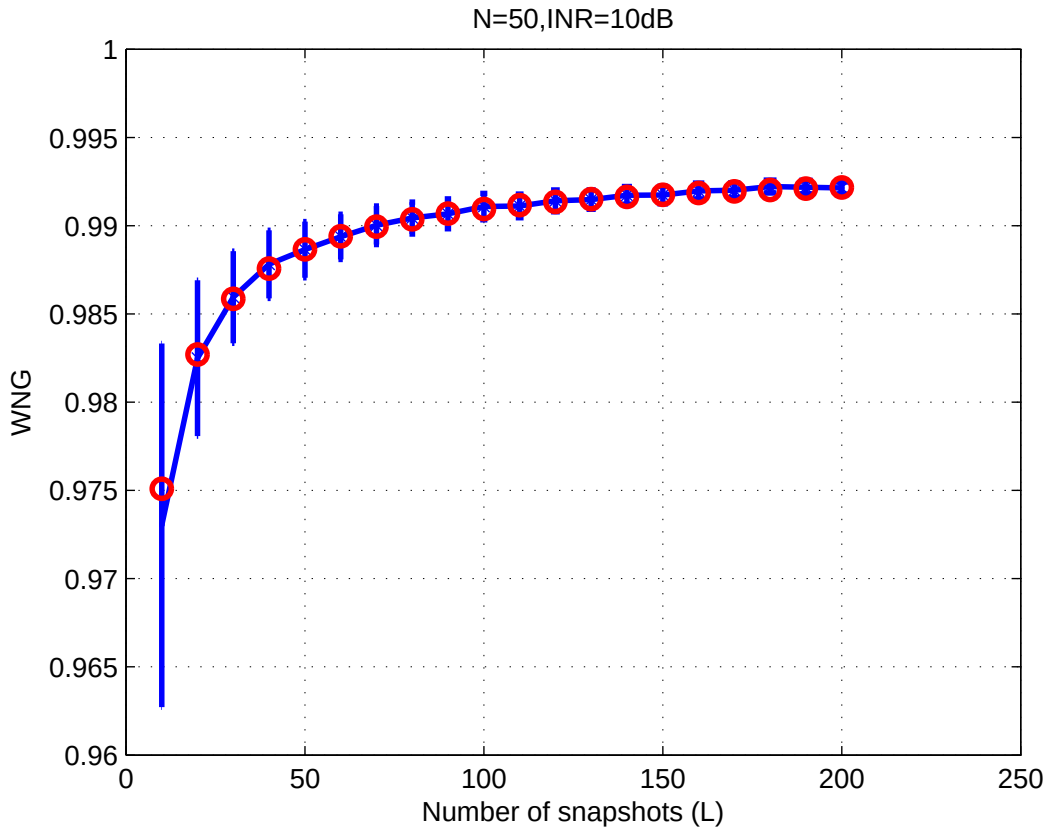

Figure 5.3 The RMT based DMR ABF WNG model predictions(red circles) and sample means of Monte Carlo simulations (blue lines) with L ranges from 5 to 200. There are $D = 3$ interferences. The example uses a 50-sensor ULA with half-wavelength spacing. Here $N = 50$, $\sigma_s^2 = 10, \sigma_1^2 = \sigma_2^2 = \sigma_3^2 = 10, \sigma_n^2 = 1$, $\theta_s = 30°$, $\theta_1 = 20°$, $\theta_2 = 60°$, $\theta_3 = 80°$.

5.5 Distribution for WNG

Let $\alpha_i = \boldsymbol{\xi}_i^H \mathbf{E_D} \mathbf{E_D}^H \boldsymbol{\xi}_i, \quad i = 1 \cdots D$, and $\alpha_{D+1} = \boldsymbol{\phi}_s^H \mathbf{E_D} \mathbf{E_D}^H \boldsymbol{\phi}_s \approx \sum_{i=1}^{D} \frac{(1-\alpha_i)}{N-D}$. For the model here [29, 40], we can get: $\boldsymbol{\xi}_i^H \mathbf{E_D} \boldsymbol{\Lambda}^k \mathbf{E_D}^H \boldsymbol{\xi}_i \approx \lambda_i^{-k} \alpha_i, \quad i = 1 \cdots D$ and $\boldsymbol{\phi}_s^H \mathbf{E_D} \boldsymbol{\Lambda}^k \mathbf{E_D}^H \boldsymbol{\phi}_s \approx \lambda_i^{-k} \alpha_{D+1}$. From [29, 40], α_i is a random variable that converges in distribution to a chi-squared variable: $\alpha_i \sim \frac{\mu_i}{D} \chi^2(D)$, where $\mu_i =$

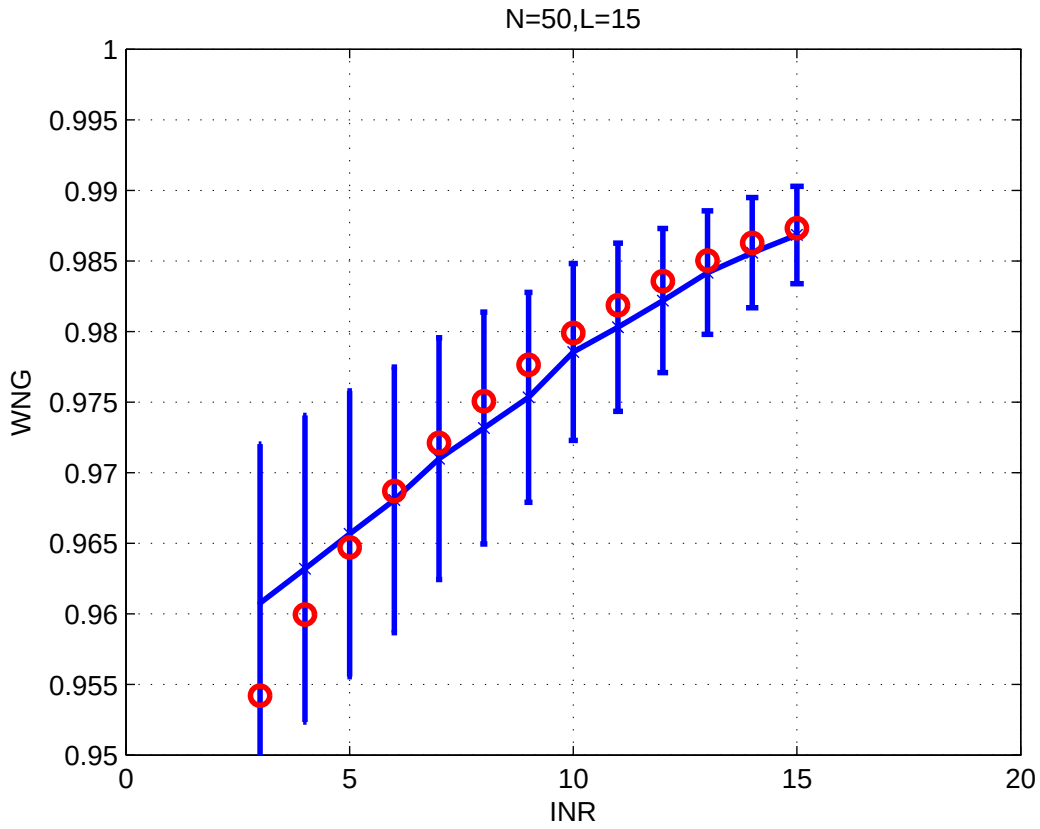

Figure 5.4 The RMT based DMR ABF WNG model predictions(red circles) and sample means of Monte Carlo simulations (blue lines) with INR ranges from $3dB$ to $15dB$. There are $D = 3$ interferences. The example uses a 50-sensor ULA with half-wave-length spacing. Here $N = 50$, $L = 15$, $\sigma_s^2 = 10, \sigma_n^2 = 1$, $\theta_s = 30°$, $\theta_1 = 20°$, $\theta_2 = 60°$, $\theta_3 = 80°$.

$\left(1 - \frac{c}{(\gamma_i/\sigma_n^2 - 1)^2}\right) / \left(1 + \frac{c}{(\gamma_i/\sigma_n^2 - 1)}\right)$. Therefore,

$$
\begin{aligned}
G_{WNG} &= \frac{\left(1 - \boldsymbol{v}_s^{\mathbf{H}} \left(\boldsymbol{\Delta}_0 - \boldsymbol{\Delta}_1\right) \boldsymbol{v}_s\right)^2}{1 - \boldsymbol{v}_s^{\mathbf{H}} \left(\boldsymbol{\Delta}_0 - \boldsymbol{\Delta}_2\right) \boldsymbol{v}_s} \\
&= \frac{\left(1 - \sum_{i=1}^{D} \left|\boldsymbol{\xi}_i^H \mathbf{v}_s\right|^2 \cdot \alpha_i \left(1 - \lambda_i^{-1}\right) - \frac{\left|\boldsymbol{\phi}_s^H \mathbf{v}_s\right|^2}{N-D} \sum_{i=1}^{D} \left(1 - \lambda_i^{-1}\right) \left(1 - \alpha_i\right)\right)^2}{1 - \sum_{i=1}^{D} \left|\boldsymbol{\xi}_i^H \mathbf{v}_s\right|^2 \cdot \alpha_i \left(1 - \lambda_i^{-2}\right) - \frac{\left|\boldsymbol{\phi}_s^H \mathbf{v}_s\right|^2}{N-D} \sum_{i=1}^{D} \left(1 - \lambda_i^{-2}\right) \left(1 - \alpha_i\right)}
\end{aligned}
\tag{5.37}
$$

where $\boldsymbol{v}_s = \left[\boldsymbol{\phi}_s^H \mathbf{v}_s \;\; \boldsymbol{\xi}_1^H \mathbf{v}_s \cdots \boldsymbol{\xi}_D^H \mathbf{v}_s\right]^T$.

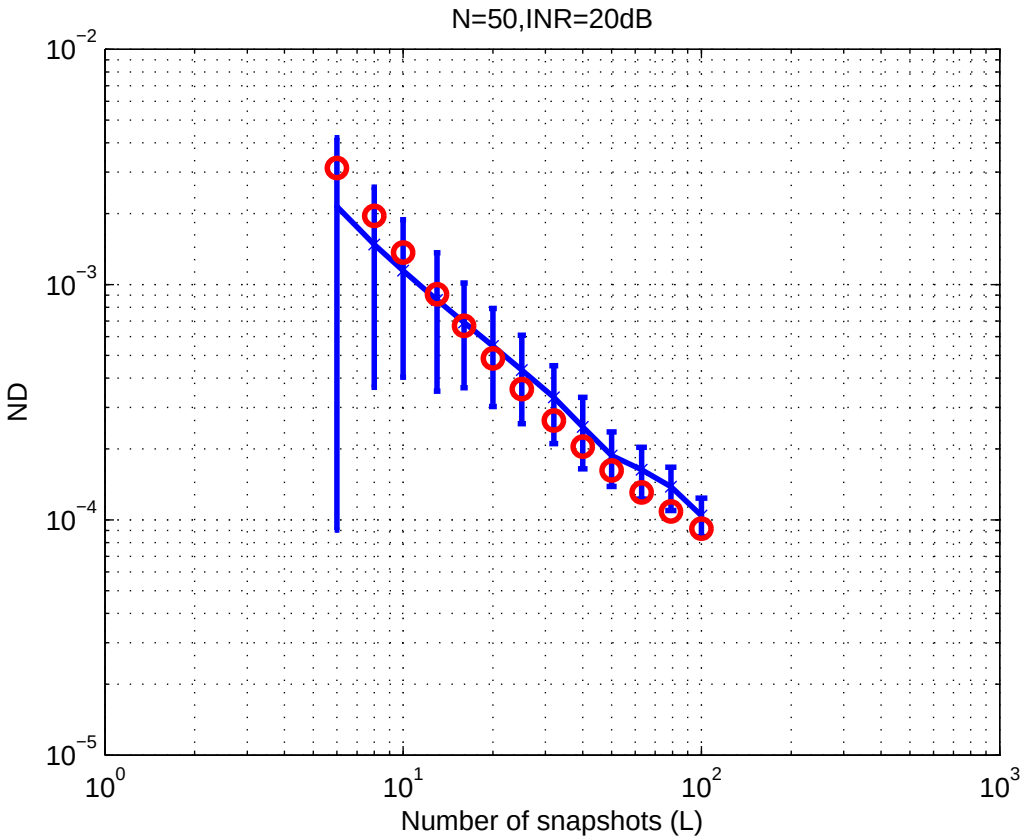

Figure 5.5 The RMT based DMR ABF ND model predictions(red circles) and sample means of Monte Carlo simulations (blue lines) with the number of snapshots ranges from 10 to 1000. There are $D = 3$ interferences. The example uses a 50-sensor ULA with half-wave-length spacing. Here $N = 50$, $\sigma_s^2 = 10, \sigma_1^2 = \sigma_2^2 = \sigma_3^2 = 100, \sigma_n^2 = 1$, $\theta_s = 30°$, $\theta_1 = 20°$, $\theta_2 = 60°$, $\theta_3 = 80°$.

5.5.1 Use ensemble eigenvalues

The DMR weight vector depends on the eigendecomposition of the SCM. In , [39], the authors investigate the relative influence of the sample eigenvalues and eigenvectors on ND. Through the comparison the standard DMR ABF (generated with sample statistics) with two alternative DMR implementations: the first one uses the ensemble eigenvectors and the sample eigenvalues to generate the structured covariance, while the second one uses the ensemble eigenvalues and the sample eigenvectors to generate the structured covariance. The results show when the ensemble eigenvectors are used to construct the covariance matrix, the resulting histogram is centered on the

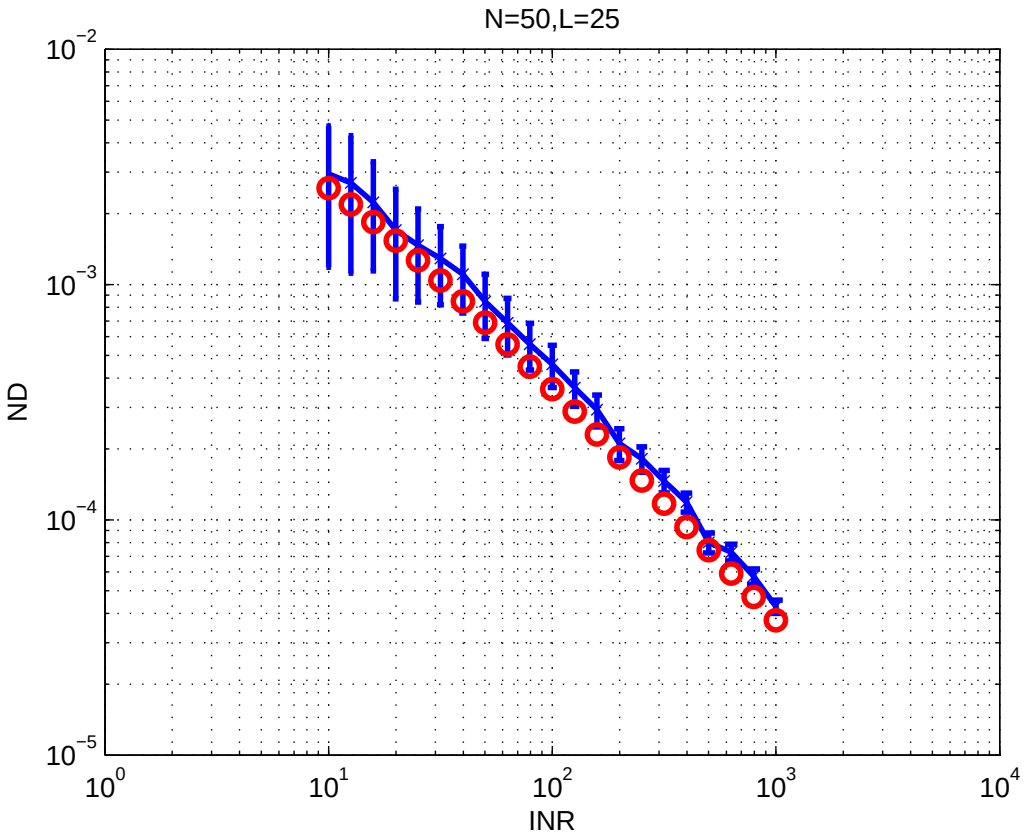

Figure 5.6 The RMT based DMR ABF ND model predictions(red circles) and sample means of Monte Carlo simulations (blue lines) with INR ranges from $10dB$ to $30dB$. There are $D = 3$ interferences. The example uses a 50-sensor ULA with half-wave-length spacing. Here $N = 50$, $L = 25$, $\sigma_s^2 = 10, \sigma_n^2 = 1$,$\theta_s = 30°$, $\theta_1 = 20°$, $\theta_2 = 60°$, $\theta_3 = 80°$.

ensemble ND. In contrast, when the sample eigenvectors are used to construct the covariance matrix , the histogram is centered on the standard DMR result. Therfore, sample eigenvectors are the dominant part rather than the sample eigenvalues. So in our equation (5.37) and (5.38), we can use ensemble eigenvalues γ_i, $i = 1 \cdots D$ to replace the sample eigenvalues λ_i, $i = 1 \cdots D$ to make a simplification.

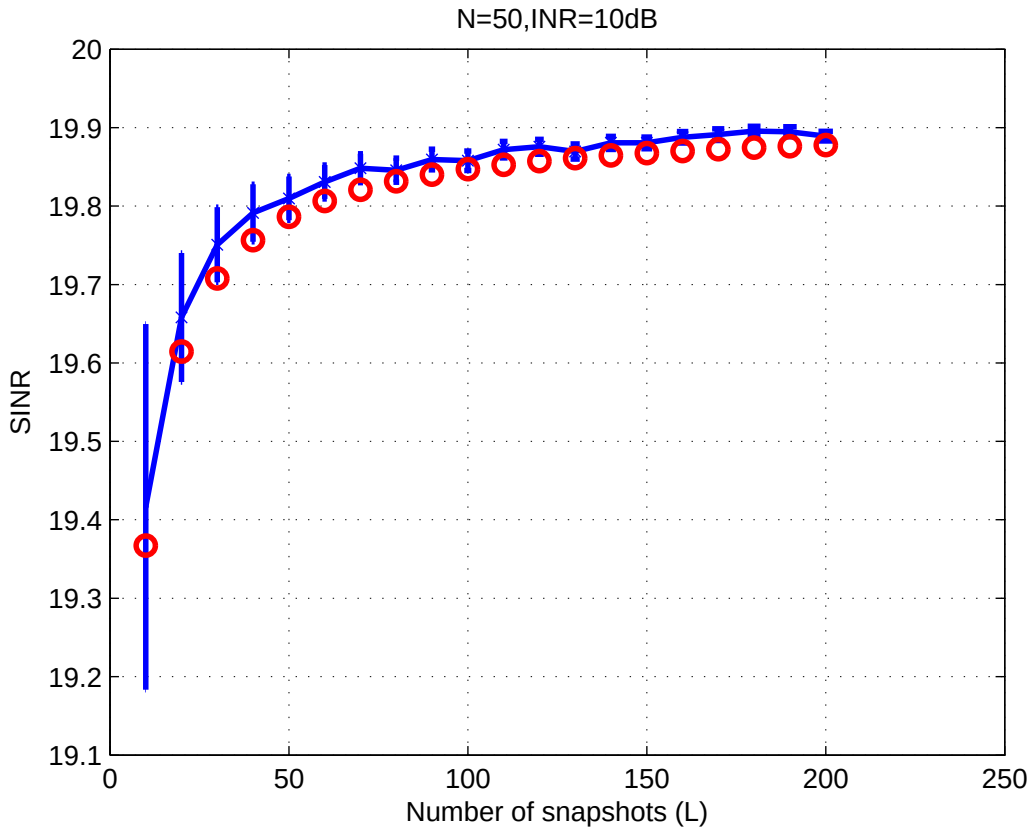

Figure 5.7 The RMT based DMR ABF SINR model predictions(red circles) and sample means of Monte Carlo simulations (blue lines) with the number of snapshots ranges from 5 to 200. The example uses a 50-sensor ULA with half-wave-length spacing. Here $N = 50$, $\sigma_s^2 = 10, \sigma_1^2 = \sigma_2^2 = \sigma_3^2 = 10, \sigma_n^2 = 1$, $\theta_s = 30°$, $\theta_1 = 20°$, $\theta_2 = 60°$, $\theta_3 = 80°$.

5.5.2 Approximated distribution for WNG

Therefore, the WNG expression can be simplified into:

$$G_{WNG} = \frac{(a\alpha + b)^2}{c\alpha + d} \tag{5.38}$$

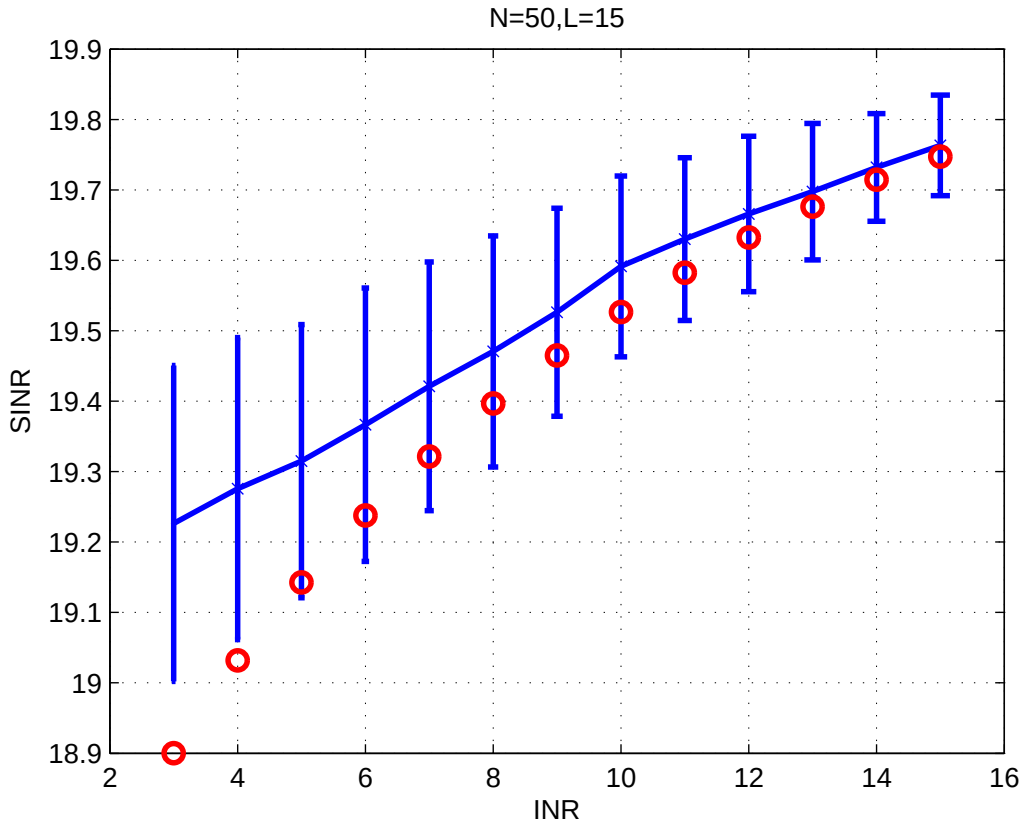

Figure 5.8 The RMT based DMR ABF SINR model predictions(red circles) and sample means of Monte Carlo simulations (blue lines) with INR ranges from $3dB$ to $15dB$. There are $D = 3$ interferences. The example uses a 50-sensor ULA with half-wave-length spacing. Here $N = 50$, $L = 15$, $\sigma_s^2 = 10, \sigma_n^2 = 1$, $\theta_s = 30°$, $\theta_1 = 20°$, $\theta_2 = 60°$, $\theta_3 = 80°$.

where $\alpha \sim \chi^2(D)$, and the rest of paramaters a, b, c, d are defined as,

$$
\begin{aligned}
a &= -\frac{1}{D}\sum_{i=1}^{D}\left|\boldsymbol{\xi}_i^H \mathbf{v}_s\right|^2\left(1-\gamma_i^{-1}\right)\mu_i + \frac{\left|\boldsymbol{\phi}_s^H \mathbf{v}_s\right|^2}{D(N-D)}\sum_{i=1}^{D}\left(1-\gamma_i^{-1}\right)\mu_i \\
b &= 1 - \frac{\left|\boldsymbol{\phi}_s^H \mathbf{v}_s\right|^2}{N-D}\sum_{i=1}^{D}\left(1-\gamma_i^{-1}\right)\mu_i \\
c &= -\frac{1}{D}\sum_{i=1}^{D}\left|\boldsymbol{\xi}_i^H \mathbf{v}_s\right|^2\left(1-\gamma_i^{-2}\right)\mu_i + \frac{\left|\boldsymbol{\phi}_s^H \mathbf{v}_s\right|^2}{D(N-D)}\sum_{i=1}^{D}\left(1-\gamma_i^{-2}\right)\mu_i \\
d &= 1 - \frac{\left|\boldsymbol{\phi}_s^H \mathbf{v}_s\right|^2}{N-D}\sum_{i=1}^{D}\left(1-\gamma_i^{-2}\right)\mu_i
\end{aligned}
\tag{5.39}
$$

Let $g = \dfrac{(a\alpha + b)^2}{c\alpha + d}$, then $\alpha = \dfrac{1}{2a^2}\left(\sqrt{(2ab - cg)^2 - 4a^2(b^2 - dg)} - (2ab - cg)\right)$

$$\left|\frac{d\alpha}{dg}\right| = \left|\frac{1}{2a^2}\left(\frac{c(cg - 2ab) + 2a^2 d}{\sqrt{(2ab - cg)^2 - 4a^2(b^2 - dg)}} + c\right)\right| \tag{5.40}$$

Through the Change-of-Variable Technique, the probability density function for G_{WNG} is:

$$f_{G_{WNG}}(g) = \frac{1}{2^{D/2}\Gamma(D/2)} \cdot \left|\frac{1}{2a^2}\left(\frac{c(cg - 2ab) + 2a^2 d}{\sqrt{(2ab - cg)^2 - 4a^2(b^2 - dg)}} + c\right)\right| \cdot g^{\frac{1}{4a^2}\left(\sqrt{(2ab-cg)^2-4a^2(b^2-dg)}-(2ab-cg)\right)-1} e^{-\frac{1}{4a^2}\left(\sqrt{(2ab-cg)^2-4a^2(b^2-dg)}-(2ab-cg)\right)} \tag{5.41}$$

5.5.3 Special case

For Figure 5.9, we find that the distribution of α_i is close to a Gaussian distribution only when there is a sufficient number of samples and a more substantial number of domiant modes. That is to say: the limit of a Chi-squared distribution will be a Gaussian distribution. This property follows from the central limit theorem, using the fact that the chi-squared distribution is obtained as the distribution of a sum of squares of independent standard normal random variables. For $\alpha_i = \boldsymbol{\xi}_i^H \mathbf{E_D} \mathbf{E_D}^H \boldsymbol{\xi}_i = \dfrac{\mu_i}{D}\alpha \sim \dfrac{\mu_i}{D}\chi^2(D), \quad i = 1 \cdots D$, or $\alpha \equiv \sum_{i=1}^{D} Z_i^2 \sim \chi^2(D)$, we have $E(\alpha) = D$ and $Var(\alpha) = 2D$. Applying the classical central limit theorem we get:

$$\lim_{D\to\infty} \mathbb{P}\left(\frac{\alpha - D}{\sqrt{2D}} \leqslant z\right) = \Phi(z) \tag{5.42}$$

Another way of writing this formal limiting result is that:

$$\frac{\alpha - D}{\sqrt{2D}} \overset{\text{Dist}}{\rightarrow} \mathrm{N}(0,1) \tag{5.43}$$

That is the formal convergence result that holds for the chi-squared distribution. Informally, for large D we have the approximate distribution: $\alpha \overset{\text{Approx}}{\rightarrow} \mathrm{N}(D, 2D)$. Though not strictly correct, sometimes this informal approximation is asserted as a kind of convergence result, informally referring to convergence where p appears on both sides.

The above results show that with a sufficient number of samples and a more substantial number of domiant modes, we can consider the distribution of α as a Gaussian distribution:

$$\alpha \overset{\text{Approx}}{\rightarrow} \mathrm{N}(D, 2D). \tag{5.44}$$

Note when the INRs are large, $\boldsymbol{\Delta}_1 \approx \boldsymbol{\Delta}_2$, that means Equation(5.37) can be simplfied into

$$G_{WNG} = \frac{\left(1 - \boldsymbol{v}_s^{\mathbf{H}} \left(\boldsymbol{\Delta}_0 - \boldsymbol{\Delta}_1\right) \boldsymbol{v}_s\right)^2}{1 - \boldsymbol{v}_s^{\mathbf{H}} \left(\boldsymbol{\Delta}_0 - \boldsymbol{\Delta}_2\right) \boldsymbol{v}_s} \approx 1 - \boldsymbol{v}_s^{\mathbf{H}} \left(\boldsymbol{\Delta}_0 - \boldsymbol{\Delta}_1\right) \boldsymbol{v}_s \tag{5.45}$$

while at the same time, in Equation(5.39) $a \approx c, b \approx d$. Therefore, Equation(5.38) can be represented as:

$$G_{WNG} = a\alpha + b \tag{5.46}$$

where $\alpha \sim \chi^2(D)$, and

$$\begin{aligned} a &= -\frac{1}{D}\sum_{i=1}^{D}\left|\boldsymbol{\xi}_i^H \mathbf{v}_s\right|^2\left(1-\gamma_i^{-1}\right)\mu_i + \frac{\left|\boldsymbol{\phi}_s^H \mathbf{v}_s\right|^2}{D(N-D)}\sum_{i=1}^{D}\left(1-\gamma_i^{-1}\right)\mu_i \\ b &= 1 - \frac{\left|\boldsymbol{\phi}_s^H \mathbf{v}_s\right|^2}{N-D}\sum_{i=1}^{D}\left(1-\gamma_i^{-1}\right)\mu_i \\ \mu_i &= \left(1-\frac{c}{\left(\gamma_i/\sigma_n^2-1\right)^2}\right)/\left(1+\frac{c}{\left(\gamma_i/\sigma_n^2-1\right)}\right), (i=1\cdots D) \end{aligned} \tag{5.47}$$

and $\gamma_i, (i = 1 \cdots D)$ are D largest eigenvalues of ECM $\boldsymbol{\Sigma}_{I+N}$.

In such cases, the distribution function of α is a Gamma distribution $\Gamma(p, \lambda)$ with parameters $p = D/2$, and $\lambda = 1/2$:

$$f(\alpha) = \frac{\alpha^{D/2-1}e^{-\alpha/2}}{2^{D/2}\Gamma(D/2)}, \qquad for \;\; \alpha \geq 0 \tag{5.48}$$

Through the Change-of-Variable Technique, the probability density function for G_{WNG} is:

$$f_{G_{WNG}}(g) = \frac{1}{a \cdot 2^{D/2}\Gamma(D/2)} \cdot \left(\frac{g-b}{a}\right)^{D/2-1} \cdot e^{-(g-b)/2a} \tag{5.49}$$

In particular, we note one thing: when $D = 1$, Equation(5.49) will reduce to the square of normal distribution variable or a chi-square distributed variable with one degree of freedom:

$$f_{G_{WNG}}(g) = \frac{1}{a\sqrt{2\pi}} \cdot \left(\frac{g-b}{a}\right)^{-1/2} \cdot e^{-(g-b)/2a}, \qquad for \;\; D = 1 \tag{5.50}$$

Table 5.1 The WND PDF plots obtained with different system parameters

	Parameters			
WNG	L	N	D	INR
Figure 10	25/100/1000	50	6	10dB
Figure 11	50	25/50/100	6	10dB
Figure 12	100	50	1/3/6	10dB
Figure 13	100	50	6	3/10/20dB

We note that when $D = 1$,

$$
\begin{aligned}
a &= \left(\frac{1}{N-1} - \left|\mathbf{v}_1^H \mathbf{v}_s\right|^2\right)\left(1 - \frac{1}{\sigma_1^2 + \sigma_n^2}\right)\left(1 - \frac{N/L}{\left(\sigma_1^2/\sigma_n^2\right)^2}\right) / \left(1 + \frac{N/L}{\sigma_1^2/\sigma_n^2}\right) \\
b &= 1 - \frac{1}{N-1}\left(1 - \frac{1}{\sigma_1^2 + \sigma_n^2}\right)\left(1 - \frac{N/L}{\left(\sigma_1^2/\sigma_n^2\right)^2}\right) / \left(1 + \frac{N/L}{\sigma_1^2/\sigma_n^2}\right) \\
E_{G_{WNG}}(g) &= a + b \\
&= 1 - \left|\mathbf{v}_1^H \mathbf{v}_s\right|^2 \cdot \left(1 - \frac{1}{\sigma_1^2 + \sigma_n^2}\right)\left(1 - \frac{N/L}{\left(\sigma_1^2/\sigma_n^2\right)^2}\right) / \left(1 + \frac{N/L}{\sigma_1^2/\sigma_n^2}\right) \\
VAR_{G_{WNG}}(g) &= 2a^2 \\
&= \left(\left(\frac{1}{N-1} - \left|\mathbf{v}_1^H \mathbf{v}_s\right|^2\right)\left(1 - \frac{1}{\sigma_1^2 + \sigma_n^2}\right)\left(1 - \frac{N/L}{\left(\sigma_1^2/\sigma_n^2\right)^2}\right) / \left(1 + \frac{N/L}{\sigma_1^2/\sigma_n^2}\right)\right)^2
\end{aligned}
\tag{5.51}
$$

In particular, for high INRs case, $\sigma_1^2 \gg \sigma_n^2$, the mean and variance can be further simplified as:

$$
\begin{aligned}
E_{G_{WNG}}(g) &\approx 1 - \left|\mathbf{v}_1^H \mathbf{v}_s\right|^2 \\
VAR_{G_{WNG}}(g) &\approx \left(\frac{1}{N-1} - \left|\mathbf{v}_1^H \mathbf{v}_s\right|^2\right)^2
\end{aligned}
\tag{5.52}
$$

This is consistent with our previous appromation result in Chapter 3, section 3.3.1. $E_{G_{WNG}}(g) \approx 1$ (in high INR scenario) and Buck and Wage's conjecture (see Figure 10 in [39]).

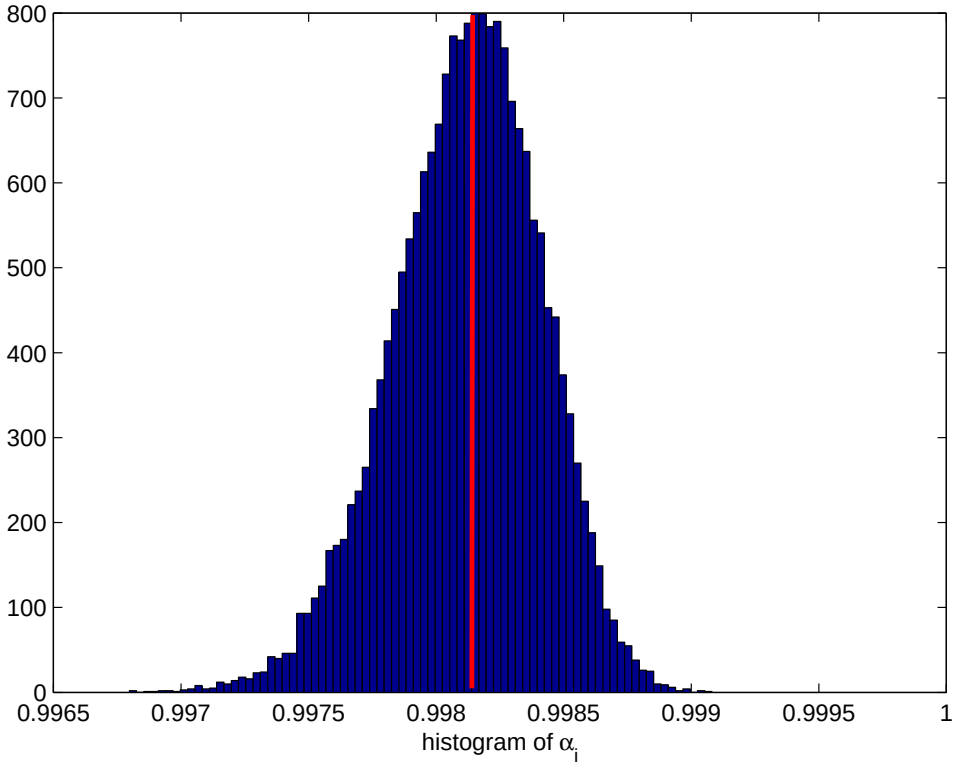

Figure 5.9 Histogram of α_i. $D = 6$, $L = 1000$, $N = 50$. 20000 trials are used.$\rho_{INR1} = \rho_{INR4} = 13dB$, $\rho_{INR2} = \rho_{INR5} = 10dB$, and $\rho_{INR3} = \rho_{INR6} = 7dB$. Red line indicates the mean.

Table 5.1 shows the WND/ND PDF plots obtained with different system parameters. Figures 5.10-13 show the probability density function (5,49) overlaid on the WNG histogram for different system parameters (L, N, D, INR). The example uses a 50-sensor ULA with half-wave-length spacing. One obvious result is that: with the increases of L/N or INR, the WNG histogram will become thinner and taller, and the mean value will be closer to 1. Moreover, Figure 5.12 illustrates the variability of the WNG with different D, the WNG with multiple interferers is less than the single interferer, this explains the fact that when $D = 1$, it can be approximated as an exponential distribution, since chi-squared distriobution with two degrees of freedom and exponential distribution have the same PDFs, since degree of freedom for complex-valued cases is supposed to be double of real-case.

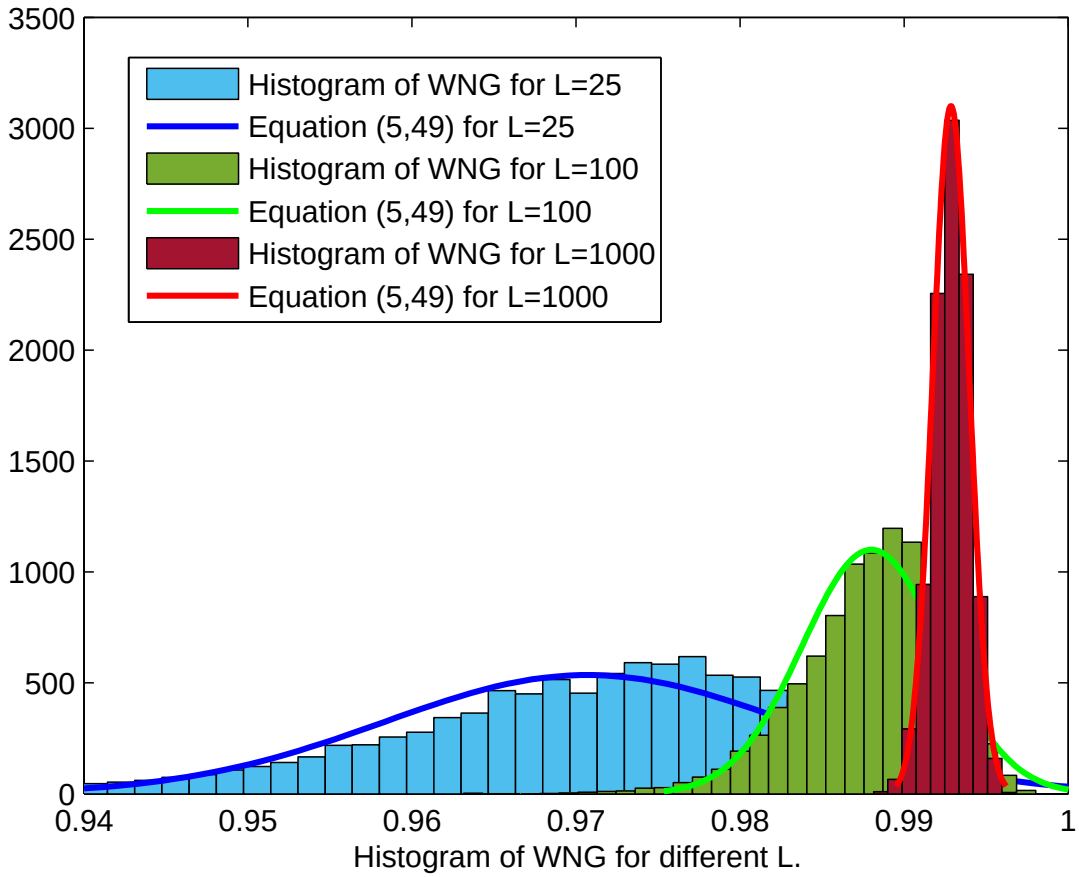

Figure 5.10 Probability density function overlaid on the WNG histogram for the multiple interference case($D = 6$). Here $N = 50$, $\rho_{INR_i} = 10dB$, $i = 1...6$. 10000 trials are used.

5.6 Summary and Conclusion

In this chapter, we focuse on an illustrative example of multiple planewave interference in spatially white noise. We show the performance analysis of DMR ABF by three standard metrics: ND, WNG, and SINR for multiple interference case. The analysis uses the RMT method for deriving and verifying the analytical results. Finally, the analytical results are compared with RMT Monte-Carlo based empirical results.

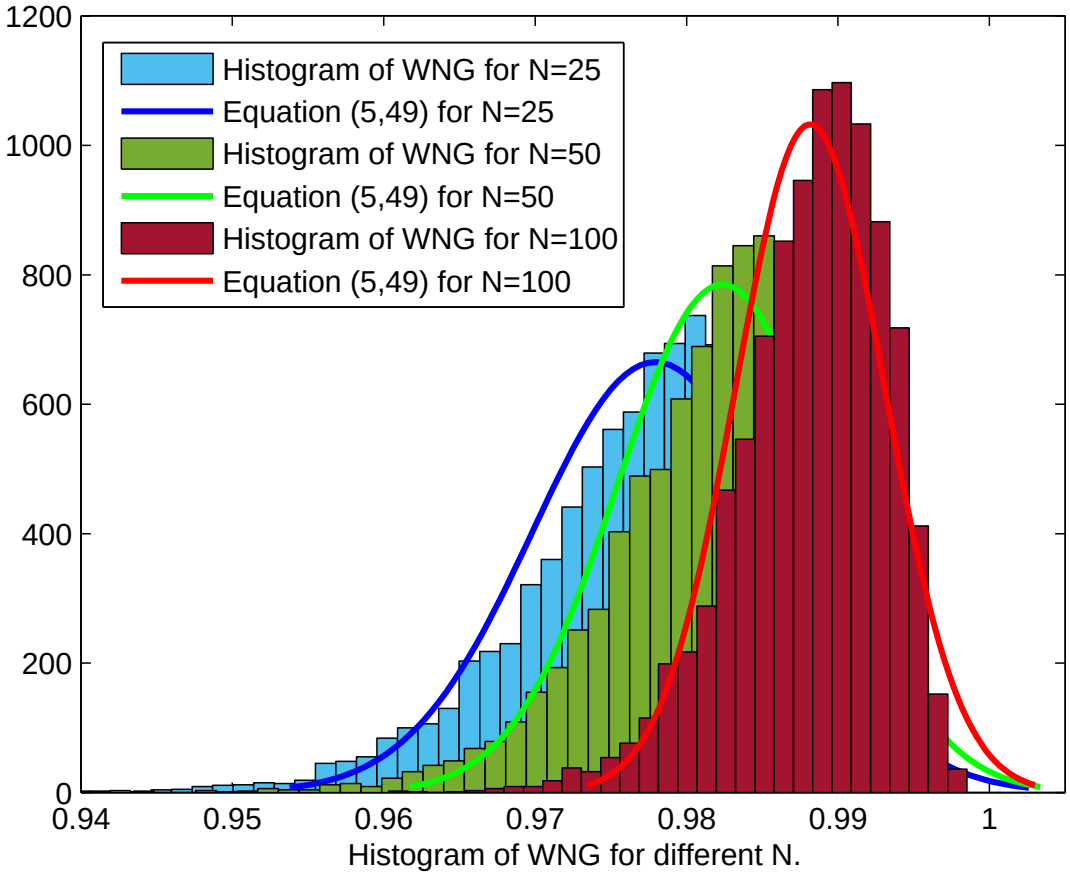

Figure 5.11 Probability density function overlaid on the WNG histogram for the multiple interference case($D = 6$). Here $L = 50$, $\rho_{INR_i} = 10dB$, $i = 1...6$. 10000 trials are used.

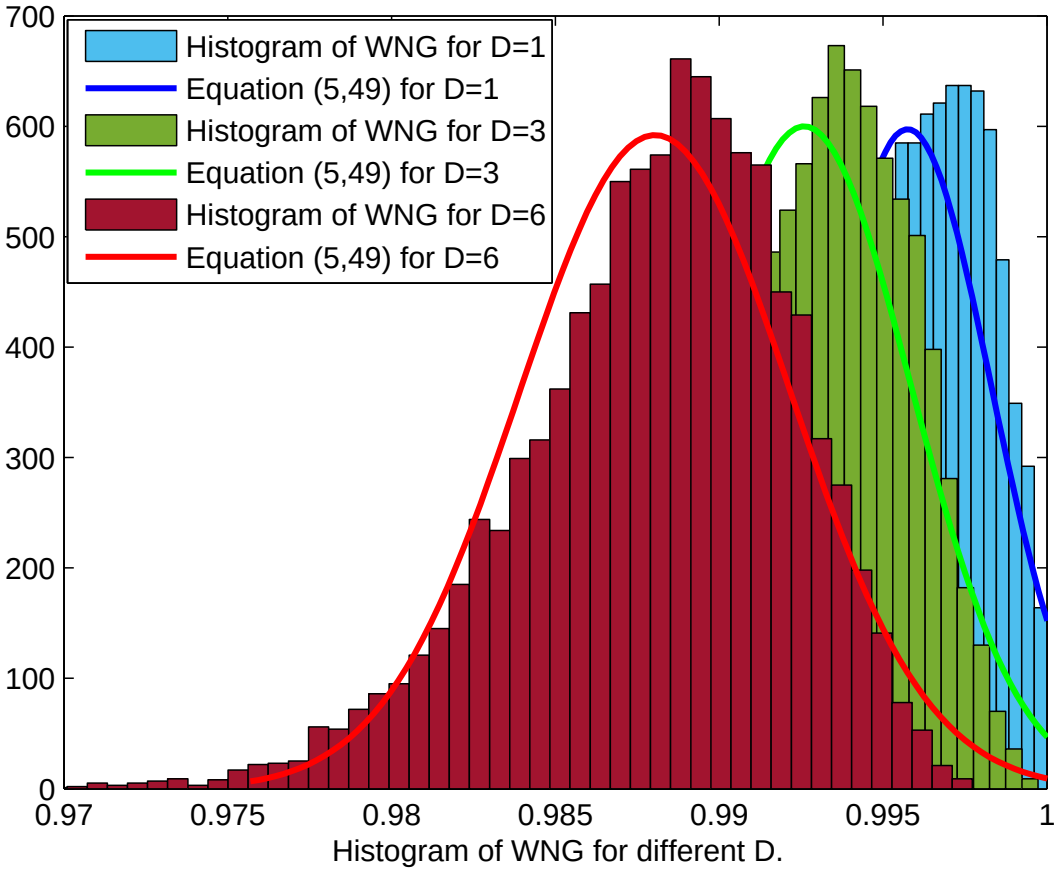

Figure 5.12 Probability density function overlaid on the WNG histogram for the single/multiple interference case. Here $N = 50$, $L = 100$, $\rho_{INR_i} = 10dB$, $i = 1...6$. 10000 trials are used.

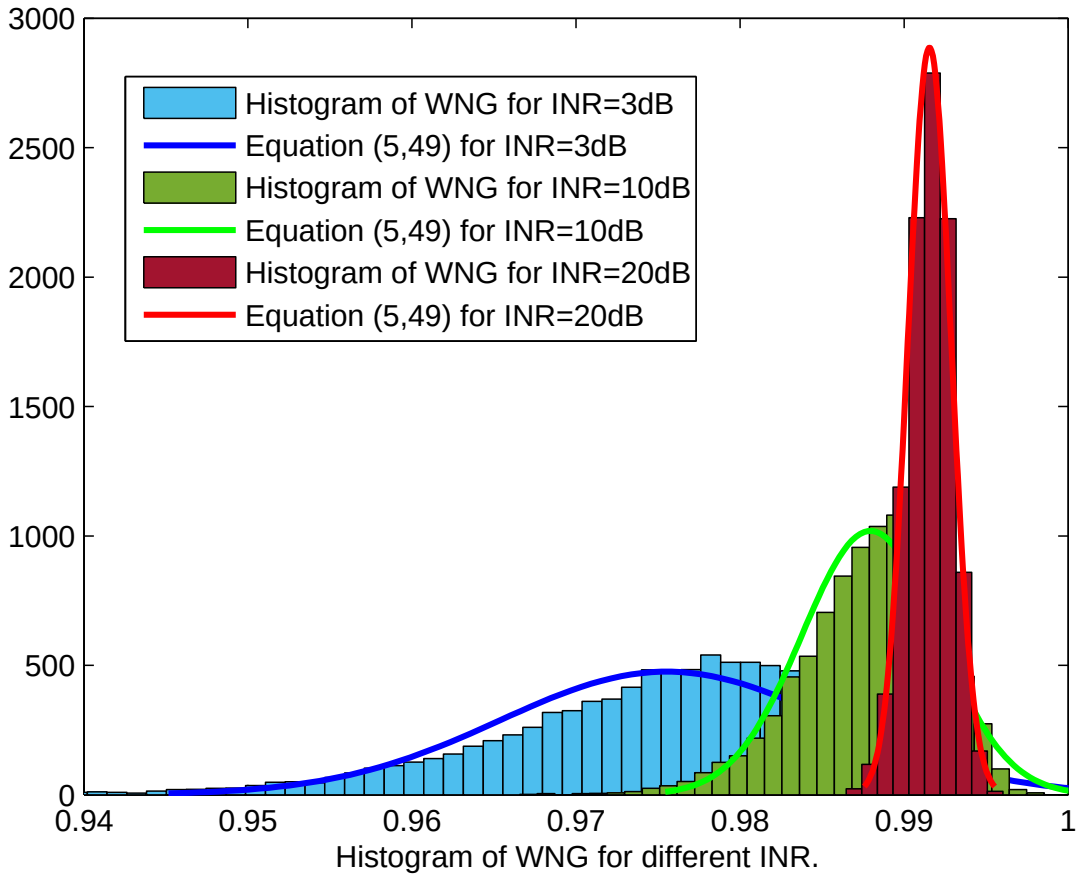

Figure 5.13 Probability density function overlaid on the WNG histogram for the multiple interference case($D = 6$). Here $N = 50$, $L = 100$. 10000 trials are used.

CHAPTER 6

CONCLUSION

This dissertation studies the performance of DMR-ABF by deriving PDFs of important metrics, namely ND, WNG, and SINR. Through three approaches for handling rank deficient sample covariance matrices, we proposed and developed data transformation methods to facilitate our study on the statistical performance of the DMR beamformer. Chapter 3 presents detailed derivation of the distribution of SINR loss ratio of the DMR beamformer for single interference case can be used a beta-distributed function to express it. Chapter 4 presents a theoretical analysis for the ND of the DMR based ABF for single interference case. A closed-form expression has been derived for the PDF of ND. Finally, the performance analysis of DMR ABF for the multiple interference case are discussed in Chapter 5, along with the RMT method for deriving and verifying the analytical results.

In summary, we have shown the performance analysis of the DMR ABF for single and multiple interference case. The analysis provides valuable insights into the research of DMR ABF.

APPENDIX A

INDEPENDENCE OF $C_{11}^{-1}\mathbf{C}_{21}$ AND C_{11}

In this appendix, we want to show $c_{11}^{-1}\mathbf{c}_{21}$ and c_{11} are independent.

We begin with a random Hermitian matrix $\mathbf{C}$. It can be represented as:

$$\mathbf{C} = \mathbf{U}^{\mathbf{H}}\mathbf{\Sigma}_{I+N}^{1/2}\mathbf{S}\mathbf{\Sigma}_{I+N}^{1/2}\mathbf{U} = \mathbf{U}^{\mathbf{H}}\mathbf{\Sigma}_{I+N}^{1/2}\left(\frac{1}{L}\sum_{l=1}^{L}\mathbf{p}\left(l\right)\mathbf{p}^{\mathrm{H}}\left(l\right)\right)\mathbf{\Sigma}_{I+N}^{1/2}\mathbf{U}$$

where $\mathbf{U}$, $\mathbf{\Sigma}$ are deteministic Hermitian matrix and $\mathbf{p}$ is $N \times 1$ sample vector. The fundamental parameters of the central complex Wishart distribution are L, the sample size, N, the number of dimensions of vector $\mathbf{p}$, and $\mathbf{I}_N$ the $N \times N$ ensemble covariance matrix of $\mathbf{C}$. Therefore, we can designate a central complex Wishart distribution with these parameters by $CW(L, N; \mathbf{I}_N)$. The partition matrixes $\mathbf{C}$ is

$$\mathbf{C} = \begin{pmatrix} c_{11} & \mathbf{c}_{12} \\ \mathbf{c}_{21} & \mathbf{c}_{22} \end{pmatrix}$$

where $\mathbf{c}_{12} = \mathbf{c}_{21}^{H}$. The PDF is given by the central complex Wishart distribution.

$$p\left(\mathbf{C}\right) = \frac{\left|\mathbf{C}\right|^{L-N}}{I(\mathbf{I}_N)} exp\left[-tr(\mathbf{C})\right)] = \frac{\left|\mathbf{C}\right|^{L-N} \cdot exp\left[-tr(\mathbf{C})\right)]}{\pi^{L(L-1)/2}\Gamma(L)\Gamma(L-1)\cdots\Gamma(L-N+1)}$$

where for a general matrix $\mathbf{M}$, the definition of $I(\mathbf{M}) = \pi^{L(L-1)/2)}\Gamma(L)\Gamma(L-1)\cdots\Gamma(L-N+1)\left|\mathbf{M}\right|^{L}$. With matrix partition, the random Hermitian matrix $\mathbf{C}$ can be factored as

$$\mathbf{C} = \begin{pmatrix} c_{11} & 0 \\ \mathbf{c}_{21} & \mathbf{I}_{N-1} \end{pmatrix}\begin{pmatrix} 1 & c_{11}^{-1}\mathbf{c}_{21}^{H} \\ 0 & \mathbf{C}_{22} - c_{11}^{-1}\mathbf{c}_{21}\mathbf{c}_{21}^{H} \end{pmatrix}$$

Hence, by Laplace's rules for computing determinants, $\left|\mathbf{C}\right| = \left|c_{11}\right|\left|\mathbf{C}_{22} - c_{11}^{-1}\mathbf{c}_{21}\mathbf{c}_{21}^{H}\right|$, one gets

$$\begin{aligned} p\left(\mathbf{C}\right) = \frac{\left|c_{11}\right|^{L-N}}{I(\mathbf{I}_N)}\left|\mathbf{C}_{22} - c_{11}^{-1}\mathbf{c}_{21}\mathbf{c}_{21}^{H}\right|^{L-N} exp\left(-c_{11} - tr\left(c_{11}^{-1}\mathbf{c}_{21}\mathbf{c}_{21}^{H}\right)\right) \\ \cdot exp\left[-tr\left(\mathbf{C}_{22} - c_{11}^{-1}\mathbf{c}_{21}\mathbf{c}_{21}^{H}\right)\right] \end{aligned}$$

Following them, make the change of variables:

$$\begin{aligned}\mathbf{D}_{11} &= \mathbf{C}_{22} - c_{11}^{-1}\mathbf{c}_{21}\mathbf{c}_{21}^{H} \\ \mathbf{d}_{12} &= \mathbf{c}_{21} \\ d_{22} &= c_{11}\end{aligned}$$

$$\begin{aligned}p\left(\mathbf{D}_{11}, \mathbf{d}_{12}, d_{22}\right) =& \frac{\left|d_{22}\right|^{L-N}}{I(\mathbf{I}_N)} \left|\mathbf{D}_{11}\right|^{L-N} \\ & exp\left(-d_{22} - tr\left(d_{22}^{-1}\mathbf{d}_{12}\mathbf{d}_{12}^{H}\right) - tr\left(\mathbf{D}_{11}\right)\right)\end{aligned}$$

where

$$p\left(\mathbf{D}_{11}\right) = \frac{1}{I(\mathbf{I}_{N-1})} \left|\mathbf{D}_{11}\right|^{L-N} exp\left(-tr\left(\mathbf{D}_{11}\right)\right)$$

a complex wishart distribution, and

$$\begin{aligned}p\left(\mathbf{d}_{12}, d_{22}\right) =& \frac{I(\mathbf{I}_{N-1})}{I(\mathbf{I}_N)} \left|d_{22}\right|^{L-N} \\ & \cdot exp\left(-d_{22} - tr\left(d_{22}^{-1}\mathbf{d}_{12}\mathbf{d}_{12}^{H}\right)\right)\end{aligned}$$

Next, let $\mathbf{e}_{12} = \mathbf{d}_{12}d_{22}^{-1} = c_{11}^{-1}\mathbf{c}_{21}, e_{22} = d_{22} = c_{11}$ so that

$$\frac{\partial\left(\mathbf{e}_{12}, e_{22}\right)}{\partial\left(\mathbf{d}_{12}, d_{22}\right)} = \begin{vmatrix} \frac{\partial \mathbf{e}_{12}}{\mathbf{d}_{12}} & \frac{\partial \mathbf{e}_{12}}{d_{22}} \\ 0 & \mathbf{I} \end{vmatrix} = \left|\frac{\partial \mathbf{e}_{12}}{\mathbf{d}_{12}}\right| = \left|e_{22}\right|^{-2}$$

then

$$p\left(\mathbf{e}_{12}, e_{22}\right) = \frac{I(\mathbf{I}_{N-1})}{I(\mathbf{I}_N)} \left|e_{22}\right|^{L-N+2} \cdot exp\left(-e_{22} - tr\left(e_{22}^{-1}\mathbf{e}_{12}\mathbf{e}_{12}^{H}\right)\right)$$

Observe the RHS, if the norm of $\mathbf{e}_{12}$ is held constant, then $\det\left(\mathbf{I_{N-1}} + \mathbf{e_{12}e_{12}^{H}}\right)$ is independent of the components of $\mathbf{e}_{12}$, hence $p\left(e_{22}\right)$ below is independent of $\mathbf{e}_{12}$. Here we can refer to the complex Wishart distribution developed by Goodman in [12]. As e_{22} has a distribution of $CW(L+1, 1; \left[1 + \mathbf{e}_{12}^{H}\mathbf{e}_{12}\right]^{-1})$, we have

$$\begin{aligned}p\left(e_{22}\right) =& \frac{1}{I(\mathbf{I}_1)} \left|e_{22}\right|^{L-N+2} \left|\mathbf{I_{N-1}} + \mathbf{e_{12}e_{12}^{H}}\right|^{L+1} \\ & exp\left(-e_{22} - tr\left(e_{22}^{-1}\mathbf{e}_{12}\mathbf{e}_{12}^{H}\right)\right)\end{aligned}$$

so

$$p\left(\mathbf{e}_{12}\right) = \frac{\Gamma\left(L+1\right)}{\Gamma\left(L-N+2\right)\Gamma\left(N-1\right)} \frac{1}{\left|\mathbf{I_{N-1}} + \mathbf{e_{12}e_{12}^{H}}\right|^{L+1}}$$
$$= \frac{\Gamma\left(L+1\right)}{\Gamma\left(L-N+2\right)\Gamma\left(N-1\right)} \frac{1}{\left|1 + \mathbf{e}_{12}^{H}\mathbf{e}_{12}\right|^{L+1}}$$

$\mathbf{e}_{12}$ and e_{22} are independent. Let $r = \mathbf{e}_{12}^{H}\mathbf{e}_{12}$, by changing to polar coordinates, one gets

$$p(r) = \frac{\Gamma\left(L+1\right)}{\Gamma\left(L-N+2\right)\Gamma\left(N-1\right)} \frac{r^{N-2}}{\left(1+r\right)^{L+1}}$$

In conclusion, we show $c_{11}^{-1}\mathbf{c}_{21}$ and c_{11} are independent.

REFERENCES

[1] D. A. Abraham and N. L. Owsley. Beamforming with dominant mode rejection. *Conference Proceedings on Engineering in the Ocean Environment*, pages 470 – 475, 1990.

[2] D. Achlioptas. Database-friendly random projections: Johnson-Lindenstrauss with binary coins. *Journal of computer and System Sciences*, (66(4)):671–687, 2003.

[3] T. W. Anderson. Asymptotic theory for principal component analysis. *The Annals of Mathematical Statistics*, 1963.

[4] J. Baik and J. W. Silverstein. Eigenvalues of large sample covariance matrices of spiked population models. *Journal of Multivariate Analysis*, 97(6):1382–1408, 2006.

[5] C. Bao. Robust high resolution dominant mode rejection beamformer for passive sonar. In *Proc. ACOUSTICS Gold Coast, Australia: Austral. Acoust. Soc*, pages 523–526, 2004.

[6] F. Benaych-Georges and R. R. Nadakuditi. The singular values and vectors of low rank perturbations of large rectangular random matrices. *Journal of Multivariate Analysis*, 111:120–135, 2012.

[7] J. Capon and N.R. Goodman. Probability distributions for estimators of the frequency-wavenumber spectrum. *Proc. IEEE*, 1970.

[8] H. Cox and R. Pitre. Robust DMR and multi-rate adaptive beamforming. In *Proc. 32nd Asilomar Conf. Signals Syst. Comput.*, pages 920–924, 1998.

[9] S. Dasgupta and A. Gupta. An elementary proof of the Johnson Lindenstrauss lemma. *Random Structures & Algorithms*, 22(1):60–65, 2003.

[10] P. Frankl and H. Maehara. The Johnson Lindenstrauss lemma and the sphericity of some graphs. *Journal of combinatorial theory. Series B*, 44(3):355–362, 1988.

[11] E. N. Gilbert and S. P. Morgan. Optimum design of directive antenna arrays subject to random variations. *The Bell System Technical Journal*, 34:637–663, 1955.

[12] N. R. Goodman. Statistical analysis based on a certain multivariate complex Gaussian distribution (an introduction). *The Annals of mathematical statistics*, 34(1):152–177, 1963.

[13] R. Pitre H. Cox and H. Lai. Robust adaptive matched field processing. In *Conference Record of Thirty-Second Asilomar Conference on Signals, Systems and Computers (Cat. No. 98CH36284)*, volume 1, pages 127–131. IEEE, 1998.

[14] R. Zeskind H. Cox and M. Owen. Robust adaptive beamforming. *IEEE Transactions on Acoustics, Speech, and Signal Processing*, 35:1365–1376, 1987.

[15] A. Haimovich. The eigencanceler: adaptive radar by eigenanalysis methods. *IEEE Transactions on Aerospace and Electronic Systems*, 32(2):532–542, 1996.

[16] E. Hu and H. Ge. The probability density function of SINR loss of the dominant mode rejection beamformer. *52nd Annual Conference on Information Sciences and Systems (CISS)*, pages 1–6, 2018.

[17] E. Hu and H. Ge. Probability density function of notch depth for dominant mode rejection beamformer. *Electronics Letters*, 55(23):1255–1258, 2019.

[18] P. Indyk and R. Motwani. Approximate nearest neighbors: towards removing the curse of dimensionality. In *30th Annual ACM Symposium on Theory of Computing*, pages 604–613, 1998.

[19] W.B. Johnson and J. Lindenstrauss. Extensions of lipschitz mappings into a Hilbert space. *Contemporary Mathematics*, 26:189–206, 1984.

[20] I. P. Kirsteins and D. W. Tufts. Adaptive detection using low rank approximation to a data matrix. *IEEE Transactions on Aerospace and Electronic Systems*, 30(1):55–67, 1994.

[21] S. M. Kogon. Robust adaptive beamforming for passive sonar using eigenvector/beam association and excision,. In *Proc. IEEE Sensor Array Multichannel Signal Process. Workshop*, pages 33–37, 2002.

[22] K. G. Larsen and J. Nelson. Optimality of the Johnson-Lindenstrauss Lemma. In *2017 IEEE 58th Annual Symposium on Foundations of Computer Science (FOCS)*, pages 633–638, 2017.

[23] J. Matousek. On variants of the Johnson Lindenstrauss lemma. *Random Struct Algorithms*, pages 142–156, 2008.

[24] T. R. Messerschmitt and R. A. Gramann. Evaluation of the dominant mode rejection beamformer using reduced integration times. *IEEE Journal of oceanic engineering*, 22(2):385–392, 1997.

[25] Y. Peng N. Li, J. Tang and X. Wang. An improved dominant mode rejection adaptive beamforming algorithm. In *2006 CIE International Conference on Radar*. IEEE, 2006.

[26] R. R. Nadakuditi and A. Edelman. Sample eigenvalue based detection of high-dimensional signals in white noise using relatively few samples. *IEEE Transactions on Signal Processing*, July 2008.

[27] E. S. Nadimi, M. H. Ramezani, and V. Blanes-Vidal. On the ratio of independent complex Gaussian random variables. *Multidimensional Systems and Signal Processing*, 29:1553–1561, 2018.

[28] B. Nadler. Finite sample approximation results for principal component analysis: a matrix perturbation approach. *The Annals of Statistics*, 36(6):2791–2817, 2008.

[29] D. Paul. Asymptotics of sample eigenstructure for a large dimensional spiked covariance model. *Statistica Sinica*, 2007.

[30] B. Picinbono. A geometrical interpretation of signal detection and estimation (Corresp.). *IEEE Transactions on Information Theory*, 26(4):493–497, 1980.

[31] T. M. Redheendran and R. A. Gramann. Iitial evaluation of the dominant mode rejection beamformer. *The Journal of the Acoustical Society of America*, 104(3):1331–1344, 1998.

[32] I. S. Reed, J. D. Mallett, and L. E. Brennan. Rapid convergence rate in adaptive arrays. *IEEE Transactions on Aerospace and Electronic Systems*, AES-10:853 – 863, 1974.

[33] C. D. Richmond. MVDR adaptive sidelobes: Extending Ruzes formula and providing an exact calculation of the probability of sidelobe suppression. *Proc. IEEE Sensor Array Multichannel Signal Process. Workshop*, pages 73–76, March 2000.

[34] A. N. Tikhonov and V. Y. Arsenin. *Solutions of Ill-Posed Problems*. Winston and Sons, Washington D.C., 1977.

[35] G. H. Tucci T.L. Marzetta and S. H. Simon. A random matrix theoretic approach to handling singular covariance estimates. *IEEE Transactions on Information Theory*, 57(9):6256–6271, 2011.

[36] S.H. Simon T.L. Marzetta and H. Ren. Capon-MVDR spectral estimation from singular data covariance matrix, with no diagonal loading. In *Proc. 14th Annu. Workshop ASAP, MIT Lincoln Laboratory*, pages 1–6, 2006.

[37] K. E. Wage and J. R. Buck. A random matrix theory model for the Dominant Mode Rejection beamformer notch depth. In *IEEE Statistical Signal Processing Workshop*, 2012.

[38] K. E. Wage and J. R. Buck. Convergence rate of the Dominant Mode Rejection beamformer for a single interferer. In *2013 IEEE International Conference on Acoustics, Speech and Signal Processing*, pages 3796–3800, 2013.

[39] K. E. Wage and J. R. Buck. Snapshot performance of the Dominant Mode Rejection beamformer. *IEEE Journal of Oceanic Engineering*, 39, no. 2,:212 – 225, April 2014.

[40] K. E. Wage and J. R. Buck. SINR loss of the Dominant Mode Rejection beamformer. In *2015 IEEE International Conference on Acoustics, Speech and Signal Processing (ICASSP)*, pages 2499–2503, 2015.

[41] K. E. Wage and J. R. Buck. Performance analysis of Dominant Mode Rejection beamforming. In *Proceedings of the 20th International Congress in Acoustics*, pages 1–6, August, 2010.

[42] M. Wax and T. Kailath. Detection of signals by information theoretic criteria. *IEEE Transactions on Acoustics, Speech, and Signal processing*, 33, 1985.